59T

E83-10363
CR-172891

ELECTROMAGNETIC DEEP-PROBING (100-1000 KMS) OF THE EARTH'S INTERIOR FROM ARTIFICIAL SATELLITES: CONSTRAINTS ON THE REGIONAL EMPLACEMENT OF CRUSTAL RESOURCES

John F. Hermance
Geophysical/Electromagnetics Laboratory
Department of Geological Sciences
Brown University
Providence, Rhode Island 02912

(E83-10363) ELECTROMAGNETIC DEEP-PROBING (100-1000 KMS) OF THE EARTH'S INTERIOR FROM ARTIFICIAL SATELLITES: CONSTRAINTS ON THE REGIONAL EMPLACEMENT OF CRUSTAL RESOURCES Final Report, Jun. 1980 - Feb. 1983 (Brown
N83-29774
Unclas
G3/43 00363

June 1983
Final Report for Period June, 1980 - February, 1983

Prepared for
GODDARD SPACE FLIGHT CENTER
Greenbelt, Maryland 20771

ORIGINAL PAGE IS
OF POOR QUALITY

BIBLIOGRAPHIC DATA SHEET

1. Report No. Final Report	2. Government Accession No.	3. Recipient's Catalog No.
4. Title and Subtitle ELECTROMAGNETIC DEEP-PROBING (100-1000 KMS) OF THE EARTH'S INTERIOR FROM ARTIFICIAL SATELLITES: CONSTRAINTS ON THE REGIONAL EMPLACEMENT OF CRUSTAL RESOURCES		5. Report Date June, 1983 6. Performing Organization Code
7. Author(s) John F. Hermance		8. Performing Organization Report No.
9. Performing Organization Name and Address Department of Geological Sciences Brown University Providence, RI 02912		10. Work Unit No. 11. Contract or Grant No. NAS 5-26138
12. Sponsoring Agency Name and Address NASA, Goddard Space Flight Center Greenbelt, MD 20771 Technical Monitor: Mr. Harold Oseroff		13. Type of Report and Period Covered Final Report June 1980 - Feb. 1983 14. Sponsoring Agency Code

15. Supplementary Notes

To be published as several separate reports in the open literature.

16. Abstract

This report summarized the reconnaissance phase of using satellite observations to studying electromagnetic induction in the solid earth. Several points are made. First, satellite data apparently suffer far less from the effects of near surface lateral heterogeneities in the earth than do ground-based data. Second, zonal ionospheric currents during the recovery phase of major magnetic storms appear to be minimal, at least in the dawn and dusk sectors where MAGSAT was flown. Hence the internal contributions that satellites observe during these times is in fact due primarily to induction in the earth with little or no contribution from ionospheric currents. Third, the interpretation of satellite data in terms of primitive electromagnetic response functions, while grossly over-simplified, results in a surprisingly well-resolved radius for an equivalent super-conductor representing the conductivity region of the earth's interior (5,370 ±120 km).

17. Key Words (Selected by Author(s)) MAGSAT Geomagnetic Variations Electromagnetic Induction		18. Distribution Statement	
19. Security Classif. (of this report)	20. Security Classif. (of this page)	21. No. of Pages Nine, with four appendices	22. Price*

*For sale by the National Technical Information Service, Springfield, Virginia 22161

RESEARCH SUMMARY

Background

On October 31, 1979, NASA launched a vector magnetometer into a fixed sun-earth orbit along the dawn-dusk meridian, at an altitude varying from 350 to 550 km. Although the mission's primary objective was to obtain data having sufficient accuracy and coverage to study static magnetization in the lithosphere, it has been recognized that there are often strong contributions from time varying external current sources in the magnetosphere, and perhaps the ionosphere, during magnetically disturbed periods. Hence this experiment presents an opportunity for studying external source fields as well as for studying the effects of electromagnetic induction in the solid earth. The purpose of this report is to describe progress in employing satellite observations to characterize the internal contribution to these rapidly varying, transient field effects - the magnetic field due to time-varying electromagnetically induced currents flowing in the earth.

Theoretical Assessment of Induction Effects at Satellite Altitudes

Hermance (1982) considered from a theoretical viewpoint several questions related to satellite-induction studies. First, are, in fact, the magnetic field effects of induced currents flowing in the earth significant for near-earth satellite observations? He found that for distant sources in the magnetosphere, magnetic fields from electric currents induced in a spherical earth may contribute from 30 to 40% of the external source field amplitude. For near-earth sources beneath the satellite, e.g. in the ionosphere, the external and internal fields tend to cancel, resulting in a much smaller total horizontal field than would be associated with sources above the satellite, or for the sources alone, if the contribution from induced currents in the earth were negligible. *Second*, Hermance (1982) investigated the effects at satellite altitudes of lateral differences in the gross conductivity structure of the earth. He found, for the particular case when the current sources are in the ionosphere (i.e., *between* the satellite and the ground), that local concentrations of induced current may generate unique magnetic field signatures at satellite altitudes. Although the absolute amplitude of the field components may be an order of magnitude smaller than for the case when the source is above the satellite, the magnetic field perturbation measured by the satellite as it crosses the geologic contact is significantly larger in relative terms for ionospheric sources. On the other hand, for the case of remote magnetospheric sources (e.g. the ring current fields), he pointed out that the contribution from lateral heterogeneities are, for all practical purposes, negligible.

In short, the theoretical studies of Hermance (1982) showed that a) the effects of induced fields were significant at near-earth satellite altitudes, b) the position of the source current (i.e. whether it was in the ionosphere, between the earth and the satellite, or whether it was remote in the magnetosphere) had a profound effect on the electromagnetic response of the structure, and c) if, in fact, the source was remote (e.g. due to the magnetospheric ring current), then the effects of lateral heterogeneities are essentially negligible.

Observational Evidence for Induction Effects in MAGSAT Data

Hermance and Rossen (1982) pursued these questions from an observational viewpoint. They identified a number of issues that needed to be addressed before the efficacy of satellite induction studies could be established. One was whether satellite data offered an improvement over ground-based observations. They found that the "noise" level during magnetic storms was significantly less at satellite altitudes, particularly on the Z component. Another issue they addressed was the presence of ionospheric current systems during major magnetic storms. In comparing ground-based and satellite observations of the Z and H components during a major magnetic storm during the MAGSAT epoch, they found little evidence for zonal ionospheric current systems. Although they detected a significant offset in the horizontal field when satellite and ground-based data were compared, which they originally felt indicated a significant contribution from ionospheric currents, they later traced this offset to an artifact introduced by uncertain base-lines. Present feeling is that there is little evidence that significant zonal ionospheric currents flow in the dawn and dusk sectors during the main and recovery phase of major magnetic storms.

Hermance and Rossen (1982) proceeded to calculate "primitive" electromagnetic response functions and determined an average radius of 5,370 (± 120) km for an equivalent super-conductor, representing the conducting region in the earth's interior. In addition they found little differences between the electromagnetic response of oceanic areas and other areas of the globe. This prompted them to more closely scrutinize MAGSAT data for the effects of lateral conductivity heterogeneities in the earth.

To evaluate the effects of lateral heterogeneities, Hermance and Rossen (1982) investigated the well-known ocean-edge effect in the vicinity of Australia. They found that the effect is of such a restricted scale-size laterally, that it is damped to negligible amplitudes at the altitude of MAGSAT - this corroborates the conclusions that Hermance (1982) reached from theoretical considerations.

Conclusions

The work summarized here is best described as the reconnaissance phase of evaluating the contribution that satellite observations can make to studying electromagnetic induction in the solid earth. Although certain elements of our analysis are qualitative, several points can nevertheless be made. First, satellite data apparently suffer far less from the effects of near surface lateral heterogeneities in the earth than do ground-based data. Second, ionospheric currents during the recovery phase of major magnetic storms appear to be minimal, at least in the dawn and dusk sectors where MAGSAT was flown. Hence the internal contributions that satellites observe during these times is in fact due primarily to induction in the earth with little or no contribution from ionospheric currents. Third, the interpretation of satellite data in terms of primitive electromagnetic response functions suggests that more quantitative interpretations hold great promise for refining models of the electrical conductivity in the upper mantle. Even the grossly over-simplified interpretation presented here results in a surprisingly well-resolved radius for an equivalent superconductor representing the conductivity region of the earth's interior (5,370 ± 120 km). This is indeed encouraging for follow-on work in this area. What is required now is a refined spectral analysis of a number of different transient events, accounting for a more complicated source field than has been assumed hitherto. Having resolved the frequency dependence of the electromagnetic response parameter, one will be able to investigate the global conductivity structure of the earth's interior using more realistic models than the one used here.

Summary of Attached Documentation

Attached as Appendices to this Final Project Report are the following items:

Appendix 1: Abstracts of Oral Presentations at National and International Meetings. This is a collection of four oral presentations describing research of which a significant portion was supported by NASA funds.

Appendix 2: Model Simulations of Possible Electromagnetic Induction Effects at MAGSAT Altitudes. A reprint of a paper which appeared in Geophys. Res. Lett., 9, 373-376, 1982.

Appendix 3: Global and Regional Electromagnetic Induction Effects in MAGSAT Satellite Data. A revised version of a paper read at the 6th Workshop on Electromagnetic Induction, held in Victoria, B.C., during August of 1982.

Appendix 4: Electromagnetic Induction by Finite Wave-Number Source Fields in 2-D Lateral Heterogeneities; The Transverse Electric Mode. A preprint of a paper submitted to Geophys. J.R. astr. Soc., 1983. The development of this theoretical effort was prompted by research supported by several funding agencies.

REFERENCES

Banks, R.J., Geomagnetic variations and the electrical conductivity of the upper mantle, Geophys. J. Roy. Astron. Soc., 17, 457-487, 1969.

Chapman, S. and J. Bartels, Geomagnetism, Clarendon Press, Oxford, 1940.

Didwall, E.M., The electrical conductivity of the Earth's upper mantle as estimated from satellite measured magnetic field variations, Ph.D. thesis, Johns Hopkins University, Baltimore, MD, 1981.

Didwall, E.M. The electrical conductivity of the upper mantle as estimated from satellite magnetic field data with implications for temperature, Submitted to J. Geophys. Res., 1983.

Hermance, J.F., Electromagnetic induction and source field effects in MAGSAT data (Abstract), Programme and Abstracts, Fourth IAGA Scientific Assembly, edited by N. Fukushima, p. 538, IUGG Publ. Office, Paris, France, 1981a.

Hermance, J.F., Are there induction effects in Dst corrections to MAGSAT data? (Abstract), EOS, 62, p. 269, 1981b.

Hermance, J.F., Finite source fields coupled to lateral conductivity heterogeneities: Effects on magnetotelluric and magnetic gradiometric deep sounding experiments (Abstract), Programme and Abstracts, Fourth IAGA Scientific Assembly, edited by N. Fukushima, p. 566, IUGG Publ. Office, Paris, France, 1981c.

Hermance, J.F., Model simulations of possible electromagnetic induction effects at MAGSAT altitudes, Geophys. Res. Lett., 9, 373-376, 1982.

Hermance, J. F. and M. Rossen, Regional and global electromagnetic induction effects in MAGSAT satellite data (Abstract), Sixth Workshop on Electromagnetic Induction in the Earth and Moon, Working Group I-S, IAGA, University of Victoria, British Columbia, Canada, 1982.

Hermance, J.F., Electromagnetic induction by finite wave-number source fields in 2-D lateral heterogeneities; The transverse electric mode, Manuscript in preparation, 1983.

Langel, R.A., Internal and external storm-time magnetic fields from spacecraft data, IAGA Program Abstracts for XVI General Assembly, Genoble, France, 1975.

Langel, R.A., R.H. Estes, G.D. Mead, E.B. Fabiano, and E.R. Lancaster, Initial geomagnetic field model from MAGSAT vector data, Geophys. Res. Lett., 7, 793-796, 1980.

Langel, R., J. Berbert, T. Jennings, and R. Horner, MAGSAT data processing: A report for investigators, Technical Memorandum 82610, 178 pp., NASA, 1981.

Langel, R.A., The magnetic earth as seen from MAGSAT, initial results, Geophys. Res. Lett., 9, 239-242, 1982.

Langel, R.A., G. Ousley, J. Berbert, J. Murphy and M. Settle, The MAGSAT mission, Geophys. Res. Lett., 9, 243-245, 1982.

Langel, R.A., J.D. Phillips, and R.J. Horner, Initial scalar magnetic anomaly map from MAGSAT, Geophys. Res. Lett., 9, 269-272, 1982.

Langel, R.A., C.C. Schnetzler, J.D. Phillips, and R.J. Horner, Initial vector magnetic anomaly map from MAGSAT, Geophys. Res. Lett, 9, 273-298, 1982.

APPENDIX I

Abstracts of Oral Presentations at National and International Meetings

Abstract of paper presented at the Spring Meeting of the American Geophysical Union, 1981.

ARE THERE INDUCTION EFFECTS IN Dst CORRECTIONS TO MAGSAT DATA?

John F. Hermance (Department of Geological
Sciences, Brown University, Providence,
Rhode Island 02912)

There is a need, when deriving residual field models from MAGSAT data, to be able to apply corrections to the data for the contribution from Dst. Unfortunately induction effects in Dst preclude in general the simple correction of the observed field by subtracting the Dst-term; one needs to account for the induced phase-shifted internal component. In addition, the temporal behavior of Dst is such that a magnetic storm with a sudden commencement has higher frequency energy at early storm-time ($T < 2$ days) and lower frequency energy at late storm-time ($2 < T < 5$ days). The result is that the ratio of internal to external fields is not a simple constant, but e plitude of the ratio changes with time during magnetic disturbance. Fortunately, simple model calculations indicate that during late storm-time the internal:external field ratio is essentially constant so that there is hope that quantitative correction factors can be applied to late storm-times in a straightforward way. As one attempts such a correction during earlier storm-time, the morphology of the Dst event has to be taken into account.

Abstract of paper presented at Fourth Scientific
Assembly of IAGA, Edinburgh, 1981.

ELECTROMAGNETIC INDUCTION AND SOURCE FIELD EFFECTS IN MAGSAT DATA

J.F. Hermance (Department of Geological Sciences, Brown
University, Providence, RI 02912

It is advantageous when compiling regional magnetic charts to be able to use satellite data during periods when the magnetic field is modestly to severely disturbed. It is necessary, therefore, to develop algorithms to compensate observed field data for the effects of time varying magnetic sources of external origin, particularly accounting for possible induction effects in the earth.

To illustrate some of the complications in such a procedure, a series of theoretical models is presented to illustrate the effects of external source fields coupling to an earth having a finite conductivity. Among the cases considered are:

1) Induction effects in the Dst index such that a storm-time dependent correction factor need be applied.

2) The electromagnetic coupling of ionospheric current systems to both a homogeneous earth having finite conductivity, and to an earth having gross lateral variations in its conductivity structure, e.g. the ocean-land interface.

Abstract of paper presented at Fourth Scientific
Assembly of IAGA, Edinburgh, 1981.

FINITE SOURCE FIELDS COUPLED TO LATERAL CONDUCTIVITY HETEROGENEITIES: EFFECTS ON MAGNETOTELLURIC AND MAGNETIC GRADIOMETRIC DEEP SOUNDING EXPERIMENTS

J.F. Hermance (Department of Geological Sciences, Brown
University, Providence, Rhode Island 02912)

Studies of the dynamical evolution of source fields in the ionosphere and magnetosphere are in many cases incompatible with global scale sources. In some cases, source fields have quadrant size dimensions, in others coherent scale distances of a few hundred km, even at mid-latitudes. The possible effect of these finite source dimensions on induction experiments therefore require renewed scrutiny, particularly as deep-sounding measurements are performed at periods greater than 10^4 sec. The magnetic variation gradiometric technique appears to suffer from source effects at least as much, and perhaps greater than, the magnetotelluric technique. When finite source fields are coupled to lateral heterogeneities, the interaction becomes quite complex. We will report on our progress in generalizing the interaction between the spatial wave-length of the source field and the scale-size of lateral heterogeneities. This is used to evaluate the conditions under which various phenomena are more dominant than others.

Abstract of paper presented at the 6th Workshop on Electromagnetic Induction in the Earth and Moon, Victoria, British Columbia, 1982.

Regional and Global Electromagnetic Induction Effects in MAGSAT Satellite Data

John F. Hermance (Department of Geological Sciences, Brown University, Providence, Rhode Island 02912)
Michael Rossen (Department of Geological Sciences, Brown University, Providence, Rhode Island 02912)

Our present analysis of MAGSAT magnetic data is separated into two stages. Both stages are designed to study the extent to which we can detect and constrain the nature of electromagnetic induction effects using satellite observations.

The first stage consists of comparison of data from contiguous orbit passes over large scale geologic boundaries, such as ocean-land interfaces, at several levels of magnetic disturbance. The purpose of these comparisons is to separate induction effects from effects of lithospheric magnetization. The procedure for reducing the data in order to make such comparisons is the following: 1) identifying and subtracting quiet time effects; 2) modelling and subtracting first order ring current effects; 3) projecting an orbit track onto a map as a nearly straight line so it can serve as an axis on which to plot the corresponding orbit pass data in the context of geography.

The second stage of our analysis consists of comparison of MAGSAT data with standard observatory hourly data. The purpose is to constrain the time evolution of ionospheric and magnetospheric current systems. Qualitative features of our ground based dataset are discussed. The methods for reducing the ground based data consists of: 1) a baseline is removed from the data; 2) a spherical harmonic analysis is performed on the data; 3) the spherical harmonic coefficients are used to reconstruct, using a suitable method of interpolation, an equivalent "ground pass" dataset corresponding to each orbit pass dataset under study; 4) a separation of the reconstructed "ground pass" data into internal and external components is made; the data are then projected up to MAGSAT altitude with the assumption that there are no intervening current systems.

Comparisons between ground passes and orbit passes are used to differentiate between the presence of ionospheric and magnetospheric current systems. Special attention is payed to analysis of long period effects, such as the storm recovery phase, with which the inclusion of hourly values in our dataset is most effective.

APPENDIX 2

GEOPHYSICAL RESEARCH LETTERS, VOL. 9, NO. 4, PAGES 373-376, APRIL 1982

A82-30809

MODEL SIMULATIONS OF POSSIBLE ELECTROMAGNETIC INDUCTION EFFECTS AT MAGSAT ACTIVITIES

John F. Hermance

Department of Geological Sciences, Geophysical/Electromagnetics Laboratory
Brown University, Providence, RI 02912

APPENDIX 3

GLOBAL AND REGIONAL ELECTROMAGNETIC INDUCTION EFFECTS IN MAGSAT SATELLITE DATA

John F. Hermance
Michael Rossen

Geophysical/Electromagnetics Laboratory
Department of Geological Sciences
Brown University
Providence, Rhode Island 02912

Revised version of a paper read at the
Sixth Workshop on Electromagnetic Induction
Victoria, British Columbia

August, 1982

INTRODUCTION

On October 31, 1979, NASA launched a vector magnetometer into a fixed sun-earth orbit along the dawn-dusk meridian, at altitudes varying between 350 km and 550 km. The resolution of the data is to within ±1 nT. The mission's primary objective was to obtain data having sufficient accuracy and coverage to produce a detailed map of static magnetization in the lithosphere (Langel et al., 1982).

It has been recognized that time varying contributions from external current sources are present in the data. This presents an opportunity for earth induction studies using vector magnetic variation data - Langel (1975), Didwall (1981, 1983), and others have attempted such analyses previously using total field scalar data from earlier satellites.

A number of issues need to be addressed before the efficacy of satellite induction studies can be established. First, do satellite measurements result in a data base which has a significantly lower noise component than ground-based measurements? Second, we must determine whether ionospheric currents are present at nominal altitudes of 110 km during magnetically disturbed periods. If present and unconstrained, such currents, since they flow beneath the satellite's orbit, would tend to bias satellite measurements of terrestrial fields.

Finally, we must ask whether the effects of electromagnetic induction in lateral heterogeneities in the earth are significant at satellite altitudes. In this report, we describe our progress in resolving these issues.

MAGNETIC STORM-TIME VARIATIONS

Reduction of Ground-Based Data

For the purposes of our present analysis we want to compare as directly as possible ground-based data from standard magnetic observatories to satellite data. Ground data is readily available from the greatest number of observatories in the form of hourly averages. Although these represent time series which are somewhat courser than desirable, they seem to be satisfactory for the type of analysis presented here. Our ground data set, therefore, consists of standard observatory hourly means for 32 sites between 55° and -55° geomagnetic latitude, as shown in Fig. 1.

The data being examined are from the period between 0:00 February 12 UT and 0:00 February 22, 1980. This epoch includes one of the most well defined geomagnetic storms to occur during the MAGSAT mission, with sudden commencement occurring at 3:09, February 14 UT (preliminary indentification; Langel *et al.*, 1981). In Figure 2 we see the H, D, and Z data from the Tucson standard magnetic observatory in the southwest United States. The H-component in particular shows a well-developed main phase on February 16-17, followed by a slow recovery phase to normal base-line values after a period of 5-6 days. Superimposed on the storm-time magnetic disturbance one can readily discern the periodic diurnal variation (Sq), which is of course strongest during local daylight hours.

Our method of reducing the ground based data is as follows:

1) All data are cast in terms of geomagnetic coordinates and geomagnetic field components (H, D, Z).
2) A baseline, calculated as an average of two hours about the quiet time local midnight immediately before the onset of the magnetic disturbance (see for example Figure 2), is removed from each component at each observatory.
3) The vector components at each observatory are geometrically corrected for the various latitudes at which they were recorded. For the lowest order surface harmonic, we assume $H = H \cos \theta_{lat}$ and $Z = Z \sin \theta_{lat}$. The coefficients H and Z are determined by dividing all H-fields by the cosine of the latitude and all Z-fields by the sine of the latitude.
4) Time series are then generated for each component as a function of storm-time for local time sectors: dusk, midnight, and dawn. This is done by calculating, for the latitudinally compensated data from each observatory, two-hour means centered at local times of 1800 hr (dusk), 0000 hr (midnight) and 0600 hr (dawn). Each observatory therefore contributes one sample in each of the three local time sectors for each day of storm-time.
5) The time series for the dusk and dawn sectors are then

directly compared with the reduced satellite data described below.

The ground-based time series for the H-component recorded during the dusk, midnight and dawn sectors, respectively, are shown in Figure 3. The midnight samples are clearly the best behaved, but all three samples display well-developed classical main and recovery phases. MAGSAT data are limited by the nature of the orbit to dawn and dusk sectors, so we are constrained to using ground-based data at only these two local times. Of these two times, dawn samples seem to display a more consistent pattern during pre-storm times as well as during the recovery phase. The well-known dawn-dusk asymmetry in main phase amplitudes is clear in Figure 3.

Both the Z-amplitudes and the H-amplitudes for ground-based data during the dawn sector are shown in Figure 4. During pre-storm time the baseline for the vertical field is well-described, however during the recovery phase a greater scatter of points is apparent - we ascribe this to the effects of lateral heterogeneities within the earth which tend to affect the vertical field more strongly than the horizontal field.

Reduction of MAGSAT Data

Five second averaged data, with the standard reference field model removed, were taken from Investigator-B tapes to form our initial dataset. Spikes were automatically culled from the data. A rotation into the geocentric magnetic dipole reference frame was then applied to both the coordinates of the satellite position and to the components of the vector magnetic field. Following convention, H, D and Z refer to the magnetic North, magnetic East and vertical down field components respectively. These basic data were then reduced in the following way:

1) H data were fit to a cosine function of magnetic latitude and Z data were fit to a sine function of magnetic latitude. The ascending (dusk) and descending (dawn) part of each orbit pass between -45 deg and 45 deg magnetic latitude were fit separately to allow observation of the dawn-dusk asymmetry.
2) The amplitudes of these cosine and sine fits of succeeding passes were gathered together as new, smoothed datasets, directly comparable to the ground based field coefficients described above. The equator-crossing times of the passes were used to form a time base for the datasets. This provided a sampling interval of about 46.5 min, or one half the orbit period. Two datasets were thus created - a dawn dataset for H and Z and a dusk dataset for H and Z. The geographic location of the actual passes used for this analysis are shown in Figure 5.

At this stage a direct comparison of the reduced satellite and ground-based data sets (Figure 6 and 7) shows that while the general form of the appropriate components is quite similar, a persistent offset between the two datasets seems to be present. Using hourly Dst values from Langel _et al_. (1981), a mean Dst value was computed for these two time intervals to determine whether an offset due to residual Dst field effects should be expected. The arithmetic mean of Dst indices for the pre-storm period (0:00 February 12 UT to 0:00 February 14 UT) was 0.9 gammas. The mean for the two and a half days at the end of the recovery phase (12:00 February 19 UT to 0:00 February 22 UT) was -10.8 gammas.

We conclude, therefore, that the Dst index, particularly at the beginning of the storm is close to zero. Langel and Estes (1983), however, have found in an independent analysis that significant external field is present even when Dst is zero. Employing a potential field separation of the MAGSAT satellite data and performing a regression of the external potential term q_1^0 on the Dst index, they find a correlation of the form:

$$q_1^0 = 19.0 - 0.65 \text{ Dst (nT)}.$$

It does not seem unreasonable, therefore, that offsets of 10-20 nT may be present in both the ground-based and satellite data, due to long term quasi-state external field contributions. Not wishing to address the issue of establishing absolute baselines to either the ground data or the satellite data at this time, we can nevertheless calculate <u>relative</u> offsets between the two data sets in the following way.

Feeling that the satellite data is least "noisy" - except for the constant offset - a smooth curve (a cubic spline) was fit in a least mean square sense to the first two days of the pre-storm satellite data (the same times indicated above). A similar curve was fit to the last two and a half days of the recovery phase. The residual could then be calculated between actual ground-based data observed at arbitrary times during these two periods and satellite observations interpolated from the smooth cubic spline functions.

The residuals for each component were sorted into bins corresponding to the prestorm period, the late recovery phase period, and the combination of both periods. In addition, the data were sorted into dawn passes and dusk passes. Histograms of the residuals are reproduced in Figures 8-11.

The average residuals from this analysis are summarized in Table 1. Their magnitudes and signs generally agree with the analysis by Langel and Estes mentioned above. The next and final step in reducing the satellite data therefore was the following.

3) The offsets indicated in Table 1 were subtracted from the corresponding satellite components. An example of one of the resulting data sets for Z and H is presented in Figure 12.

This represents the final reduced satellite data. Note that the data from both components show significantly lower scatter than the corresponding ground-based data in Figure 4. This comparison graphically depicts the potential advantages in using satellites to study magnetic storm phenomena - particularly earth induction effects. We feel that a substantial contribution to the noise in the ground-based data of Figure 4 is due to effects of lateral conductivity heterogeneities within the earth. The field components at some observatories may suffer from contamination due to edge-effects encountered near discontinuities in the electrical structure; in other cases, the fields may be perturbed by different conductivity structures beneath the observatories.

The satellite data and ground-based data for the dawn and the dusk sectors, respectively, are actually overlaid in Figures 13 and 14. These figures again illustrate the lower scatter in the reduced satellite components. However, in spite of the somewhat higher noise level in the ground data, there are specific time intervals and events for which the tracking of the two datasets is quite remarkable. In spite of the simplicity of our approach, the results are encouraging.

On the Possibility of Ionospheric Currents

We now address the issue as to whether appreciable ionospheric currents flow at low and mid-latitudes during disturbed periods. Ionospheric currents flow at a nominal altitude of 110 km and during magnetically quiet times, these currents are usually limited to the daylight hours. Indeed, MAGSAT's orbit was located in the dawn-dusk sector in order to minimize the contribution of ionospheric currents to magnetic field observations. However, several workers have detected the effects on low latitude ($\pm 20^{\circ}$) MAGSAT data from what they believe to be quiet-time ionospheric currents (e.g. Maeda et al., 1982). The effects have been largely on the D component in the dusk sector and the source has been inferred to be a meridional current system restricted to a latitude range of $\pm 20^{\circ}$, and contributing a maximum D field variation of ±20 nanoteslas.

The question we address here is whether appreciable ionospheric currents develop during magnetically disturbed periods, i.e. during major magnetic storms. The answer is essential to whether one can readily use satellite data to study electromagnetic induction in the solid earth. The satellite trajectory is well above any ionospheric current system. Any attempt to downward continue satellite field data through the ionosphere will be biased by the effects of the current sheet source. If the current system is known and constrained, one may be able to compensate for this bias. However, if the current system is unknown, then satellite induction studies may not be feasible because of the presence of this unknown bias.

The presence of ionospheric currents can in principle be detected by comparing ground-based and satellite measurements (a quantitative basis for this approach is presented in Hermance, 1982 and Hermance, 1983). A simple geometric model which illustrates our approach is presented in Figure 15. A time-varying sheet current source in the ionosphere induces oppositely directed image currents in the earth. At the surface of the earth a simple application of the right-hand rule indicates that the horizontal field from each current system (the source and the induced currents) will combine constructively, which results in a total horizontal field which is generally from 1.4 to 2.0 times the horizontal source field alone.

However at satellite altitudes a similar application of the right hand rule will show that the two horizontal field contributions combine destructively and tend to cancel. In this case the total horizontal field at satellite altitudes is as little as 5% to 20% of the horizontal source field alone.

Hence, comparing ground and satellite observations of the horizontal field is a sensitive means to detect ionospheric current systems. Returning to our inspection on Figures 13 and 14 we see little evidence for the presence of systematic offsets in either Z or H for any length of time between our satellite and ground-based data. In particular we feel that these data suggest that during the recovery phase of the storm (and perhaps during the main phase as well) there is little evidence for significant ionospheric current flow on the disturbed Z and H components (our analysis of D is currently in progress). This implies that large-scale zonal ionospheric current systems are minimal during these times. Our pending analysis of the D component will allow us to evaluate, in a future paper, the effects of meridional current systems during major magnetic disturbances. At present, however, we feel that our analysis to-date is encouraging regarding the use of satellite data to study electromagnetic induction in the solid earth, particularly those studies which rely primarily on observations of the Z and H disturbed components.

STORM-TIME ELECTROMAGNETIC INDUCTION EFFECTS

Primitive Electromagnetic Response Functions

Data from magnetic storms during the MAGSAT mission having the quality shown in Figures 13 and 14 are limited. Although a number of magnetically disturbed periods were experienced, few major magnetic storms occurred. Hence at this point we feel that a refined analysis of the data to determine an electromagnetic response function is not warranted. On the other hand, an analysis directed at extracting some of the first order features of the effects of induction may be quite appropriate. To do this we calculate what we term to be a "primitive" response function. Essentially this is a gross, wide-band induction parameter determined from the recovery phase of the magnetic storm, where short term temporal fluctuations are minimal and where the source field can most likely be represented by a first order surface harmonic.

To assess global induction effects we assume that, to the first-order, the earth is spherically symmetric and is illuminated by the magnetic field of an equivalent ring current system. Therefore, the source field, $\underline{B}_o$, is assumed to be uniform and polarized perpendicular to the ecliptic plane over the earth's diameter. We adopt the usual spherical coordinate conventions such that in a geocentric coordinate system is the geomagnetic colatitude and r is the radial distance. The effects of asymmetries in the ring-current and gradients in the source field are assumed to have second order effects on the results of our discussion.

It is well-known that under these assumptions (e.g. Chapman and Bartels, 1940) the magnetic field relations can be derived from the gradient of a scalar potential ($B = -\nabla U$), where

$$U(r,\theta) = r_o\{I_1(r_o/r)^2 + E_1(r/r_o)\} \cos\theta \quad ,$$

I_1 and E_1 are the so-called internal and external potential field coefficients, respectively; r_o is the radius of the earth, r is the radial position of the observer and θ is the colatitude.

For the purpose of our present discussion we will approximate a region of high conductivity in the earth's interior as a super-conductor ($\sigma = \infty$) having a radius a. The magnetic field component normal to the surface of our super-conductor, $B_r = -\partial U/\partial r$, is zero at $r = a$.

This condition leads to

$$I_1 = 1/2\ \left(\frac{a}{r_o}\right)^3 E_1 \quad ,$$

where $E_1 = -B_o$. Differentiating the above expression for the scalar potential with respect to r and θ, respectively, we obtain the conventional geomagnetic vector components

$$\hat{Z} = -\left[1 - \left(\frac{a}{r}\right)^3\right] B_o \cos\theta \quad ,$$

$$\hat{H} = \left[1 + 0.5\left(\frac{a}{r}\right)^3\right] B_o \sin\theta \quad .$$

These expressions can be written in terms of latitude invariant amplitude coefficients, analogous to those used in our previous discussion, above, such that

$$\hat{Z} = Z \cos\theta \quad ,$$

$$\hat{H} = H \sin\theta \quad .$$

The Z and H terms correspond to the amplitude coefficients, introduced earlier. Upon taking the ratio of Z to H we obtain the electromagnetic response parameter

$$Z/H = - \frac{[1 - (a/r)^3]}{[1 + 0.5(a/r)^3]} \quad ,$$

which a number of workers have employed in ground-based magnetic studies (e.g. Banks, 1969).

Returning now to inspecting Figures 13 and 14, we see that the Z and H components both show the well-known exponential decrease in amplitude over a number of days during the recovery phase of the storm. In addition there are some shorter term fluctuations during which Z and H track quite well, with little phase shift. The close visual correlation between the Z and H time series prompts us to plot Z and H as a correlogram, or scatter diagram. A linear trend for the entire storm was subtracted from each data set, using a linear least squares fit to the first 12 hours and the last 12 hours of the satellite data shown in Figures 13 and 14. A correlogram of the detrended simultaneous $Z(t_i)$ and $H(t_i)$, sampled at various times, t_i, for the recovery phase of the storm is shown in Figure 16. A linear relation between Z and H is evident, which is to be expected. The slope of the best-fitting straight line through these points, <Z/H>, is precisely the primitive electromagnetic response parameter which we will employ in our subsequent analysis. We also note little systematic difference between dawn and dusk passes.

These data are further segregated in Figure 17, where dawn and dusk passes are subdivided into passes primarily over the ocean (i.e. less than 10% of its path in a particular sector between $\pm 45^{o}$ geomagnetic latitude was over a continental land mass, see Figure 18) and all other passes. Again at this level of our analysis, there appears to be little systematic difference between our data subsets.

A Simple Statistical Approach

By performing a mean least squares linear regression of $Z(t_i)$ on $H(t_i)$, where t_i represents the set of observation times, we can determine the ratio <Z/H> and estimate certain statistics, such as the correlation coefficient. The parameter <Z/H>, our primitive response function, will be used to infer some of the gross effects from electromagnetic induction in the earth.

The assumptions that our source field can be represented by a first order surface harmonic and that aliasing effects due to short term fluctuations between satellite passes are negligible, seem to be most reasonable during the later portion of the recovery phase of the magnetic storm we are using. Hence we will begin our regression at the last point of the storm and systematically increase the number of samples by running backward in time, all the while evaluating the statistical parameters associated with our estimate of <Z/H>.

The late phase of the storm in which we compare samples reversed in time suggests a distinct correlation of two magnetic channels $H(t_i)$ and $Z(t_i)$ which we denote, respectively, by the usual convention x_t and y_t. We assume that data points in this phase are correlated with coefficient , and have a bivariate normal distribution whose probability density function, for all physically possible storms, is given by:

$$p(x,y) = \frac{1}{2\pi\sigma_x\sigma_y\sqrt{1-\rho^2}} \exp\{-[(x/\sigma_x)^2-(2\rho xy/\sigma_x\sigma_y) + (y/\sigma_y)^2]/[2(1-\rho^2)]\} ,$$

where σ_x and σ_y are the standard deviations of x and y observations, the mean assumed to be 0. The correlation estimate

$$\bar{\rho} = \frac{\left(\sum_{t=t_1}^{t=t_n} x_t y_t\right)^2}{\Sigma x_t^2 \Sigma y_t^2}$$

is a statistic whose Fisher z-transform

$$z = \frac{\sqrt{n}}{2} \ln \left[\frac{(1+\bar{\rho})}{(1-\bar{\rho})} \cdot \frac{(1-\rho)}{(1+\rho)}\right]$$

is a statistic with a standard normal distribution of mean = $\frac{\sqrt{n}}{2} \ln \left(\frac{1+\rho}{1-\rho}\right)$ and variance = 1.

In time, the statistic z tends to increase to a maximum as more points are included in averaging the various estimates toward the beginning of the storm. Qualitatively, this implies that the significance of the correlation increases up to this point. That is, the probability that the observed points could be produced by a weakly correlated or uncorrelated signal pair is decreasing to this point.

However, as data from earlier phases of the storm are included in the averages, a decrease in correlation occurs, leading us to conclude that the decline in the z-statistic may be implying the modification of our basic model - perhaps the configuration of the source field is more complicated and our simple model is no longer applicable. Therefore we could reject any points after this local maximum, even though the correlation begins to eventually rise again as different phenomena become dominant.

Given the hypothesis that $\rho = \bar{\rho}$ observed at the cutoff, we may generate confidence intervals for $\bar{\rho}$ which will in turn give a (crude) error bar for the slope of the correlation, by considering the values of the slope corresponding to cutoff points within the confidence interval for $\bar{\rho}$.

The results of this simple analysis are presented in Table 2 for various sets of satellite passes. Our primitive induction parameter, <Z/H>, is the slope of the best-fitting line through the points shown in the scatter diagrams of Figures 16 and 17. The data analysed spans the period from 6 hours after the main phase maximum throughout the recovery phase of the storm. For comparison in Table 2 we indicate the actual values of the magnetic field amplitudes at this time (approximately 6 hours after the main phase maximum), the ratio of the mean amplitudes, Z/H, the primitive induction parameter <Z/H> with the estimated range of uncertainty, and the respective correlation coefficients.

The Importance of Source Field Effects as Opposed to Lateral Conductivity Variations

In studying Table 2, one obtains the impression that the difference between dawn and dusk estimates of <Z/H> (.37 ± .02 versus .42 ± .02) seem to be significantly larger than the variation between passes over open ocean and passes over other regions. At this point therefore we are led to conclude that source field effects, e.g. the well-known dawn-dusk asymmetry in magnetic field amplitudes and perhaps other source field configurations, is a major contributor to the uncertainty in obtaining valid estimates of <Z/H>.

A Globally Averaged Conductivity Model

Clearly, the uncertainty in our induction parameter does not warrant a refined interpretation, but it may be appropriate to make some general observations. For example, what does a value of approximately 0.40 (.37 to .42) for <Z/H> imply about the actual conductivity structure of the earth?

Upon rearranging our theoretical relation between Z/H and (a/r) given above, we obtain

$$a/r = \left[\frac{1 + (Z/H)}{1 - 0.5(Z/H)}\right]^{1/3} \quad .$$

We may now substitute our estimate <Z/H> for the Z/H term in this expression and solve for a/r. Note that the value of a/r is relatively insensitive to uncertainties in <Z/H>, because of the cube root. In other words, the radius of an equivalent superconductor is a robust parameter to estimate from our data base.

The result of such calculations are summarized in Table 3 for dawn and dusk passes, and for the averge of both. The appropriate r, of course, is the radial position of the satellite at a nominal altitude of 400 km, so that r = 6770 km.

Surprisingly, in view of the grossly simplifying assumptions we have made, the radius of an equivalent superconductor seems to be well estimated at a value of 5,370 (± 120) km, corresponding to a depth below the earth's surface of 990 (± 120) km.

A SEARCH FOR OCEAN EDGE-EFFECTS ON SATELLITE INDUCTION STUDIES

The Ocean Coast Effect

One of the more profound examples of lateral heterogeneities is the difference in conductivity between oceans and continents. This sharp boundary leads to intense concentrations of electric currents, induced by transient magnetic field variations. The resulting secondary magnetic fields give rise to what is classically known as the "coast" or "ocean" effect by ground-based electromagnetic workers. We've chosen the southern shore of Australia as a region in which to observe this phenomenon and the storm-time enhanced westward directed ring current as our external inducing source. Thus we have a combination of a low order inducing field, a region where unhindered east-west global current circulation is possible, and a large scale perturbing structure of relatively simple geometry contained wholly within this region of electromagnetically induced current flow. It is an ideal setting in which to observe the coast effect.

Figure 19 is an example of MAGSAT total field magnitude data from two contiguous passes over central Australia (passes are considered contiguous if they are within two degrees longitude of one another). In the bottom portion of the figure, one of the satellite tracks is plotted against a backdrop of a rotated Mercator map projection of the world. It serves t[illegible] convenient reference.

An order 14 standard reference field has been subtracted from the data. In addition, we've removed spikes which are apparently due to satellite orientation. The data at the bottom were taken during a magnetic quiet period selected on the basis of Kp and Dst indices. On the top we have data obtained during the main phase of a major storm during the MAGSAT epoch, beginning on February 14, 1980. The highly disturbed character of the top trace compared to the quiet time data is quite evident. In particular, we notice that in mid and lower latitudes, the field has a smooth well-behaved low order shape that one would expect from a ring current source. We also note that a well-defined dawn-dusk asymmetry is in evidence during this period of storm time.

Upon closely inspecting the quiet time pass, we can see small scale perturbations throughout the record They range from 5 nT to 20 nT in magnitude. In many cases, they are due to static magnetization of the lithosphere. We feel the resolution of the MAGSAT data is consistently of sufficient quality to show <u>induction</u> effects of these magnitudes. Hence the <u>lithospheric</u> anomalies must be removed. They are separable from among the perturbations by means of two criteria:

1) They must be repeatable from pass to pass over the same region.
2) Being insensitive to external time varying fields, their magnitudes must be invariant between contiguous quiet and disturbed passes.

We turn now to the vertical field (Z) data, the Z component being particularly sensitive to the ocean edge-effect. In Fig. 20, we have plotted this component from five contiguous quiet time passes over Australia. The scale is enlarged about six fold beyond the scale in the previous figure. We note remarkable repeatability of the data in the mid latitudes, and to some extent even in the auroral regions. Correlation of small scale features of magnitudes as low as 5 nT, such as over Australia and over Brazil, is evident.

In Figure 21, we compare a quiet time pass (bottom-trace), a disturbance time pass from February 16 (middle-trace), and the difference between the two (disturbed minus quiet; top trace). The top trace, therefore, shows the residual of the storm time Z data after removal of lithospheric effects via subtraction of the quiet time pass.

At low and mid latitudes the field is dominated by enhanced ring current effects, as is clear from the smooth low order trend of the Z component.

We see no indication of fluctuation in the data when the satellite crosses the south shore of Australia that would characterize the presence of an ocean edge-effect. This pass was one of the most disturbed during the entire MAGSAT mission.

It is well established, of course, that an ocean effect does indeed exist near the coast of Australia. What our analysis presents therefore is a constraint on the scale size of this phenomenon. That is to say, induced currents flowing in the ocean adjacent to Australia have a characteristic spatial wavelength that is small enough so that the effect is attenuated below the noise level at satellite altitudes. We may obtain an estimate for the maximum wavelength of the ocean effect at the surface in the following way.

First we note that the coast effect as observed at ground level along the south coast of Australia results in an enhancement of the Z component adjacent to the coast of at least a factor of 2 relative to observations 300 km or more inland (Parkinson and Jones, 1979). As we noted above, such an anomalous perturbation near the coastline in Australia is not apparent in the MAGSAT data in Figure 21. In fact, if a perturbation were present, it must have an amplitude less than 10-20% of "normal" Z. We are seeing, therefore, a geometrical attenuation of the coast effect at MAGSAT altitudes by at least a factor of 10 to 20. If λ_s is typically the longest spatial wavelength of the lateral dimensions of the coast effect, then one might expect an attenuation at a height, h, which behaves as $\exp(-2\pi h/\lambda_s)$. At a nominal satellite altitude of 400 km, this expression decreases by a factor of 10 to 20 for spatial wavelengths shorter than 1,100 km and 840 km, respectively. Typical scale dimensions of the coast effect observed at the ground in land areas apparently are well below these values (generally less than 300 km). Therefore, one can conclude with reasonable confidence, based on both the analytical expression indicated above, as well as by inspection of actual MAGSAT data (e.g. Figure 21), that one of the most profound electrical "edge-effects" which influence ground-based magnetic induction studies has a minimal contribution to magnetic field components at MAGSAT altitudes.

CONCLUSIONS

The work summarized here is best described as the reconnaissance phase of evaluating the contribution that satellite observations can make to studying electromagnetic induction in the solid earth. Although certain elements of our analysis are qualitative, several points can nevertheless be made. First, satellite data apparently suffers far less from the effects of near surface lateral heterogeneities in the earth than do ground-based data. Second, zonal ionospheric currents during the recovery phase of major magnetic storms appear to be minimal, at least in the dawn and dusk sectors where MAGSAT was flown. Hence the internal contributions that satellites observe during these times is in fact due primarily to induction in the earth with little or no contribution from ionospheric currents. Third, the interpretation of satellite data in terms of primitive electromagnetic response functions suggests that more quantitative interpretations hold great promise for refining models of the electrical conductivity in the upper mantle. Even the grossly over-simplified interpretation presented here results in a surprisingly well-resolved radius for an equivalent superconductor representing the conductivity region of the earth's interior (5,380 ± 120 km). This is indeed encouraging for follow-on work in this area. What is required now is a refined spectral analysis of a number of different transient events, accounting for a more complicated source field than has been assumed hitherto. Having resolved the frequency dependence of the electromagnetic response parameter, one will be able to investigate the global conductivity structure of the earth's interior using more realistic models than the one used here.

Table 1. Calculated offsets between ground-based and satellite data.

Residual = Smoothed satellite data - ground-based data

Component	Residual	
	Dawn Sector	Dusk Sector
H	-24.3(±6.0)*	-19.8(±10.6)*
Z	24.1(±9.6)*	16.9(±10.4)*

* ±1 standard deviation

Table 2. Estimates of the primitive induction parameter $\langle Z/H \rangle$ for various types of satellite passes.

	No. of samples	H_{max}	Z_{max}	$\overline{Z}/\overline{H}$	$\langle Z/H \rangle$	Correlation coefficient
Dawn						
All passes	69	-45.	16.	-.36	-.37(±.02)	.89
Ocean passes	19	-30.	10.	-.36	-.37(±.02)	.89
All but ocean passes	50	-45.	16.	-.36	-.37(±.02)	.89
Dusk						
All passes	79	-84.	30.	-.44	-.42(±.02)	.93
Ocean passes	23	-80.	32.	-.47	-.46(±.02)	.97
All but ocean passes	56	-84.	30.	-.43	-.40(±.02)	.91

ORIGINAL PAGE IS
OF POOR QUALITY

Table 3. Range of simple conductivity models for the earth based on primitive response function from satellite data.

	Response Parameter, <Z/H>	Radius of Equivalent Super-Conductor
Dawn	-.37 (±.02)	5,480 (±75) km
Dusk	-.42 (±.02)	5,300 (±80) km
"Average"	-.40 (±.03)	5,370 (±120) km

REFERENCES

Banks, R.J., Geomagnetic variations and the electrical conductivity of the upper mantle, Geophys. J. Roy. Astron. Soc., 17, 457-487, 1969.

Chapman, S. and J. Bartels, Geomagnetism, Clarendon Press, Oxford, 1940.

Didwall, E.M., The electrical conductivity of the Earth's upper mantle as estimated from satellite measured magnetic field variations, Ph.D. thesis, Johns Hopkins University, Baltimore, MD, 1981.

Didwall, E.M. The electrical conductivity of the upper mantle as estimated from satellite magnetic field data with implications for temperature, Submitted to J. Geophys. Res., 1983.

Hermance, J.F., Electromagnetic induction and source field effects in MAGSAT data (Abstract), Programme and Abstracts, Fourth IAGA Scientific Assembly, edited by N. Fukushima, p. 538, IUGG Publ. Office, Paris, France, 1981a.

Hermance, J.F., Are there induction effects in Dst corrections to MAGSAT data? (Abstract), EOS, 62, p. 269, 1981b.

Hermance, J.F., Finite source fields coupled to lateral conductivity heterogeneities: Effects on magnetotelluric and magnetic gradiometric deep sounding experiments (Abstract), Programme and Abstracts, Fourth IAGA Scientific Assembly, edited by N. Fukushima, p. 566, IUGG Publ. Office, Paris, France, 1981c.

Hermance, J.F., Model simulations of possible electromagnetic induction effects at MAGSAT altitudes, Geophys. Res. Lett., 9, 373-376, 1982.

Hermance, J. F. and M. Rossen, Regional and global electromagnetic induction effects in MAGSAT satellite data (Abstract), Sixth Workshop on Electromagnetic Induction in the Earth and Moon, Working Group I-S, IAGA, University of Victoria, British Columbia, Canada, 1982.

Hermance, J.F., Electromagnetic induction by finite wave-number source fields in 2-D lateral heterogeneities; The transverse electric mode, Submitted to Geophys. J.R. astr. Soc., 1983.

Langel, R.A., Internal and external storm-time magnetic fields from spacecraft data, IAGA Program Abstracts for XVI General Assembly, Genoble, France, 1975.

Langel, R.A. and R.H. Estes, Large-scale, near-earth, magnetic fields from external sources and the corresponding induced internal field, NASA Technical Memorandum 85012, Goddard Space

Flight Center, April, 1983.

Langel, R.A., R.H. Estes, G.D. Mead, E.B. Fabiano, and E.R. Lancaster, Initial geomagnetic field model from MAGSAT vector data, Geophys. Res. Lett., 7, 793-796, 1980.

Langel, R., J. Berbert, T. Jennings, and R. Horner, MAGSAT data processing: A report for investigators, Technical Memorandum 82610, 178 pp., NASA, 1981.

Langel, R.A., The magnetic earth as seen from MAGSAT, initial results, Geophys. Res. Lett., 9, 239-242, 1982.

Langel, R.A., G. Ousley, J. Berbert, J. Murphy and M. Settle, The MAGSAT mission, Geophys. Res. Lett., 9, 243-245, 1982.

Langel, R.A., J.D. Phillips, and R.J. Horner, Initial scalar magnetic anomaly map from MAGSAT, Geophys. Res. Lett., 9, 269-272, 1982.

Langel, R.A., C.C. Schnetzler, J.D. Phillips, and R.J. Horner, Initial vector magnetic anomaly map from MAGSAT, Geophys. Res. Lett, 9, 273-298, 1982.

Maeda, H., T. Iyemori, T. Araki and T. Kamei, New evidence of a meridional current system in the equatorial ionosphere, Geophys. Res. Lett., 9, 337-340, 1982.

Parkinson, W.D. and F.W. Jones, The geomagnetic coast effect, Rev. Geophys. and Space Phys., 17, 1999-2015, 1979.

FIGURE CAPTIONS

Figure 1. Locations of standard magnetic observatories used in this study.

Figure 2. Ground-based vector component magnetic data from the Tucson standard observatory. Hourly averages were low pass (Hann) filtered such that full amplitudes are present at a 12 hour period, the amplitudes are reduced to one-half at a 6 hour period and to zero at a 3 hour period. The arrow labeled "MDNT" denotes the local midnight values which were used to establish the zero baseline.

Figure 3. Reduced global ground-based data for the H-component during the dusk, midnight, and dawn sector. The time extends from 00:00 hrs. Feb 12 to 00:00 hrs. Feb 23, 1980.

Figure 4. Reduced ground-based data for the Z and H components during the dawn sector, 00:00 hrs. Feb 12 to 00:00 hrs Feb 23, 1980.

Figure 5. Geographic location of satellite passes used in this study. Geomagnetic latitudes of $\pm 45^{\circ}$ are shown for comparison. Data gaps are shown as interruptions in each satellite track.

Figure 6. H-field amplitude coefficients for satellite data (solid pts.) compared with ground-based data (open circles). Note the similarity in form, but the presence of a small, persistent offset.

Figure 7. Z-field amplitude coefficients for satellite data (solid pts.) compared with ground-based data (open circles).

Figure 8. Histograms of offset residuals during the dusk sector for the H component satellite data minus the ground data. Top: two days at the beginning; Middle: two and a half days at the end; Bottom: the total of both beginning and end.

Figure 9. Histograms of offset residuals during the dawn sector for the H component. See caption for Figure 8.

Figure 10. Histograms of offset residuals during the dusk sector for the Z component. See caption for Figure 8.

Figure 11. Histograms of offset residuals during the dawn sector for the Z component. See caption for Figure 8.

Figure 12. Z-component amplitude coefficients (top) and H-component amplitude coefficients (bottom) for the satellite data during the dawn sector with constant offset removed.

Figure 13. Comparison of fully reduced satellite data (solid

points) with ground-based data (open circles) for the dawn sector.

Figure 14. Comparison of fully reduced satellite data (solid points) with ground-based data (open circles) for the dusk sector.

Figure 15. The geometry of external ionospheric source currents and internal induced currents.

Figure 16. Correlogram of simultaneous Z and H amplitudes for all satellite passes during the recovery phase of the storm from approximately 6 hours after the main phase maximum to 00:00 hr. Feb 23, 1980. Results for the dusk sector are shown as solid points, those for the dawn sector are open circles.

Figure 17. Segregation of Z and H amplitudes into correlograms for passes over open ocean (OCN) and all other pases (ALL). These are shown for the dusk and dawn sectors, to see if a source effect is evident.

Figure 18. Those satellite tracks classified as ocean passes between geomagnetic latitudes of $\pm 45^{o}$.

Figure 19. MAGSAT total field magnitude data from two contiguous passes (within 2^{o} of each other) for the satellite track shown.

Figure 20. MAGSAT vertical field (Z) data from five contiguous quiet time passes. Scale is enlarged about 6 fold relative to Figure 19.

Figure 21. Comparison of MAGSAT vertical field (Z) data for a quiet time pass (bottom-trace), a disturbance time pass (middle-trace) and the difference between the two (disturbed minus quiet; top-trace).

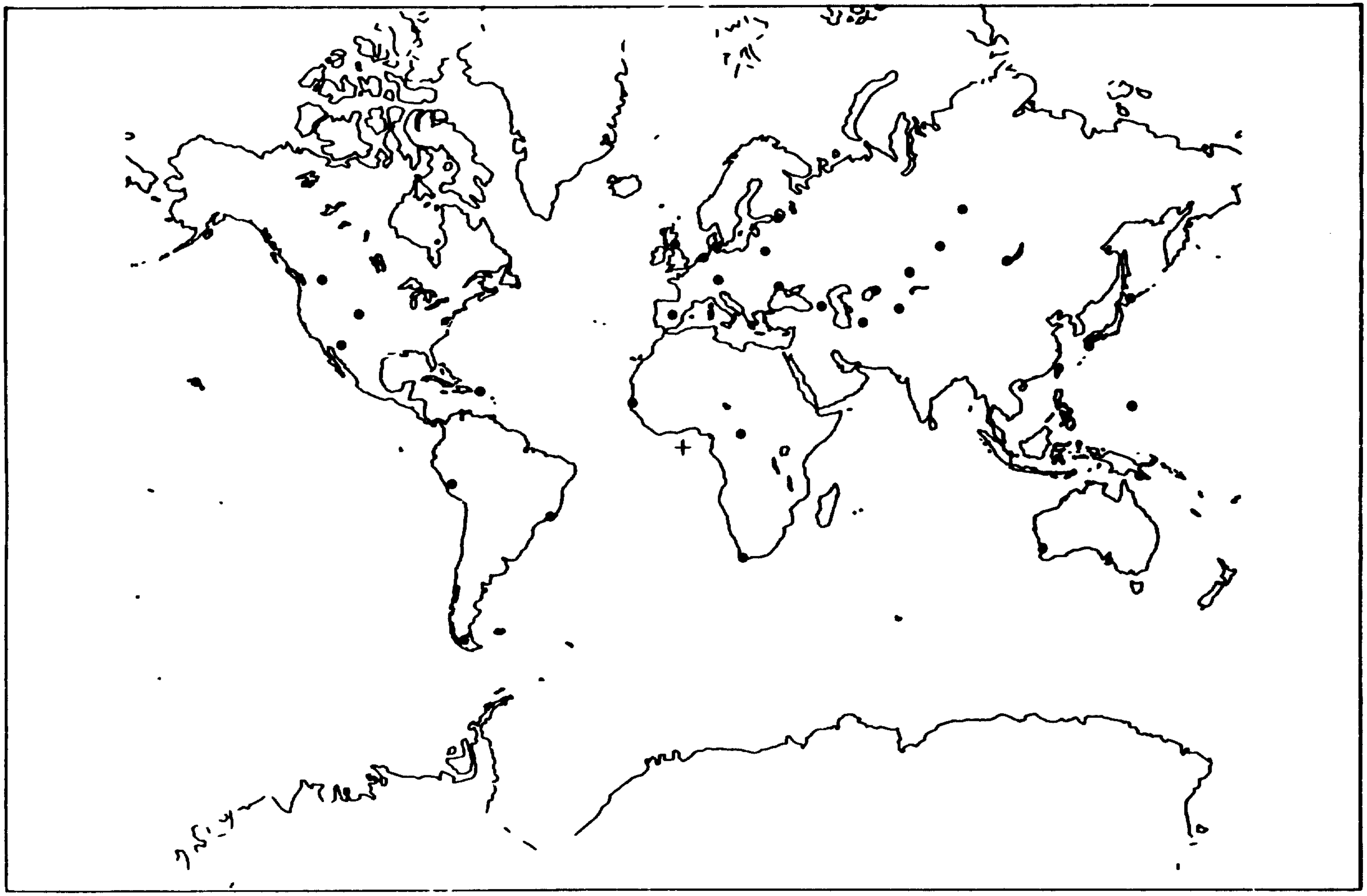

FIGURE 1.

ORIGINAL PAGE IS
OF POOR QUALITY

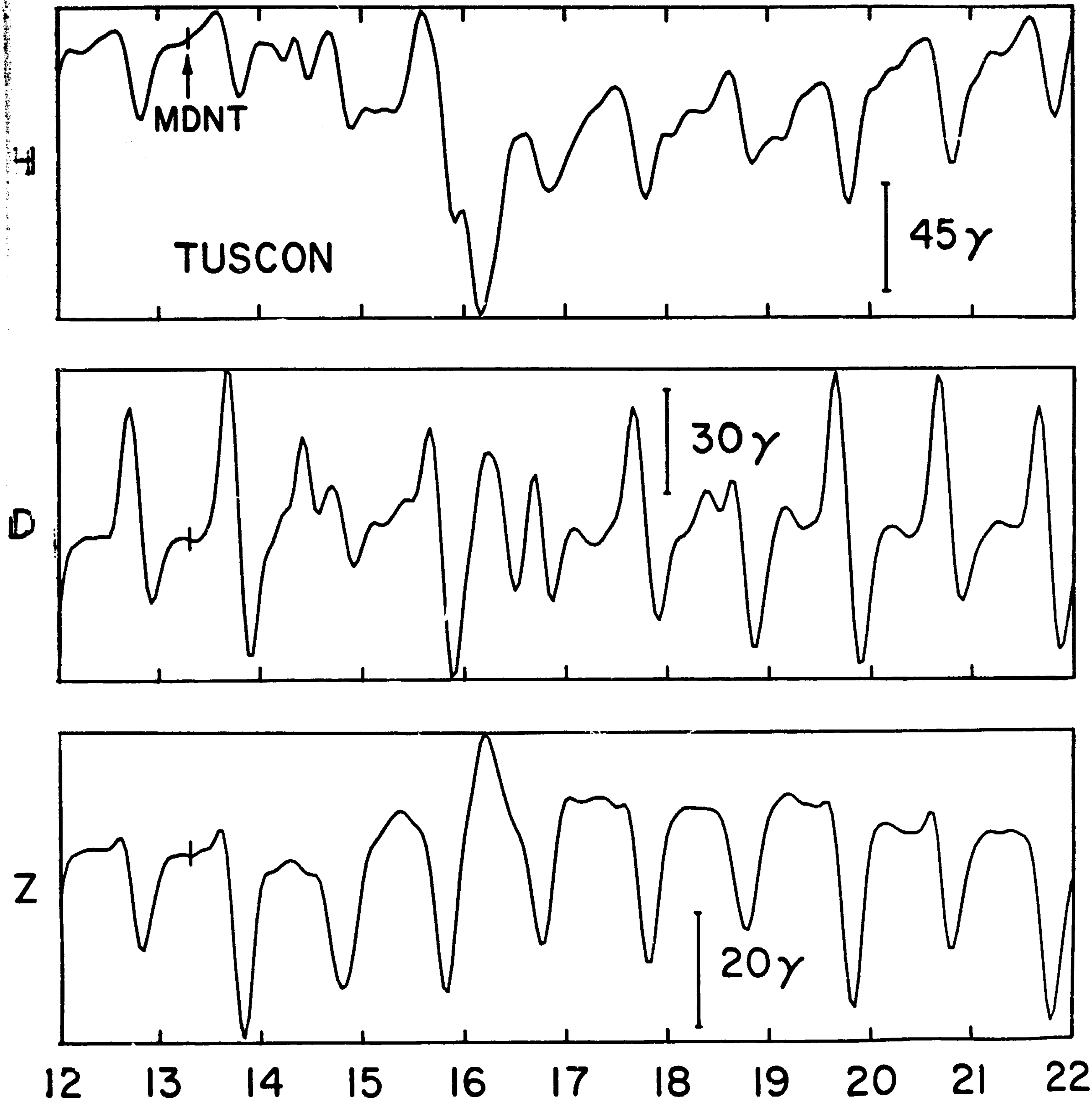

GREENWICH DAY, FEB. 1980

FIGURE 2.

ORIGINAL PAGE IS
OF POOR QUALITY

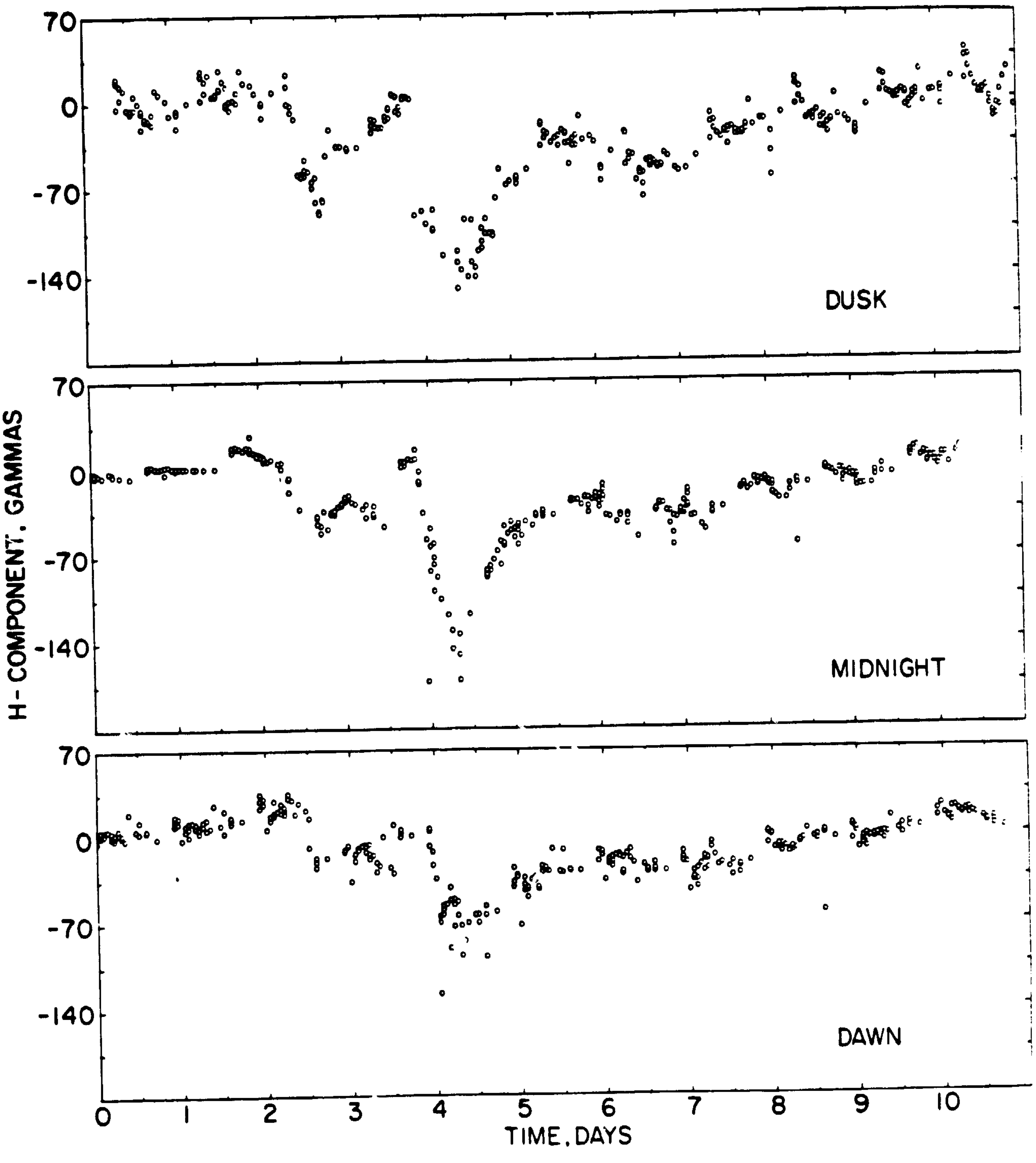

FIGURE 3.

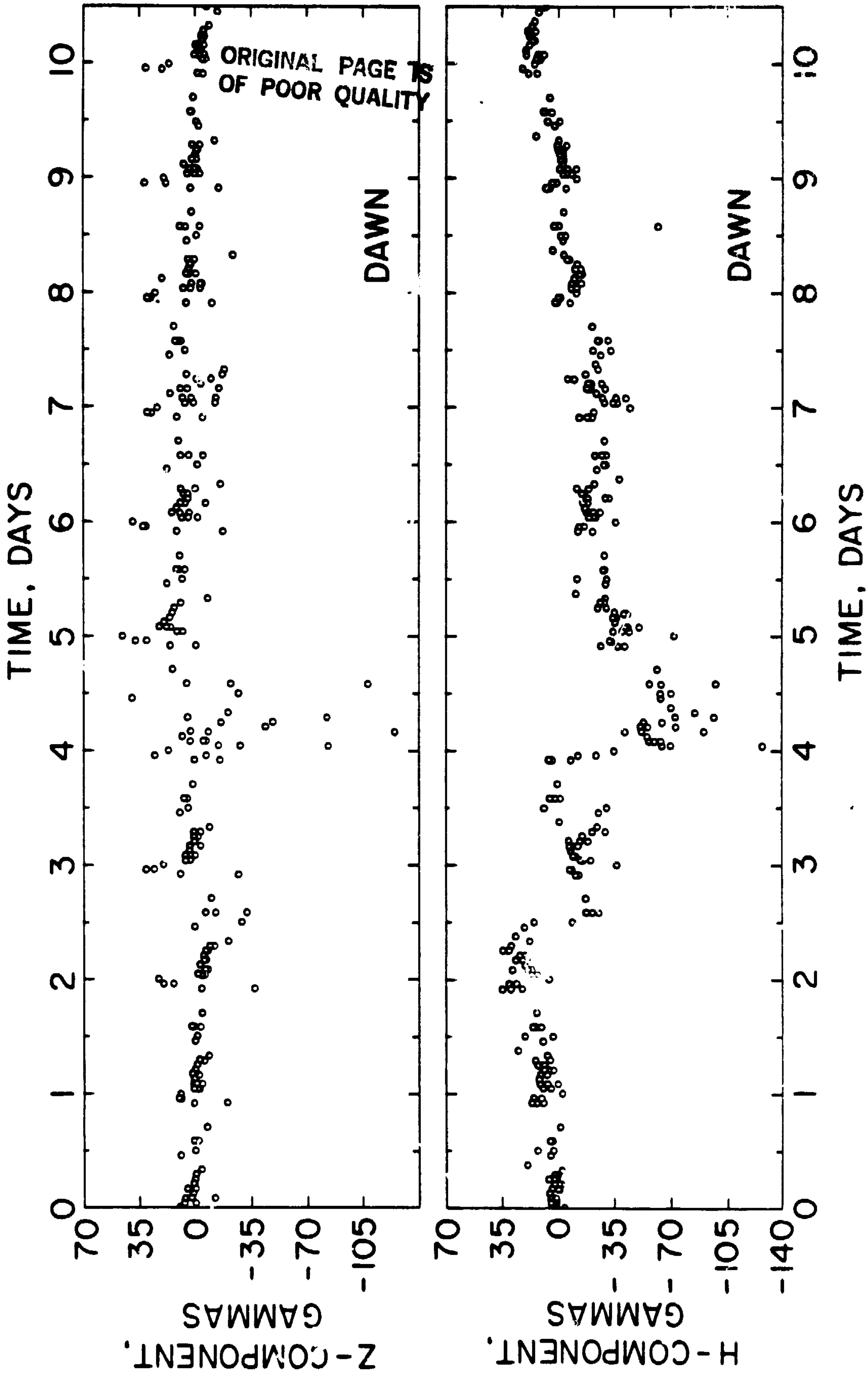
TIME, DAYS
0
1
2
3
4
5
6
7
8
9
10
DAWN
Z-COMPONENT, GAMMAS
70
35
0
-35
-70
-105
H-COMPONENT, GAMMAS
70
35
0
-35
-70
-105
-140

FIGURE 4.

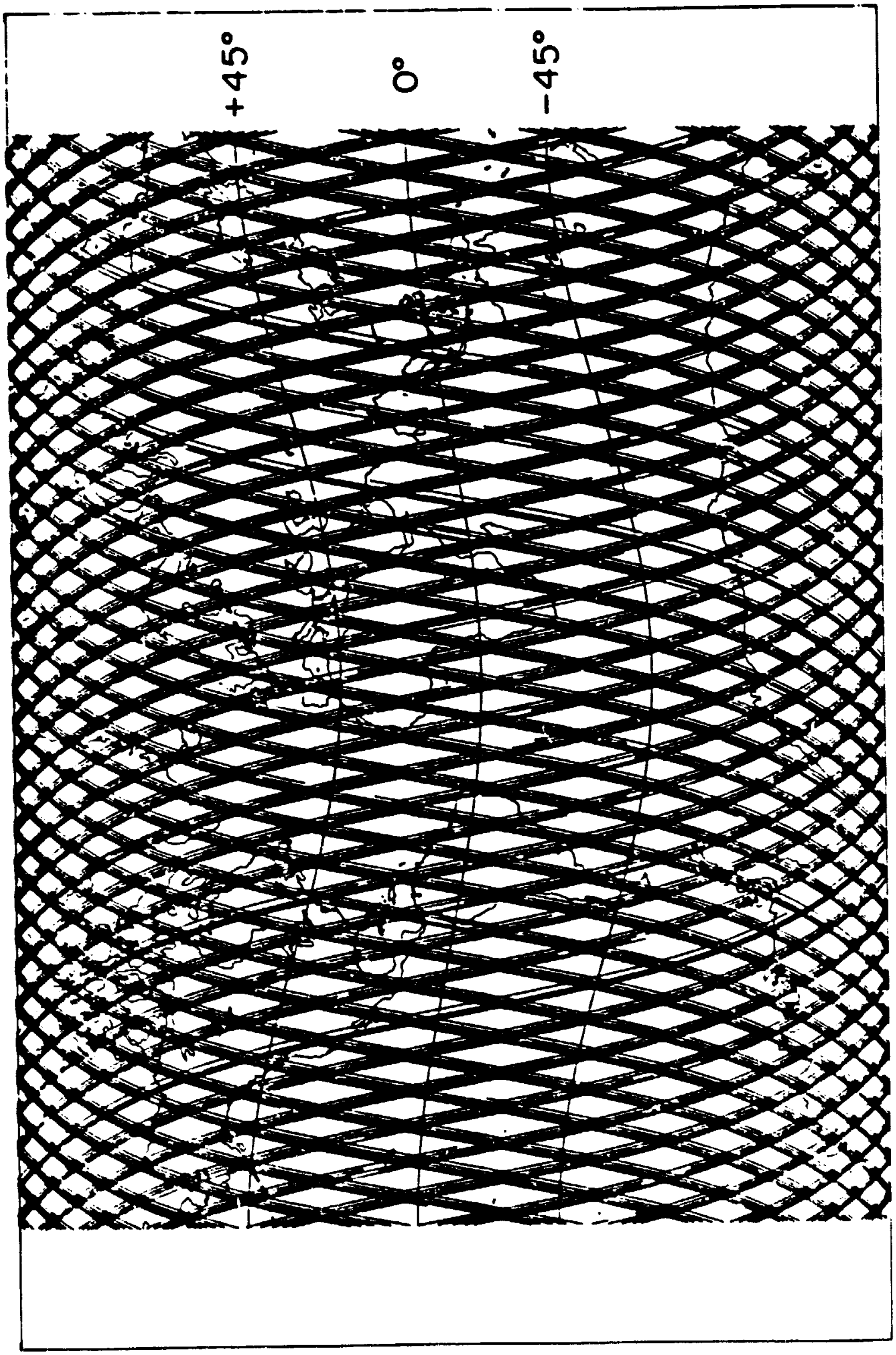

FIGURE 5.

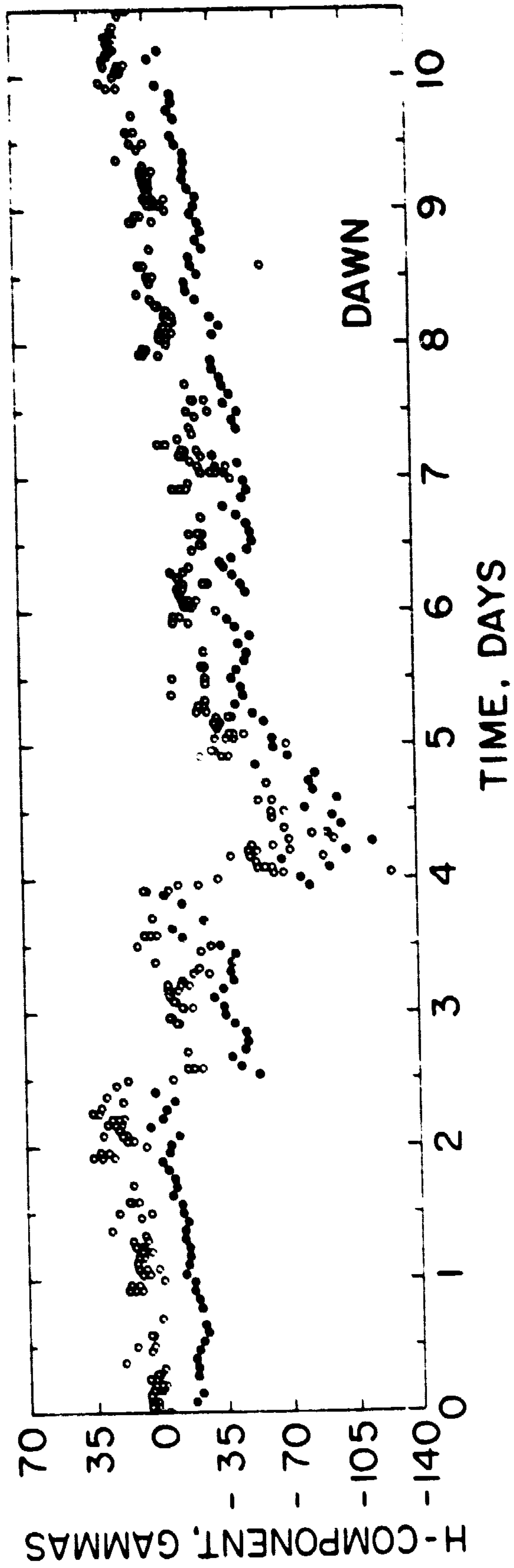
DAWN
TIME, DAYS
0
1
2
3
4
5
6
7
8
9
10
H-COMPONENT, GAMMAS
70
35
0
-35
-70
-105
-140

FIGURE 6.

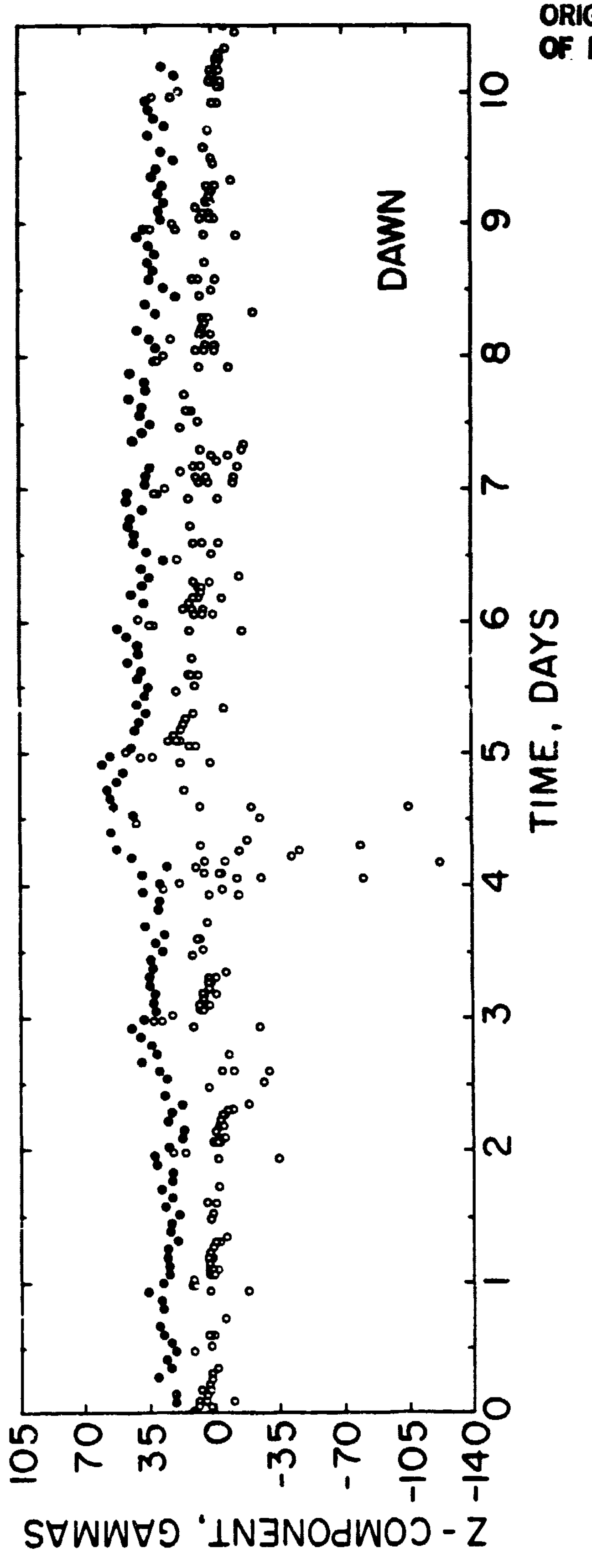
DAWN
TIME, DAYS
0
1
2
3
4
5
6
7
8
9
10
Z - COMPONENT, GAMMAS
105
70
35
0
-35
-70
-105
-140

FIGURE 7.

ORIGINAL PAGE IS
OF POOR QUALITY

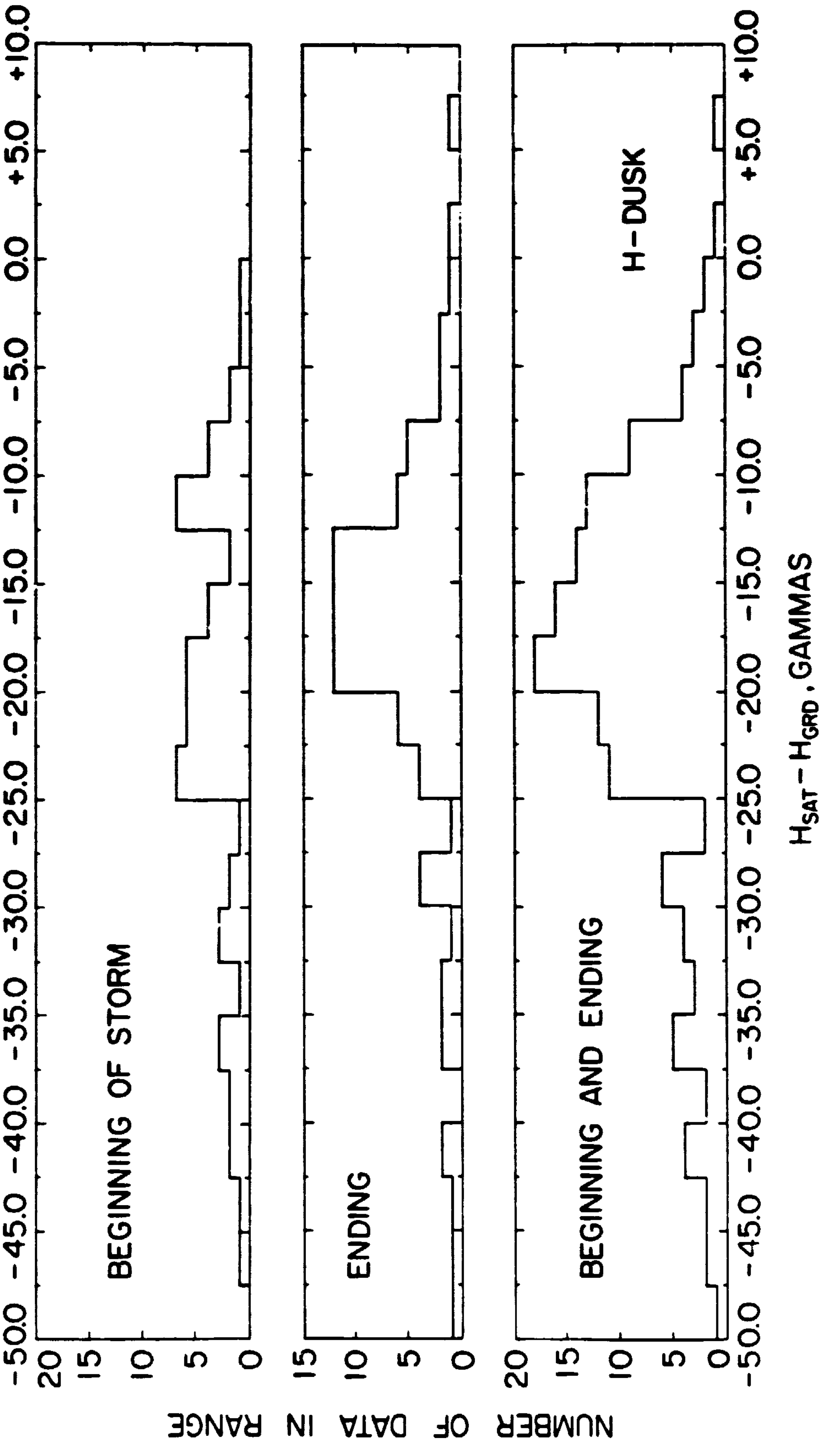

FIGURE 8.

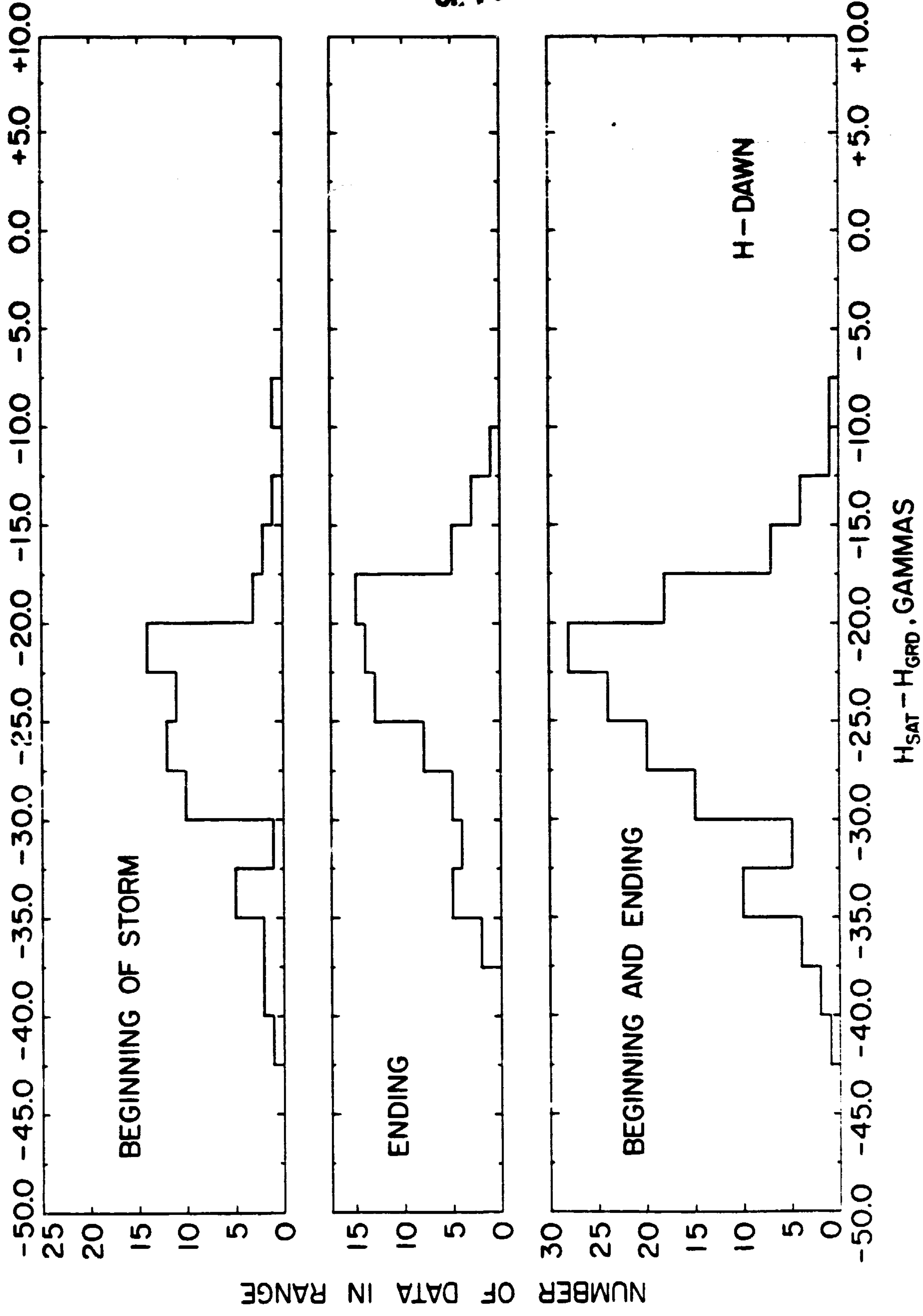
BEGINNING OF STORM
ENDING
BEGINNING AND ENDING
H-DAWN
-50.0
-45.0
-40.0
-35.0
-30.0
-25.0
-20.0
-15.0
-10.0
-5.0
0.0
+5.0
+10.0
25
20
15
10
5
0
15
10
5
0
30
25
20
15
10
5
0
$H_{SAT} - H_{GRD}$, GAMMAS
NUMBER OF DATA IN RANGE

FIGURE 9.

ORIGINAL PAGE IS
OF POOR QUALITY

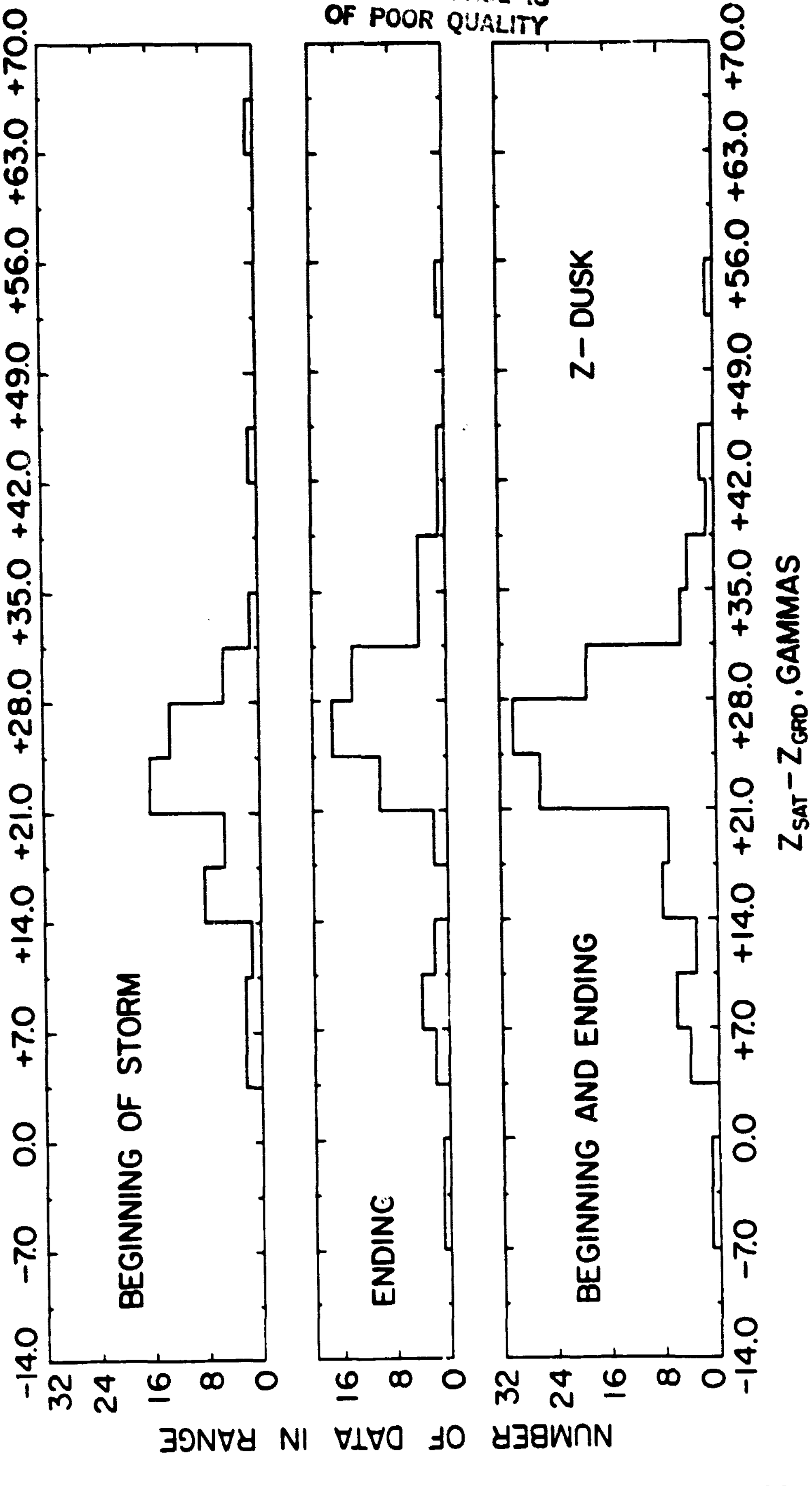

FIGURE 10.

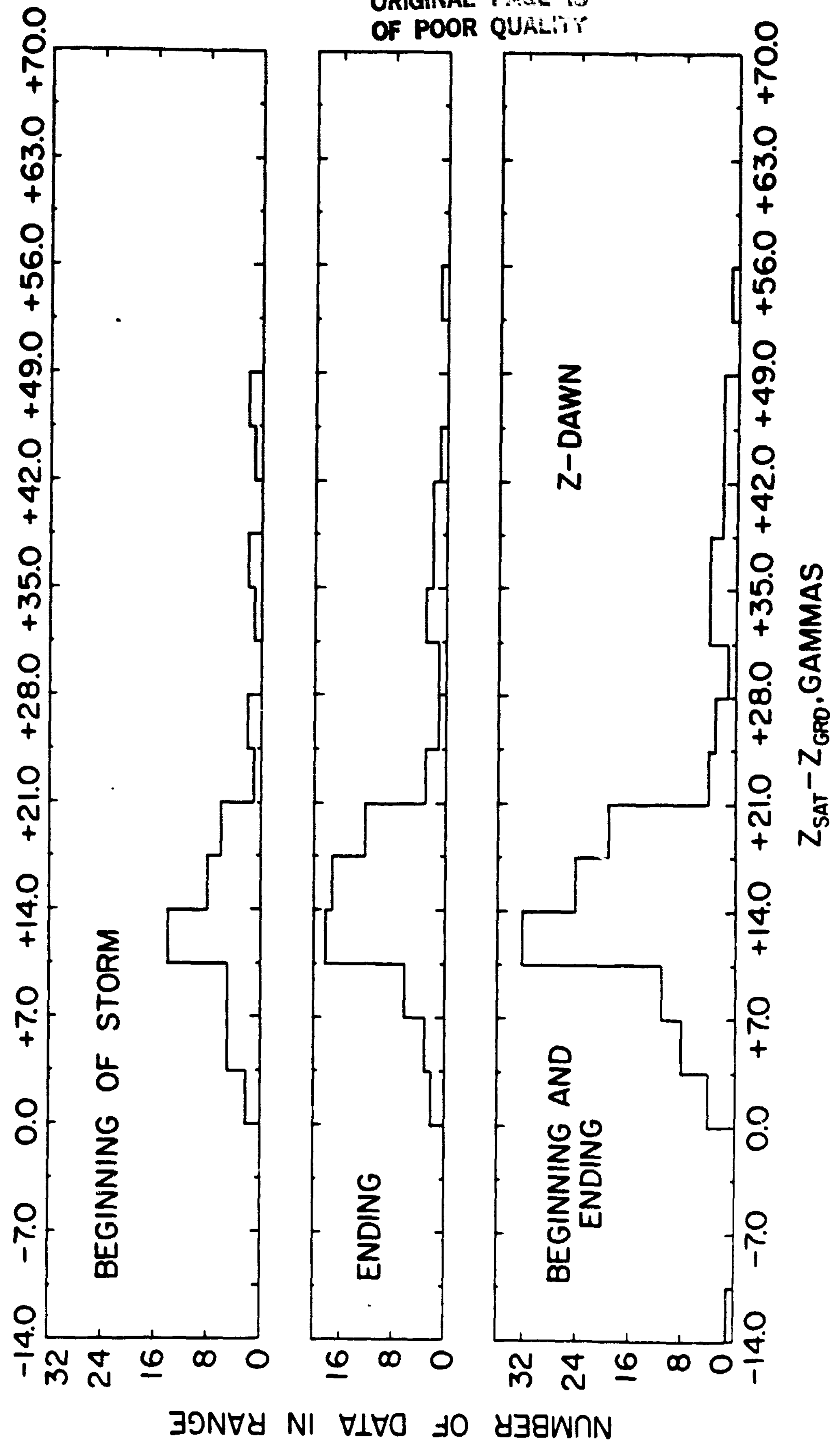
BEGINNING OF STORM
ENDING
BEGINNING AND ENDING
Z-DAWN
-14.0
-7.0
0.0
+7.0
+14.0
+21.0
+28.0
+35.0
+42.0
+49.0
+56.0
+63.0
+70.0
32
24
16
8
0
$Z_{SAT}-Z_{GRD}$, GAMMAS
NUMBER OF DATA IN RANGE

FIGURE 11.

ORIGINAL PAGE IS
OF POOR QUALITY

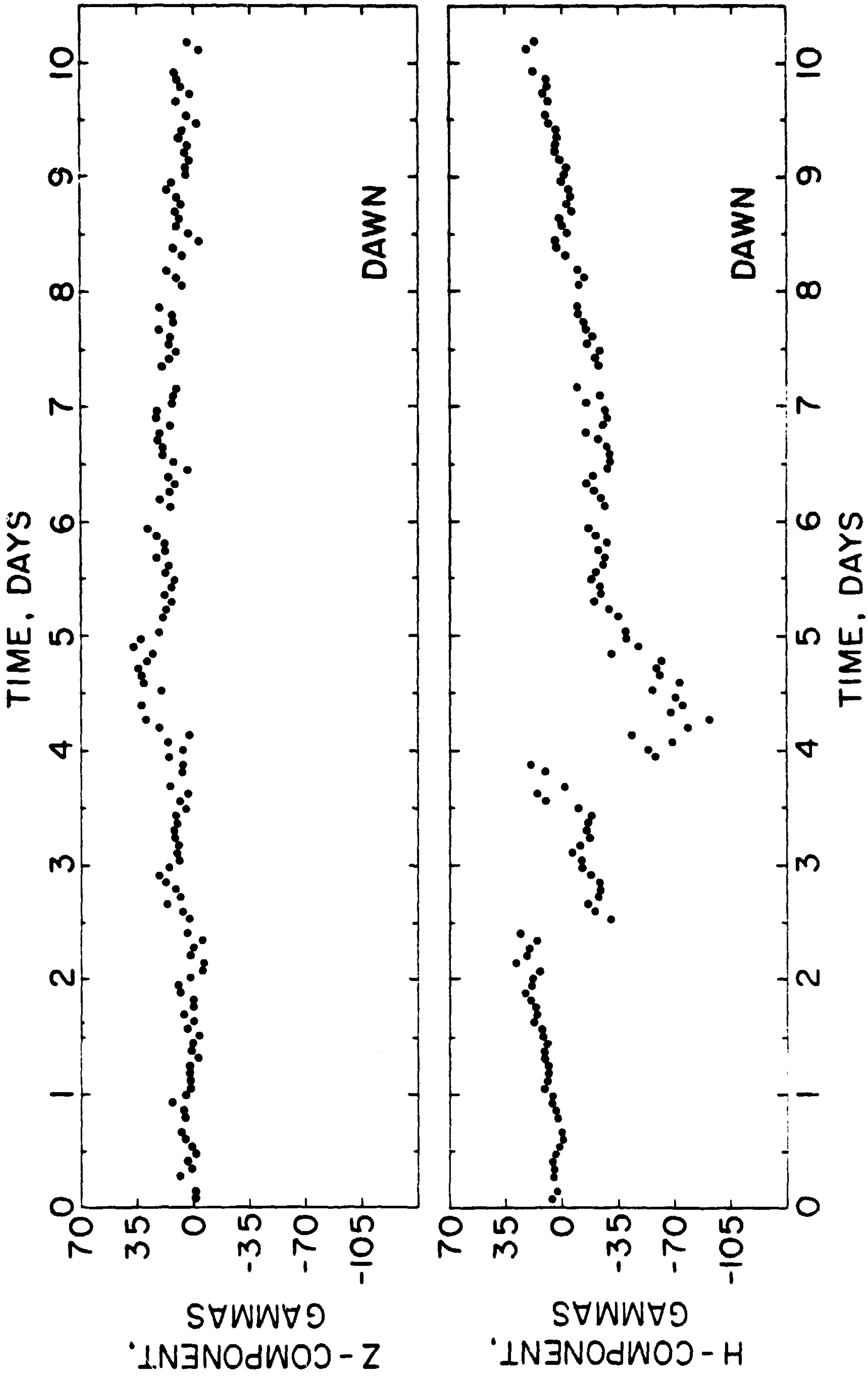

FIGURE 12.

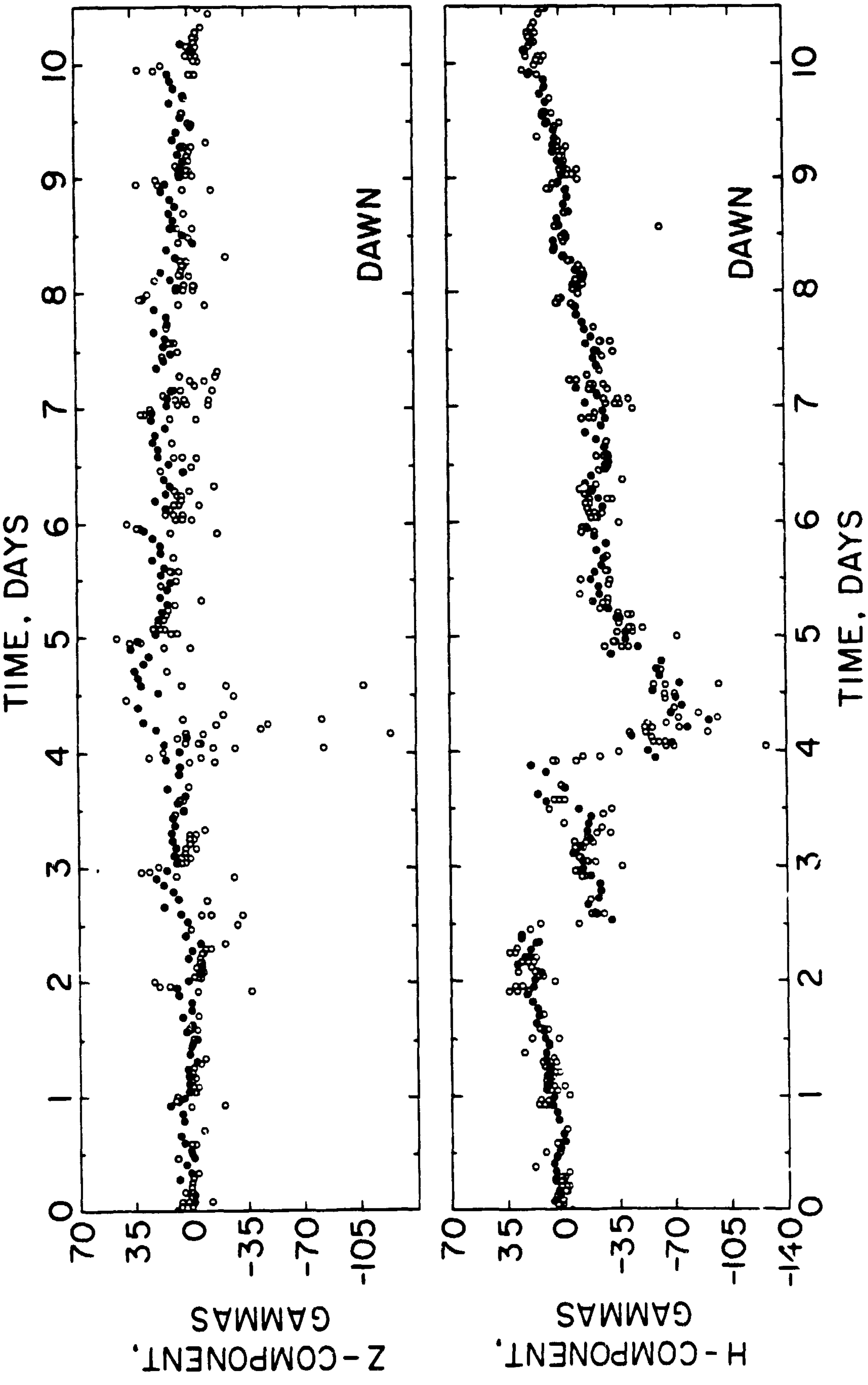
Z-COMPONENT, GAMMAS
H-COMPONENT, GAMMAS
TIME, DAYS
DAWN
70
35
0
-35
-70
-105
-140
0
1
2
3
4
5
6
7
8
9
10

FIGURE 13.

ORIGINAL PAGE IS
OF POOR QUALITY

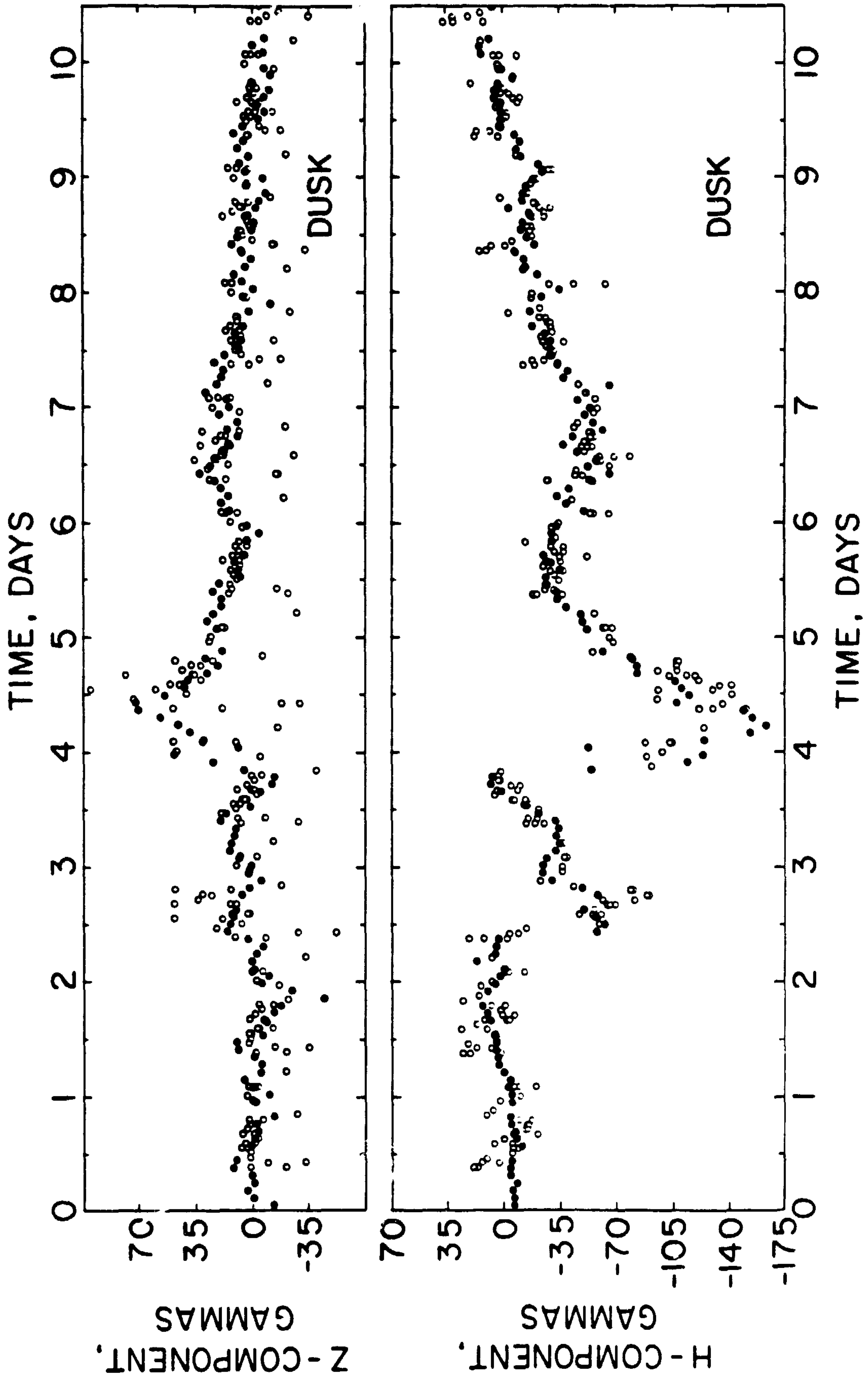

FIGURE 14.

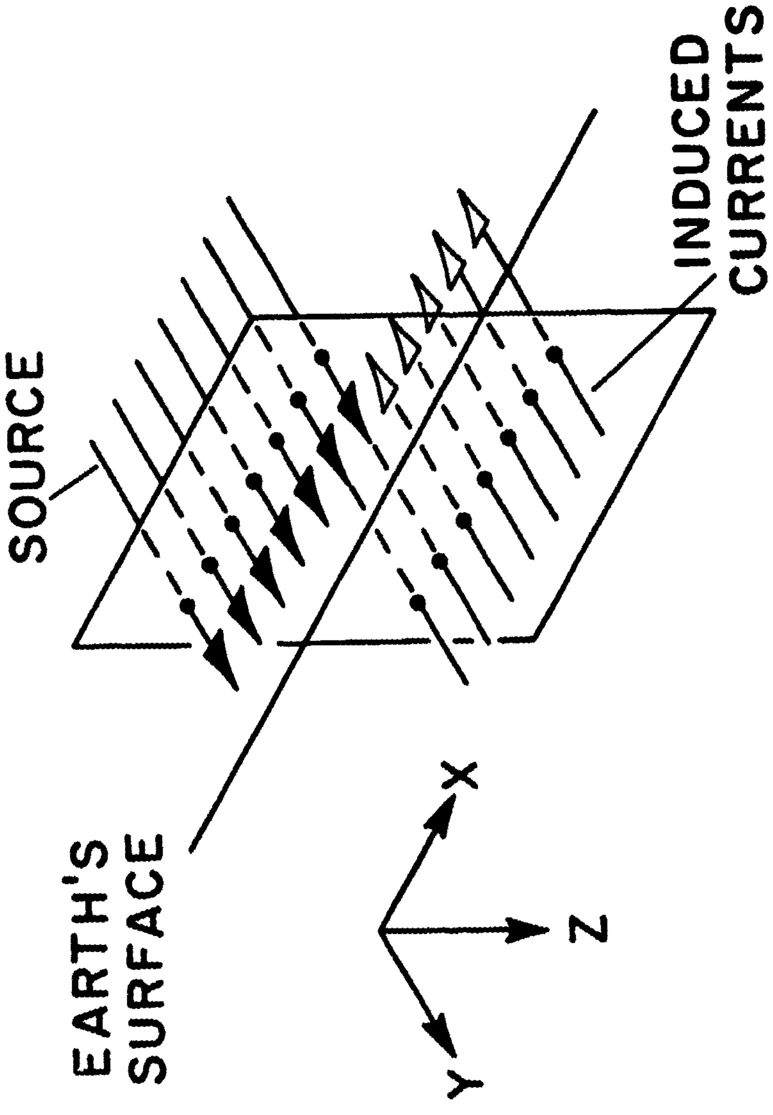

FIGURE 15.

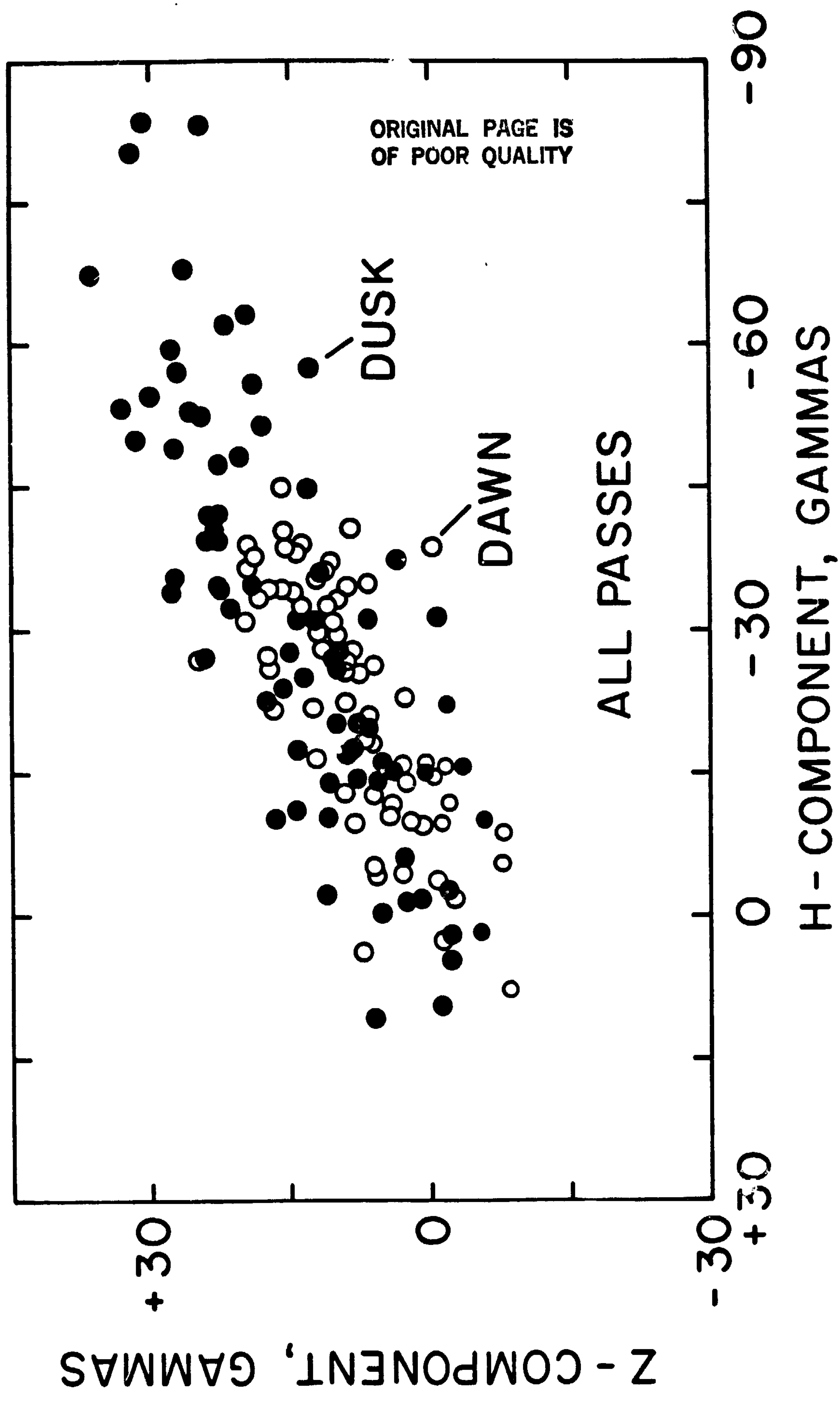
ALL PASSES
DUSK
DAWN
H-COMPONENT, GAMMAS
Z-COMPONENT, GAMMAS
-90
-60
-30
0
+30
+30
0
-30

FIGURF 16.

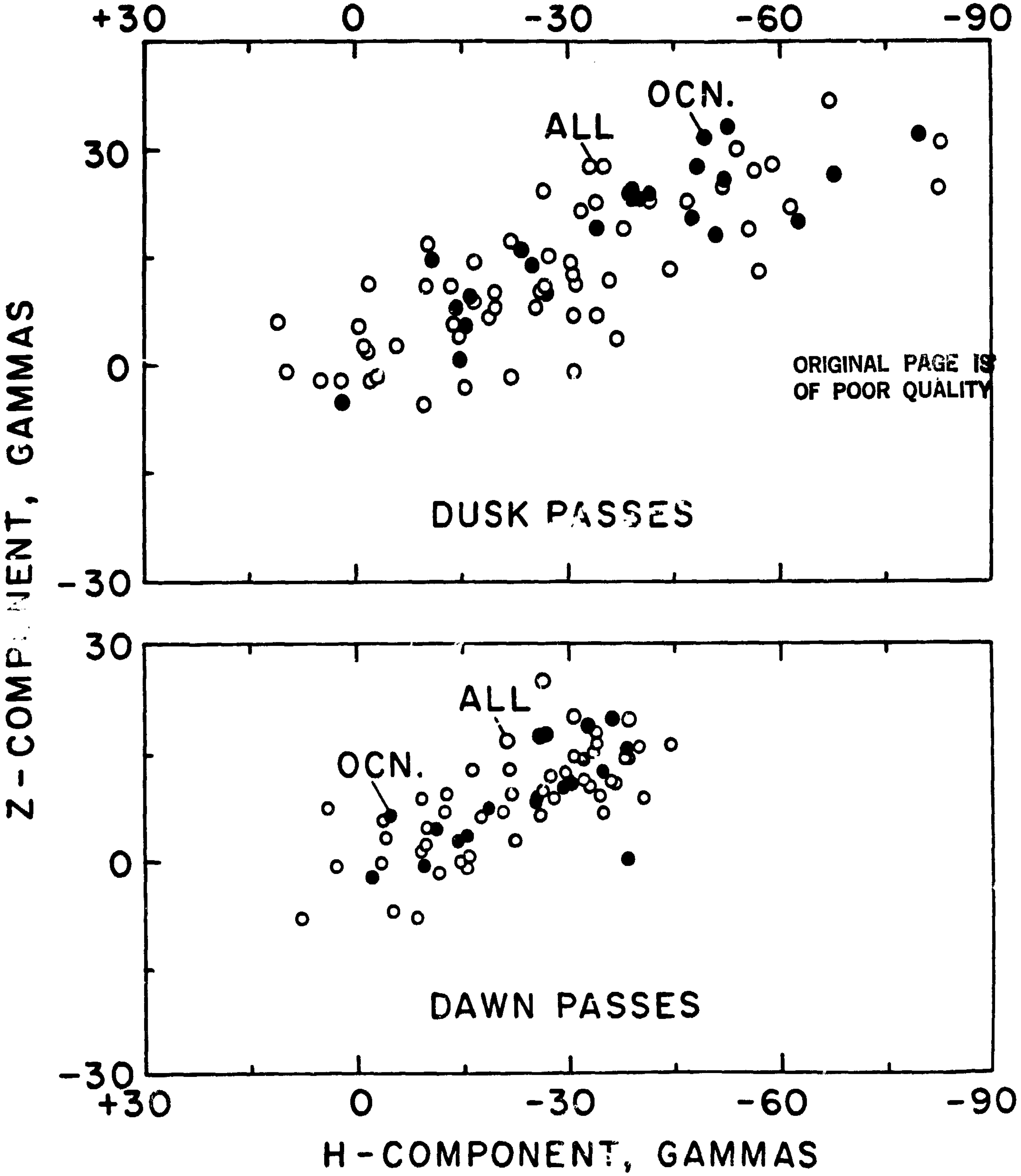
+30
0
-30
-60
-90
30
0
-30
OCN.
ALL
ORIGINAL PAGE IS
OF POOR QUALITY
DUSK PASSES
ALL
OCN.
DAWN PASSES
Z-COMPONENT, GAMMAS
H-COMPONENT, GAMMAS

FIGURE 17.

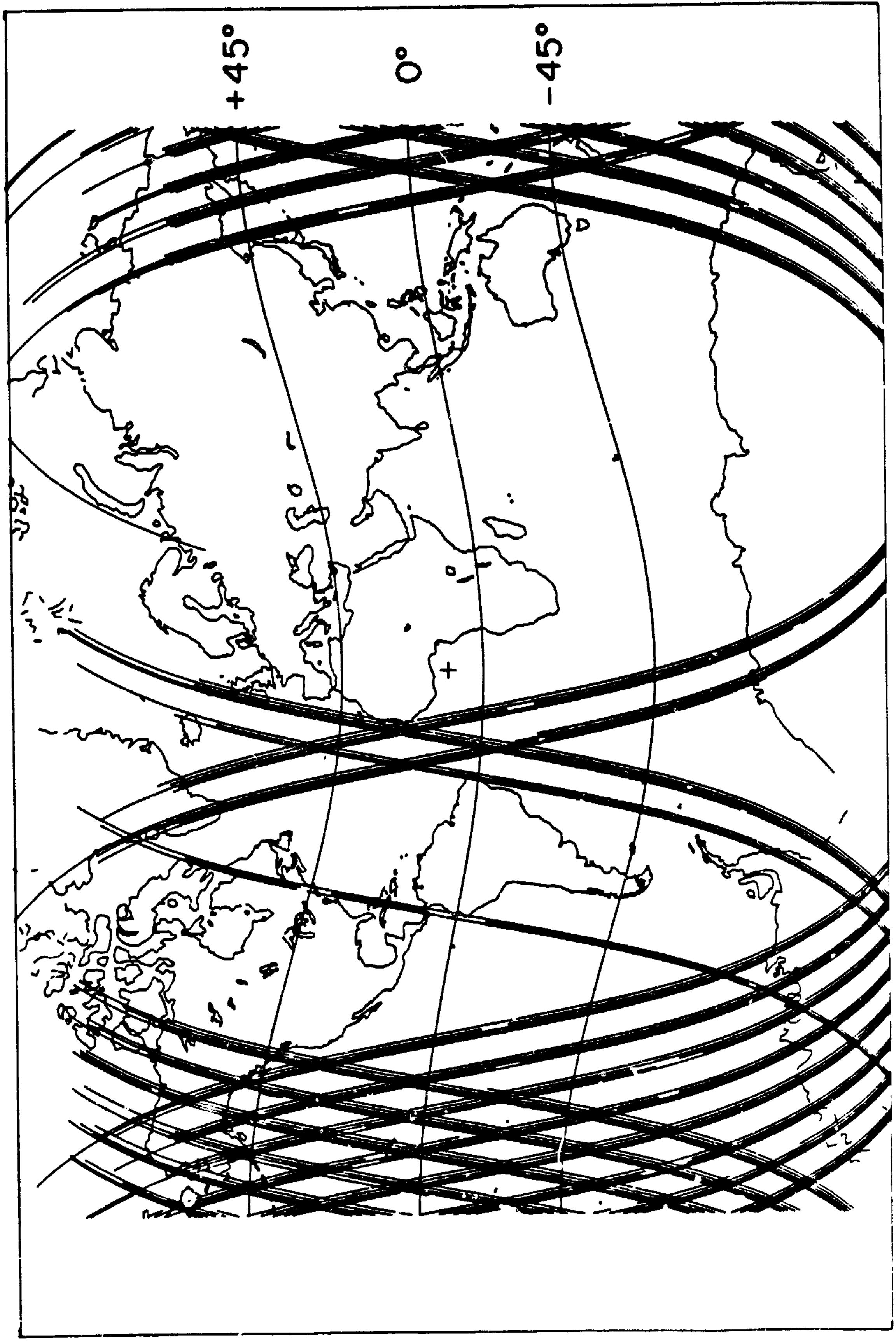

FIGURE 18.

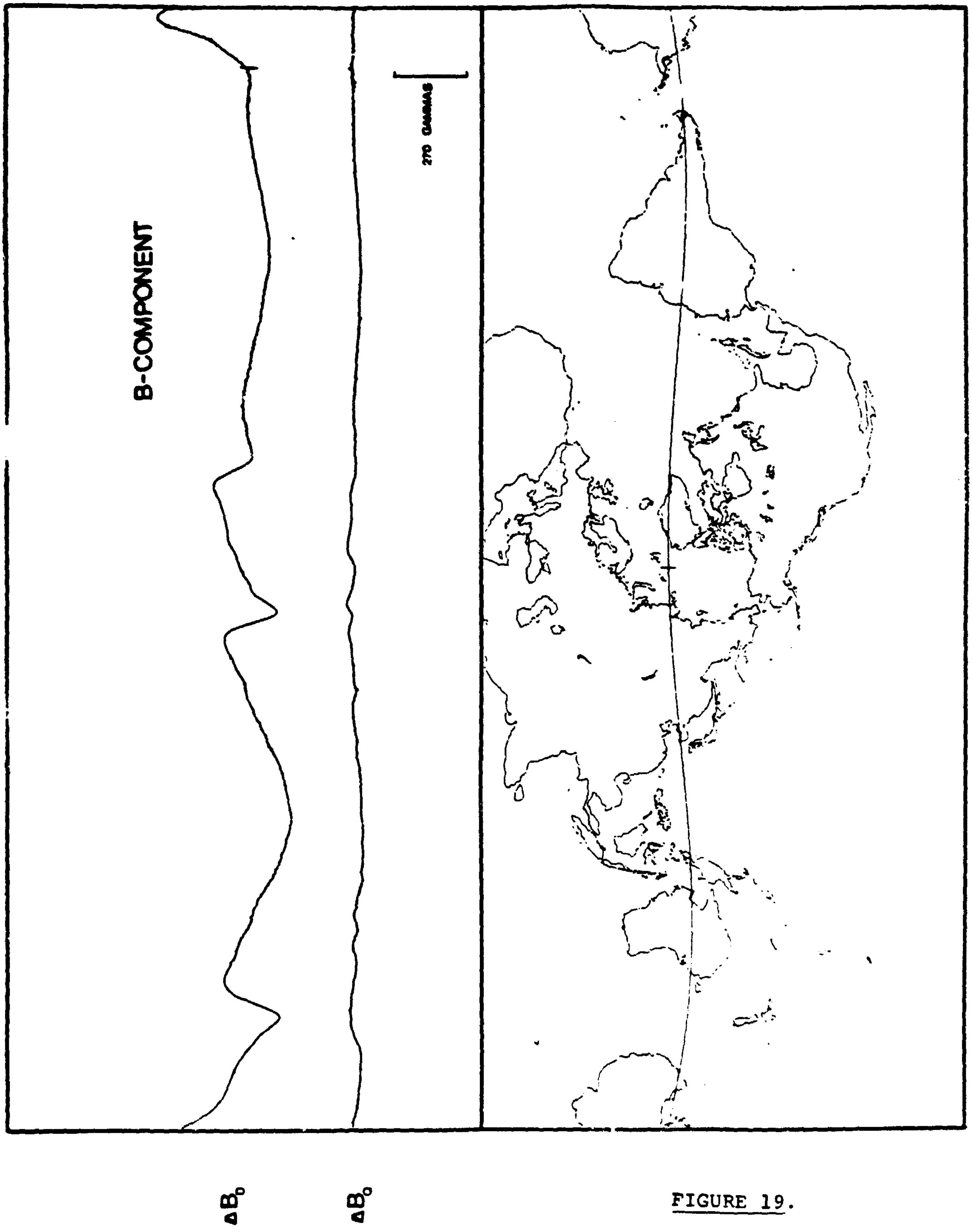

FIGURE 19.

ORIGINAL PAGE IS
OF POOR QUALITY

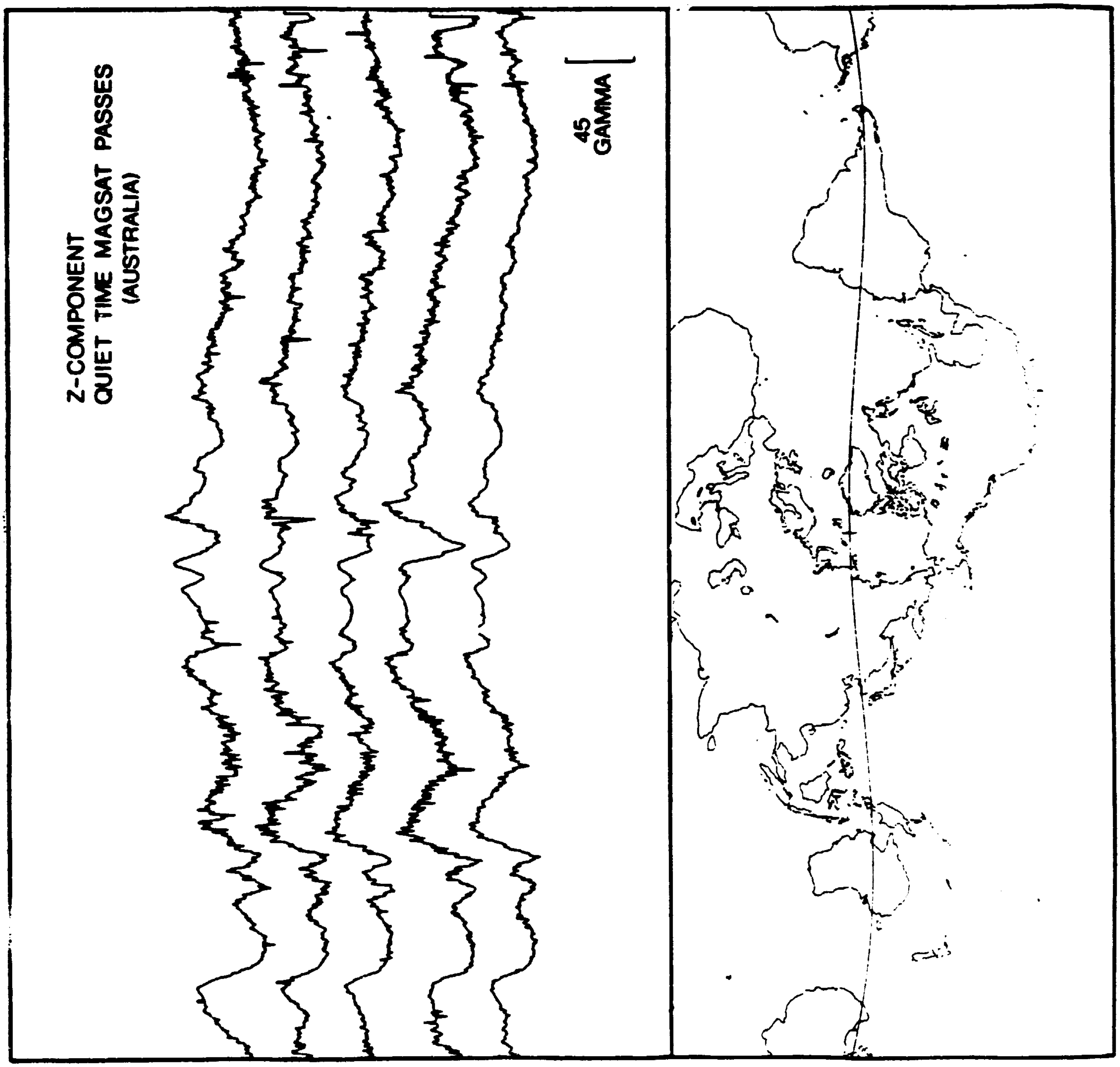

FIGURE 20.

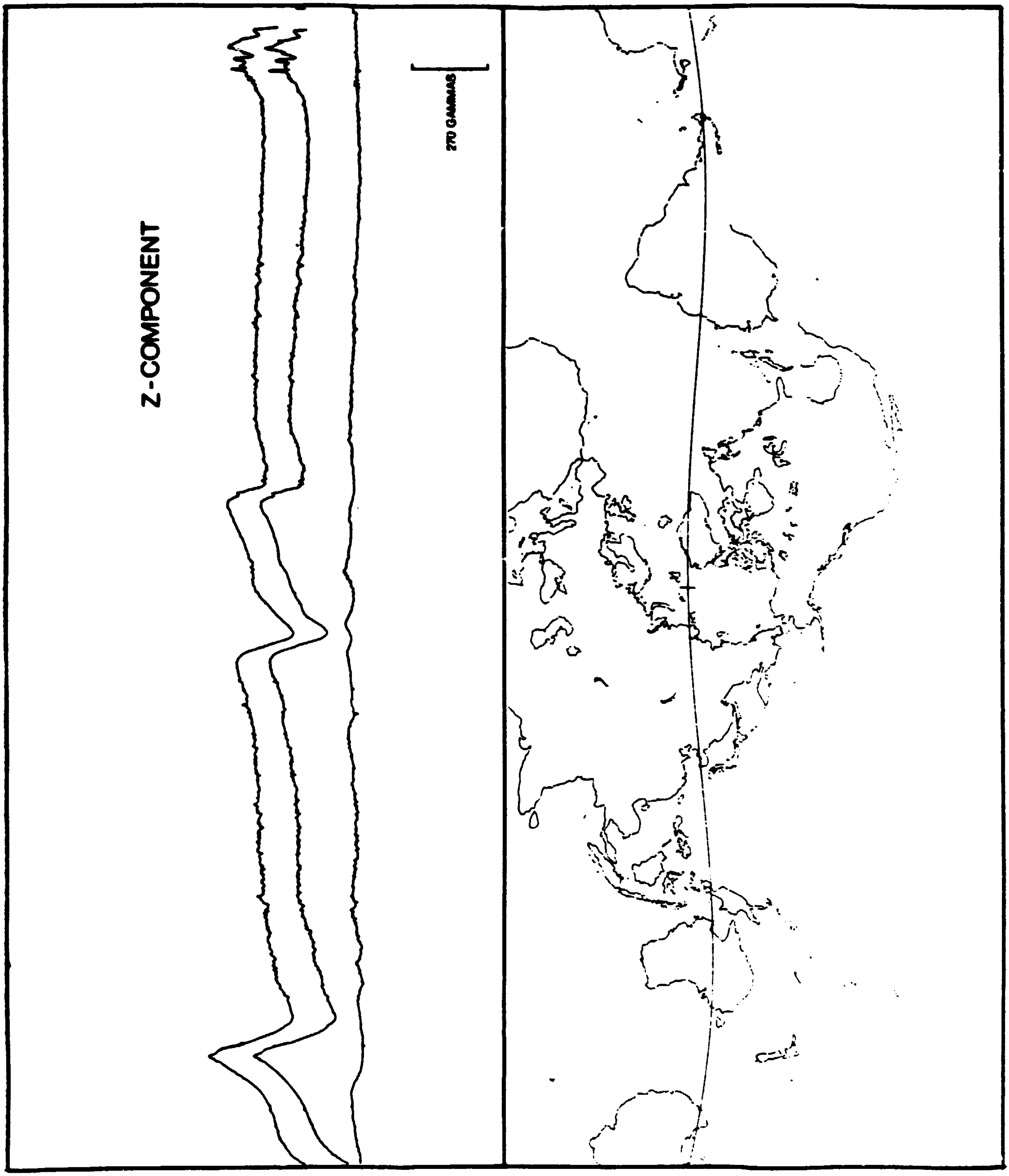

FIGURE 21.

APPENDIX 4

ELECTROMAGNETIC INDUCTION BY FINITE WAVE-NUMBER SOURCE FIELDS IN 2-D LATERAL HETEROGENEITIES; THE TRANSVERSE ELECTRIC MODE

John F. Hermance
Geophysical/Electromagnetics Laboratory
Department of Geological Sciences
Brown University
Providence, Rhode Island 02912

Preprint of a paper submitted to the
GEOPHYSICAL JOURNAL OF THE ROYAL ASTRONOMICAL SOCIETY
May, 1983

ABSTRACT

Interest in electromagnetic induction in a laterally heterogeneous earth by a finite source field spans a variety of geophysical disciplines. Most efforts reported to date are somewhat restricted in that certain scaling relations cannot be violated, or else the modelling results become invalid. For example certain approaches are appropriate only when the dimensions of the heterogeneity are small compared to the scale size of the source field. In addition, interest has recently developed in using satellites to study induction in the earth. The particular case when the satellite is above the source (such as for ionospheric current systems) is one which poses special problems to several existing approaches.

This paper describes a more general approach to solving these problems and broadens the range of scaling relations over which such models can be applied. The specific geometry considered is an equivalent 2-D current source directed parallel to the strike of a 2-D anomalous structure within the earth having a characteristic dimension of L; this geometry represents the transverse electric (TE, or E-parallel) induction mode.

A finite source field, which is located at some position within the modelling region, is simulated by discontinuities in the magnetic (or electric) field appropriate to the current flowing in the source. However, the fields reflected from the earth are continuous through the source region. Such an

approach not only has certain mathematical advantages, but also allows us to evaluate the electromagnetic fields above current sources in the ionosphere such as might be observed by satellites.

The case when the source field itself has a finite dimension imposes additional considerations for the problem of designing adequate 2-D models. The mesh spacing must be sufficiently dense to allow quadratic forms employed by the numerical algorithm to adequately represent trigonometric functions in the horizontal direction and exponentially damped functions in the vertical dimension. Moreover, in some cases, close to electrical discontinuities the induced field may behave more like $1/r$ or $1/r^2$. This often necessitates excessively close nodal spacing near electrical discontinuities. Whereas for the case of uniform source fields incident on a 2-D earth, one often increases the nodal spacing to very large values as one approaches the edges of the model, this is generally inappropriate for finite source fields.

Our results suggest that while fields may be perturbed in the close vicinity of lateral heterogeneities, at even modest offset distances from the contact the fields are more influenced by what is beneath the observer than by what is at some lateral distance away. This implies that in many cases, simple 1-D plane-layered models may be appropriately used in interpreting field data in a "piece-wise" sense, even when the total structure is more complicated laterally.

The fact that the fields induced by finite sources tend to decouple fairly rapidly with distance to either side of a vertical discontinuity prompted us to consider the effects that this phenomenon has on magnetic gradiometric experiments. Our results are encouraging in that, at least in some cases, regional gradients of the horizontal field (even where the sites span a major discontinuity) can be combined with local values of the vertical field, to yield reliable estimates of electromagnetic response functions.

At satellite altitudes, the difference between the results for the uniform source field and those for a finite source field in the ionosphere are profound. The total horizontal field amplitude produced by the uniform source is approximately unity, suggesting that for remote sources in the magnetosphere the horizontal field is insensitive to the effects of lateral variations in the earth's conductivity. On the other hand, the total horizontal field amplitude produced by the finite source field in the ionosphere is reduced by more than an order of magnitude. This is due to the fact that the satellite is <u>above</u> the source so that the induced and the source horizontal field components tend to cancel and the resultant H-field is quite small. In contrast, the finite source produces an anomalous vertical field at satellite altitudes which is of the same order of magnitude as that produced by the uniform source.

INTRODUCTION

Motivation

This paper considers electromagnetic induction in a laterally heterogeneous earth by a source field having finite dimensions. Interest in this problem spans a variety of geophysical disciplines which range from exploration studies, using artificial source fields, to global induction studies, using natural sources in the ionosphere and magnetosphere.

While a number of investigations have been reported in the literature which deal with various aspects of this problem, most efforts are somewhat restricted in that certain scaling relations cannot be violated, or else the modelling results become invalid. For example certain approaches are appropriate only when the dimensions of the heterogeneity are small compared to the scale size of the source field.

In addition, interest has recently developed in using satellites to study the coupling of finite source fields to the conducting earth (e.g., Hermance, 1982). The particular case when the satellite is above the source (such as for ionospheric current systems) is one which poses special problems to several existing approaches and has not been studied up to the present time except for simple, plane-layered earth models.

The following discussion describes our progress in developing a more general approach to solving these problems. We not only want to broaden the range of scaling relations over which our model can be applied, but we are especially interested in addressing those problems related to the effects of induction as seen at satellite altitudes (Hermance, 1982). The geometry considered in this paper is illustrated in Figure 1, which shows an equivalent 2-D current source directed along the y axis and flowing in the ionosphere at some height above the earth's surface. The source current varies in time according to exp(iωt) and flows parallel to the strike of a 2-D anomalous structure within the earth having a characteristic dimension of L. In the parlance of theoretical electromagnetism, this geometry represents the transverse electric (TE, or E-parallel) induction mode.

The procedure we follow involves establishing analytical relations between field quantities at the boundaries of our modelling region and then solving for the fields within our modelling region using a numerical algorithm. In principle this is a standard approach to such problems.

Previous Work

In the past, some workers have preferred an algorithm whereby the uppermost boundary of the modelling region (shown as the dashed line in Figure 2) is actually below the source, and the value of the field is constrained to represent the sum of that of the incident source from above and that of the induced field from below. To account for the induced field one needs to introduce an a priori value for the average reflectance of the earth. This in general is most appropriate when the characteristic spatial wavelength of the source (λ_s) as well as the height of the top-most boundary is much greater than the characteristic dimension (L) of the anomalous region.

Other workers have preferred boundary conditions such that in the vicinity of the source, one "sees" the effects of the source field alone (Figure 3), while at "infinity", the electromagnetic fields go to 0. These conditions are appropriate when λ_s is small compared to the characteristic dimension of the model - in some sense, this is the opposite extreme of the case illustrated in Figure 2.

Swift (1971) used a transmission surface analog of a finite difference approach to simulate induction by a line current in an imbedded heterogeneity. He imposed a plane-wave characteristic impedance boundary condition of

$$Z_i = (i\omega\mu/\sigma)^{1/2}$$

at the top, sides and bottom of the model. Although this approximation is correct for some cases, it is not correct in general. The impedance (defined as $-E_y/H_x$) of a homogeneous earth to a line current source flowing in the y-direction is generally not the same as the impedance of a homogeneous earth to a plane wave source (see for example, Wait, 1953). In the case where the impedance of the earth to either source is approximately the same (i.e. when $\delta << \lambda_s$, δ being the depth of penetration), then these boundary conditions are appropriate when the distance to the boundaries is large when compared with the characteristic dimension of the source field as well as when compared with the characteristic dimension of the lateral heterogeneity (or the depth of penetration).

Stoyer and Greenfield (1976) also used plane-wave characteristic impedance boundary conditions at the edges of their model. They found that their results within the interior of the model, close to the source, appeared to be reasonably reliable when compared with analytical (but numerically integrated) solutions. However when the edge of the model was approached, the quality of their results degraded appreciably.

Coggon (1971; p. 140) felt that when simulating induction by a line source parallel to a two-dimensional heterogeneity (E-polarization), the appropriate condition to apply at exterior boundaries is that the secondary electric field is zero. This, of course, also implicitly assumes that either the scale size of the source is small or that the dimensions of the lateral heterogeneity are small.

Hibbs and Jones (1973) adapted the numerical algorithm of Jones and Pascoe (1971) and Pascoe and Jones (1972) to treat the case of induction by finite source fields in a two-dimensional current system flowing parallel to the strike of conductive heterogeneities (E-polarization). An implicit restriction on their model, although one they did not emphasize, was that the plane-layered structure must be the same at either vertical edge of their exterior boundaries. Moreover, in the example they discussed, they assumed uniform reflectivities at an altitude of only 50 km which implies the effects of lateral heterogeneities are minimal at this height. This assumption is appropriate if the scale size (L) of the lateral heterogeneity is small compared to the height at which this condition is applied. In the case they considered, the lateral heterogeneity must have a dimension $L << 50$ km.

Quon *et al*. (1979) have considered the effects of what are probably extreme cases of dipole and line current sources at heights of only 110 km. Although they do not discuss their numerical algorithm in detail, they describe an example of induction by finite sources in an earth which consists of two quarter-spaces (of resistivity 100 and 10 ohm-m, respectively) separated by a vertical contact. Each sub-region extends to infinity in its respective quarter-space.

Weaver and Thompson (1972) have shown for a restricted case the importance of properly selecting the dimensions of a numerical model and specifying the boundary conditions at its edges. They point out that improperly posed boundary constraints often perturb numerical results over significant regions of the model's interior.

Present Model

The case to be considered here is somewhat more generalized than much of the previous work. As illustrated in Figure 4, we want to simulate a finite source field which is located at some position within the modelling region. The presence of the source is simulated by discontinuities in the magnetic (or electric) field appropriate to the current flowing in the source, but the fields reflected from the earth are continuous through the source region. Such an approach has certain mathematical advantages, but also allows us to evaluate the electromagnetic fields above current sources in the ionosphere such as might be observed by satellites. Alternative formulations, such as the class of models represented in Figure 2, are sometimes not compatible with this application.

At the top-most and bottom-most boundaries, characteristic impedance conditions are applied (accounting, of course, for the finite wave-number of the source). In addition, the earth is assumed to be plane layered at either of the side boundaries (but the vertical structure can be different at either side). In the interior of the model, the theory allows for quite arbitrary 2-D lateral heterogeneities. Clearly, however, it is required by the physics of the problem that all boundaries be far from the localized effects of fields associated with electrical discontinuities within the model's interior. In the following sections we consider in detail the implementation of these concepts, first in an analytical sense and then in terms of numerical operators.

BOUNDARY CONDITIONS AT THE LEFT AND RIGHT EDGES OF THE MESH

Plane-Layered Earth at $x = \pm\infty$

For the class of problems we wish to consider in the present analysis, we follow the conventional assumptions employed for two-dimensional models using uniform-source fields (Madden and Swift, 1969; Wright, 1970; Jones and Price, 1970): the earth is plane-layered at the extreme left and right vertical edges of the mesh (i.e. the outer-most column of nodes); and that these edges are sufficiently far from scattering centers that one may neglect the effects of lateral heterogeneities on the fields at the edges. We wish to assume, however, that in general the horizontal layers along the left edge may be different from those along the right edges. This assumption allows us to apply Dirichlet boundary conditions at the edges approximate for a finite source above a plane-layered earth, a problem which is solvable analytically (Price, 1950; Wait, 1953; Hermance and Peltier, 1970; Peltier and Hermance, 1971, Hermance, 1978). We now describe the application of these boundary conditions to our finite difference simulation.

A Surface Impedance Recursion Relation

Expressions for determining the downward-looking impedance at an arbitrary surface above a n-layered earth have been derived by many workers (e.g. Wait, 1953) and the problem need not be discussed in detail here. However for the sake of consistency in notation etc., we briefly outline the development.

To derive the impedance recursion relation, we begin by considering the orthogonal electric and magnetic field components, E_x and H_y, and assume E_y and E_z are 0. For self-consistency, the electric and magnetic fields must be related through Maxwell's equation, for example

$$\nabla x \underline{E} = -\partial \underline{B}/\partial t \ , \tag{1}$$

or

$$(\nabla x \underline{E})_y = -i\omega\mu H_y \ , \tag{2}$$

where

$$(\nabla x \underline{E})_y = \partial E_x/\partial z \ . \tag{3}$$

Therefore

$$H_y = -(1/i\omega\mu)\partial E_x/\partial z \ . \tag{4}$$

If, in the jth medium, the electric field follows a relation of the form

$$E_{xj} = (A_j e^{\gamma_j z} + B_j e^{-\gamma_j z})\cos\theta_x \ , \tag{5}$$

where $\theta_x = k(x-x_o)$ and $\gamma_j = (k^2 + i\omega\mu\sigma_j - \omega^2\mu\varepsilon)^{1/2}$, then

$$H_{yj} = -(\gamma_j/i\omega\mu)[A_j e^{\gamma_j z} - B_j e^{-\gamma_j z}]\cos\theta_x \ . \tag{6}$$

At the jth interface, we define the surface impedance,

$$Z^j = E_{xj}/H_{yj} \ , \tag{7}$$

which of course is not to be confused with the generalized charracteristic impedance, $Z_j = (i\omega\mu/\gamma_j)$, of a strictly homogeneous medium.

Relative to a coordinate system located at the jth interface, the ration E_{xj-1}/H_{yj-1} formed from (5) and (6), and evaluated at $z = 0$ is given by

$$[E_{xj-1}/H_{yj-1}]\Big|_{z=0} = -Z_{j-1}(A_{j-1} + B_{j-1})/A_{j-1} - B_{j-1}) \ , \tag{8}$$

which we term our generalized surface impedance at the top of the jth medium; in other words, denoting this parameter with a subscript j, we obtain

$$Z^j = -Z_{j-1}(A_{j-1} + B_{j-1})/(A_{j-1} - B_{j-1}) \ , \tag{9}$$

which can be rearranged to the form

$$A_{j-1}(Z^j + Z_{j-1}) = B_{j-1}(Z^j - Z_{j-1}) \ . \tag{10}$$

Expressions such as (5) and (6) can be used to express the generalized surface impedance at the top of the j-1 layer, relative to a coordinate system at the jth interface:

$$Z^{j-1} = [E_{xj-1}/H_{yj-1}]\Big|_{z=-\Delta d_{j-1}}$$

$$= -Z_{j-1}\left\{\frac{A_{j-1}e^{-\alpha_{j-1}} + B_{j-1}e^{\alpha_{j-1}}}{A_{j-1}e^{-\alpha_{j-1}} - B_{j-1}e^{\alpha_{j-1}}}\right\} \tag{11}$$

where the argument of the exponent is given by $\alpha_{j-1} = \gamma_{j-1}\Delta d_{j-1}$. However a relation between A_{j-1} and B_{j-1} is expressed in (10), so, for example, upon solving (10) for A_{j-1}, substituting the resulting expression into (11), rearranging terms and cancelling the B_{j-1} terms which appear in the numerator and denominator, we obtain

$$Z^{j-1} = -Z_{j-1}\left\{\frac{(Z^j - Z_{j-1})e^{-\alpha_{j-1}} + (Z^j + Z_{j-1})e^{\alpha_{j-1}}}{(Z^j - Z_{j-1})e^{-\alpha_{j-1}} - (Z^j + Z_{j-1})e^{\alpha_{j-1}}}\right\} \tag{12}$$

Combining like terms in Z^j and Z_{j-1}, respectively, we obtain

$$Z^{j-1} = Z_{j-1}\left\{\frac{Z^j\cosh\alpha_{j-1} + Z_{j-1}\sinh\alpha_{j-1}}{Z^j\sinh\alpha_{j-1} + Z_{j-1}\cosh\alpha_{j-1}}\right\} \tag{13}$$

or upon dividing through by cosh α_{j-1}, we arrive at the form

$$Z^{j-1} = Z_{j-1}\frac{Z^j + Z_{j-1}\tanh\alpha_{j-1}}{Z^j\tanh\alpha_{j-1} + Z_{j-1}}\quad , \tag{14}$$

for the surface impedance at the top of the j-1 layer, where Z^j is the surface impedance at the top of the jth layer (or the bottom of the j-1 layer).

Clearly we may use expression (14) as a recursion relation. Assuming that a homogeneous medium is present beneath the bottommost interface ($j = n$), we have $Z^n = Z_n$. Using (14) we can propagate this relation to the next higher interface ($j = n-1$) to determine Z^{n-1}. This recursive operation can be continued to progressively shallower depths until we reach the node directly beneath our source current.

ELECTROMAGNETIC FIELDS OF THE SOURCE

Source Current Density

It is well-known (e.g. Hermance, 1978) that an arbitrary two-dimensional source flowing in the y-direction, having a current density $J_y(x,z,t)$, can be expressed as a superposition of elementary sources having a spatial wavelength λ_s, or wavenumber $k = 2\pi/\lambda_s$. For the case of a thin horizontal current sheet flowing at a fixed height ($z = z_o$) above the earth's surface (Figure 5) we can express the current density as

$$J_y(k) = I_o(k)\delta(z-z_o)\cos[k(x-x_o)] \qquad (15)$$

where $\delta(z-z_o)$ is the Dirac delta function and $I_o(k)$ is the magnitude of the coefficient associated with the kth spatial wave number (which we assume has the dimensions of a sheet current density, i.e. amperes/m). For the present discussion we will only consider sources of the above form, recognizing that if needbe, more complicated sources can be easily synthesized from the resulting expressions (Hermance, 1978). In the present context we emphasize that sheet currents such as (15), which may be reconstructed from ground-based magnetic field measurements, may not represent actual current systems in nature. In some cases they should be looked upon as only <u>hypothetical</u> current systems which produce magnetic fields at the earth's surface which are equivalent to the magnetic fields produced by actual ionospheric or magnetospheric current systems - the <u>actual</u> current systems may have quite a different geometry in three dimensions. As an example, even certain classes of electrojets, which may in fact be terminated at either end by field-aligned currents, generate electromagnetic field variations over restricted regions at the earth's surface which can be represented as the fields of equivalent current sheets such as (15). Above the source of course, or within the source, the expressions will be completely different. However the concept of equivalent sheet current sources is a useful artifice for evaluating electromagnetic perturbations at the earth's surface when the sources are some distance above; particularly when the sources become quasi two-dimensional as they seem to do for many classes of electromagnetic phenomena ranging from pulsations to magnetic substorms. In order to emphasize that it is the <u>effects</u> of the current system that we are attempting to simulate over a limited region of interest, rather than attempting to physically model the sources themselves, the sheet current represented in (15) will be termed an <u>equivalent</u> sheet current density (e.g. used by Price, 1962).

Electromagnetic Field Components

Directly beneath the source represented by (15) and immediately adjacent to it, we must have, for the source field alone,

$$H_x = J_y/2 \quad , \tag{16}$$

where, for convenience in this and all following equations, we suppress the k index whenever possible without leading to confusion in the resulting terms.

An appropriate form for the horizontal component of the magnetic field observed at a position (x,z) beneath a source at (x_o,z_o) in a homogeneous medium is, according to Hermance (1978),

$$H_x = (I_o/2)\ \exp[-\gamma(z-z_o)]\cos k(x-x_o) \quad , \tag{17}$$

where $\gamma = (k^2 + i\omega\mu\sigma - \omega^2\mu\varepsilon)^{1/2}$. For convenience we will use the following constants to represent the arguments of the terms in (17):

$$\theta_z = \gamma(z-z_o) \quad , \tag{18a}$$

$$\theta_x = k(x-x_o) \quad . \tag{18b}$$

For the class of problems considered here, we will assume $\underline{B} = \mu_o \underline{H}$ everywhere, where $\mu_o = 4\pi \times 10^{-7}$ henries/m is the permeability of free space. In this case

$$\nabla \cdot \underline{H} = 0 \tag{19}$$

everywhere, and we are led to the following condition on the derivatives:

$$\partial H_z/\partial z = -\partial H_x/\partial x \ . \tag{20}$$

Upon substituting (17) for H_x, and taking the derivative with respect to x on the right hand side, we have

$$\partial H_z/\partial z = (I_o k/2)\ \exp(-\theta_z)\sin\theta_x \ , \tag{21}$$

which can be easily integrated to the form

$$H_z = -[I_o k/(2\gamma)]\ \exp(-\theta_z)\sin\theta_x \ . \tag{22}$$

The electric field has only a y-component and is related to the magnetic field components through Faraday's Law of Induction. In other words, if we assume the following form for the electric field of the source:

$$E_y = B_o^s\ \exp(-\theta_z)\cos\theta_x \ , \tag{23}$$

the coefficient B_o^s is determined from

$$\underline{H} = -(1/i\omega\mu)\nabla\mathrm{x}\underline{E} \ . \tag{24}$$

Upon taking the curl of the electric field on the right hand side of (24), we obtain

$$H_x = (1/i\omega\mu)\ \partial E_y/\partial z \tag{25a}$$

$$= -(\gamma/i\omega\mu)B_o^s\ \exp(-\theta_z)\cos\theta_x \ , \tag{25b}$$

and

$$H_z = (k/i\omega\mu)B_o^s\ \exp(-\theta_z)\sin\theta_x \ . \tag{26}$$

By comparison of (25) with (17), or (26) with (22) it is clear that

$$B_o = -[i\omega\mu I_o/(2\gamma)] \ . \tag{27}$$

To summarize, we assume an equivalent sheet current having the spatial form

$$J_y = I_o \ \delta(z-z_o)\cos\theta_x \tag{28}$$

where I_o is the fixed amplitude of the spatial harmonic at the wavenumber k, and $\theta_x = k(x-x_o)$ so that the source is centered at $x = x_o$. In this case the source-field electromagnetic field components at a distance $z - z_o$ in a homogeneous medium beneath the source are given by

$$E_y = -[i\omega\mu I_o/(2\gamma)] \ \exp(-\theta_z)\cos\theta_x \ , \tag{29a}$$

$$H_x = (I_o/2) \ \exp(-\theta_z)\cos\theta_x \ , \tag{29b}$$

$$H_z = -[I_o k/(2\gamma)] \ \exp(-\theta_z)\sin\theta_x \ , \tag{29c}$$

where $\theta_z = \gamma(z-z_o)$. On the other hand, in the medium above the source we have the following expressions for the source field components:

$$E_y = -[i\omega\mu I_o/(2\gamma)] \ \exp(+\theta_z)\cos\theta_x \ , \tag{30a}$$

$$H_x = -(I_o/2) \ \exp(+\theta_z)\cos\theta_x \ , \tag{30b}$$

$$H_z = -[I_o k/(2\gamma)] \ \exp(+\theta_z)\sin\theta_x \ . \tag{30c}$$

Hence the electric field of the source has the same spatial dependence as the horizontal magnetic field component, whereas it has the opposite sense to the direction of current flow. A few moments thought and the right-hand-rule will justify the fact that H_z is maximum at positions of x for which J_y and H_x are minimum.

A Downward-Propagating Recursion Relation

We assume that in the medium between each node along the left and right hand vertical boundaries we have the following expressions for the total (source plus induced) electromagnetic field components:

$$E_{yj} = [A_j \exp(\gamma_j z) + B_j \exp(-\gamma_j z)]\cos\theta_x \ , \tag{31a}$$

$$H_{xj} = (\gamma_j/i\omega\mu)[A_j \exp(\gamma_j z) - B_j \exp(-\gamma_j z)]\cos\theta_x \ , \tag{31b}$$

$$H_{zj} = (k/i\omega\mu)[A_j \exp(\gamma_j z) + B_j \exp(-\gamma_j z)]\sin\theta_x \ . \tag{31c}$$

The subscript j refers to field values and material constants appropriate for the jth medium, defined in our convention as the region directly below the jth node, but above the j + 1 node.

To be definite, we assume the equivalent sheet current source is in free-space above, but infinitesimally close to the $j = j_s$ node. We also assume that the surface impedance $Z^j\big|_{j_s}$ at this node has already been calculated, hence we have the condition that

$$Z^j\Big|_{j_s} = -E_{yj}/H_{xj}\Big|_{j_s} \tag{32}$$

For the special case when $j_s = 1$, we will assume the source is immediately above, but closely adjacent to the topmost row of nodes. In the latter situation we will assume that it is appropriate to apply Dirichlet boundary conditions along the topmost row of nodes which represent the total (source plus induced) field components above a plane-layered earth. For this to be possible, any lateral heterogeneities must be well within the interior of our finite difference mesh, the left and right hand conductivity structure must be plane-layered and identical, and the scale-size of the heterogeneity must be small compared to its distance from any boundary. Although somewhat restrictive, these conditions still permit asymmetric source fields (i.e. in general $\cos\theta_x^{lhs} \neq \cos\theta_x^{rhs}$), and the lateral heterogeneity need not be symmetric.

We assume that in the infinitesimally thin region between the source and the j_s interface, the electric field can be represented by

$$E_y = -[i\omega\mu I_0/(2\gamma_0)]\{\exp(-\gamma_0 z) - R(k)\exp(\gamma_0 z)\}\cos\theta_x \ , \quad (33)$$

where $\gamma_0 = (k^2 - \omega^2\mu\varepsilon)^{1/2}$ and $R(k)$ is the reflection coefficient. The corresponding horizontal magnetic field is given by

$$H_x = (I_0/2)\{\exp(-\gamma_0 z) + R(k)\exp(\gamma_0 z)\}\cos\theta_x \ . \quad (34)$$

Upon taking the ratio of (33) to (34) at $z = 0$ and equating the result to the surface impedance $-Z^j\big|_{j_s}$ we obtain

$$-Z^j\Big|_{j_s} = -(i\omega\mu/\gamma_0)\{[1-R]/[1+R]\} \quad (35)$$

which can be solved for the reflection coefficient

$$R(k) = [(Z_o - Z^j)/(Z_o + Z^j)]_{j=j_s} \tag{36}$$

where $Z_o = i\omega\mu/\gamma_o$ is the generalized characteristic impedance of free-space (i.e. includes the spatial wavenumber, k).

At the j_s interface we equate the horizontal electric field components across the j_s-1 and j_s media, as well as the horizontal magnetic field components. Using (31a) and (31b), this leads to

$$E_y\Big|_{j_s} = (A_j + B_j)\cos\theta_x \quad , \tag{37}$$

$$H_x\Big|_{j_s} = (1/Z_o)(A_j - B_j)\cos\theta_x \quad , \tag{38}$$

the left hand sides of the equations being given by (33) and (34) respectively. We might note at this point the general applicability of relations of this form to any interface, such that the electric and magnetic field components at the bottom of any layer, j-1, is related to the coefficients in the layer, j, below, through the forms

$$E_y^{j-1}\Big|_j = (A_j + B_j)\cos\theta_x \ , \tag{39}$$

$$H_x^{j-1}\Big|_j = (1/Z_j)(A_j - B_j)\cos\theta_x \ , \tag{40}$$

where the expressions are evaluated at the j interface. We can solve for the coefficients

$$A_j = (1/2)[E_y^{j-1}\Big|_j + Z_j H_x^{j-1}\Big|_j]/\cos\theta_x \quad , \tag{41a}$$

$$B_j = (1/2)[E_y^{j-1}\Big|_j - Z_j H_x^{j-1}\Big|_j]/\cos\theta_x \quad . \qquad (41b)$$

Using the forms (31a) and (31b) we can now determine the electric and magnetic field components at the <u>bottom</u> of the jth layer through (31a) and (31b) such that

$$E_y^j\Big|_{j+1} = [A_j \exp(\alpha_j) + B_j \exp(-\alpha_j)]\cos\theta_x \quad , \qquad (42a)$$

and

$$H_x^j\Big|_{j+1} = (1/Z_j)[A_j \exp(\alpha_j) - B_j \exp(-\alpha_j)]\cos\theta_x \ , \quad (42b)$$

where $\alpha_j = \gamma_j d_j$.

We now have the architecture for developing a recursion relation for the downward propagation of field values at each node. We begin at the interface directly below the source by determining the surface impedance, and from (36), the reflection coefficient. The reflection coefficient is substituted into (33) and (34) to yield E_y and H_x, respectively. These expressions are substituted into (41a) and (41b), along with the appropriate characteristic impedance Z_j, to yield the coefficients A_j and B_j. The coefficients are next substituted into (42a) and (42b) multiplied by the exponential factors which are indicated and result in values for the electric and magnetic field components at the next lower interface. We have essentially continued our fields downward from the jth interface to the j+1 interface.

This process can be iterated until we reach the bottom of the grid. If this is done numerically, then it is usually advantageous to evaluate the magnitude of the field components, normalized by the values directly beneath the source, say, and when the magnitudes become vanishingly small, to set nodal values at greater depth equal to zero.

Propagating the Recursion Relation Above the Source

In the medium above the source we must consider source terms which decrease with altitude. For the sake of simplicity, we neglect the effects of reflections above the source so that at the jth node we have

$$E_y = -[i\omega\mu I_o/(2\gamma_o)]\{\exp(\alpha_j) - R(k)\exp(\alpha_j)\}\cos\theta_x \quad , \qquad (43a)$$

$$H_x = (I_o/2)\{-\exp(\alpha_j) + R(k)\exp(\alpha_j)\}\cos\theta_x \quad , \qquad (43b)$$

and

$$H_z = -[I_o k/(2\gamma_o)]\{\exp(\alpha_j) - R(k)\exp(\alpha_j)\}\sin\theta_x \quad , \qquad (43c)$$

where $\alpha_j = \gamma_o z_j$, such that $\gamma_o = (k^2 - \omega^2\mu\varepsilon)^{1/2}$, and z is measured relative to a coordinate system having its origin (z=0) at the source, $j=j_s$ (z increasing positive downward). These relations are simply used to calculate E_j, H_{xj} and H_{zj} at each node, j, above the source, after z_j is specified.

BOUNDARY CONDITIONS AT THE TOP-MOST AND BOTTOM-MOST ROW OF NODES

Impedance Boundary Conditions

We assume that all sources are contained within the region spanned by the model and that no reflections occur from above the top-most nor from below the bottom-most row of nodes. Hence the flow of power is everywhere outward through the top and bottom boundaries of our model and we are able to impose a generalized impedance condition on the fields crossing these boundaries.

At the top-most boundary we impose the condition that

$$E_y/H_x\Big|_{z=z_t} = Z_t \quad , \tag{44a}$$

$$= i\omega\mu/\gamma_t \quad , \tag{44b}$$

where $\gamma_t = (k^2 + i\omega\mu\sigma_t - \omega^2\mu\varepsilon)$; the subscript, t, denoting the material parameters associated with the homogeneous region at and beyond the top boundary. The positive impedance term in (44a) is compatible with the upward flux of power.

We have, of course, from Faraday's Law of Induction (1), that

$$H_x = (1/i\omega\mu)\partial E_y/\partial z \quad , \tag{45}$$

so that the condition (44b) can be posed as a condition on the electric field E_y and its vertical derivative such that, at $z=z_t$,

$$E_y - (1/\gamma_t)\partial E_y/\partial z = 0 \quad . \tag{46}$$

At the bottom-most boundary we have downward flowing power and impose the condition that

$$E_y/H_x\Big|_{z=z_b} = -Z_b \qquad (47a)$$

$$\approx -i\omega\mu/\gamma_b \qquad (47b)$$

which, upon invoking (45), can be expressed at $z=z_b$ as

$$E_y + (1/\gamma_b)\partial E_y/\partial z = 0 \ . \qquad (48)$$

IMPLEMENTATION OF THE THEORY
USING FINITE DIFFERENCE SIMULATION

A General Finite Difference Operator

The numerical solution of problems concerned with electromagnetic induction in heterogeneous structures can be accomplished using a number of techniques (see, for example, the review by Ward et al. 1974). Of these techniques, we have chosen to employ the finite difference method. In brief, the present formulation has the following four features.

First, complex field quantities are calculated directly. This facilitates setting up and checking the original finite difference simulation. It is, however, advisable to use double precision arithmetic in the computer code to minimize round-off error.

Second, variable node spacing is permitted throughout. Although this feature is in the code published by Jones and Pascoe (1971), the simulation discussed below is generally of a higher degree approximation. On the other hand, a simulation published by Ward et al. (1974), although of the same degree approximation as the one considered here, is for a single-valued constant nodal spacing.

Third, the earth may be generally heterogeneous in two dimensions. The simulation is developed so that the nodes are placed at the corners of infinitely long two-dimensional rectangular prisms. Each neighboring prism can be assigned a distinct value of resistivity. The general finite difference template then uses a five-point, second degree approximation for the most pathologic situation - the case of four dissimilar rectangular prisms abutting one another in the vicinity of the center point. Clearly, all cases of lesser pathology can be deduced from this situation and, in the case of a homogeneous material with equal nodal spacing, our general template reduces to the simple homogeneous finite difference simulation of the time-harmonic diffusion equation (Ward et al. 1974).

Fourth, and finally, machine coding using the general operator is enormously simplified because the boundary conditions to be applied between dissimilar materials are implicitly handled by the relation. Therefore, to determine the coupling matrix, one needs only to specify the resistivity of each rectangular prism and then simply apply the operator sequentially centered at each nodal point. Although this latter feature is present in the code of Jones and Pascoe (1971), from their discussion one is not aware of the degree of accuracy of their approximation in the vicinity of discontinuities. Furthermore, even though Jones and Thompson (1974) acknowledge that the suggestions of Williamson et al. (1974) can improve the degree of approximation in a homogeneous region, they have not shown the degree of approximation in the neighborhood of discontinuities. It seems appropriate therefore at the present state of literature to formulate a finite difference scheme with careful attention to the approximations involved. This is the intention of the following discussion.

Decoupling the Field Equations. It is well known that Maxwell's equations in the M.K.S.A. system reduce to the following forms:

$$\nabla \times \underline{H} = (\sigma_{dc} + i\omega\varepsilon)\underline{E} \tag{49}$$

$$\nabla \times \underline{E} = -i\omega\mu\ \underline{H} \tag{50}$$

$$\nabla \cdot \underline{E} = 0 \tag{51}$$

$$\nabla \cdot \underline{H} = 0 \tag{52}$$

when one assumes the usual constitutive relations (σ_{dc} being the true of d.c. conductivity), a time dependence of the form $\exp(i\omega t)$, and that ε, the permittivity, and μ, the permeability, are the same everywhere. Equation (49) leads to the condition that the total current is divergence-free, or that

$$\nabla \cdot (\underline{J} + \partial\underline{D}/\partial t) = 0 \tag{53}$$

where $\underline{J}$ is the true conduction current and $\partial\underline{D}/\partial t$ is the displacement current. Assuming that the tangential magnetic field is continuous across interfaces is sufficient to ensure that (53) is implicitly observed. A second boundary condition is that the tangential electric field is continuous across interfaces. We simplify the writing of (49) somewhat if we let $\sigma = \sigma_{d.c.} + i\omega\varepsilon$, where we call σ the total conductivity and let it be equal to the sum of the d.c. conductivity, $\sigma_{d.c.}$, plus the term $i\omega\varepsilon$.

If one is in the principal coordinate system of a two-dimensional inhomogeneity such that the structure strikes in the y-direction, then for the class of source fields considered here, all derivatives of the fields with respect to y vanish. Moreover, the set of equations (49) through (52) decouples into two independent modes.

One mode is determined by the set of equations relating E_x, E_z and H_y through

$$\sigma E_x = -\partial H_y/\partial z \tag{54a}$$

$$\sigma E_z = \partial H_y/\partial x \tag{54b}$$

$$i\omega\mu H_y = -(\partial E_x/\partial z - \partial E_z/\partial x) \tag{54c}$$

and is known as the magnetic polarization, the H-parallel or the TM (transverse magnetic) mode. We see that if in some way the <u>magnetic field</u> component parallel to strike (H_y) is determined everywhere, then E_x and E_z can be determined using (54a) and (54b) respectively.

The other mode is determined by the set of equations relating H_x, H_z and E_y through

$$\sigma E_y = (\partial H_x/\partial z - \partial H_z/\partial x) \tag{55a}$$

$$i\omega\mu H_x = \partial E_y/\partial z \tag{55b}$$

$$i\omega\mu H_z = -\partial E_y/\partial x \tag{55c}$$

and is known as the electric polarization, the E-parallel or the TE (transverse electric) mode. We see, in this case, that if in some way the <u>electric field</u> component parallel to strike

(E_y) is determined everywhere, then H_x and H_z can be determined using (55b) and (55c), respectively.

Clearly the behavior of the fields for an arbitrary polarization of the source field can be decomposed into two principal modes and, conversely, the two principal modes can be used to synthesize the solution for any arbitrary polarization. In the case considered here, the two-dimensional heterogeneity is oriented so that its strike is parallel to the direction of current flow in the source, hence we need to consider induction for the transverse electric (TE or E-parallel) case. The TM (or transverse magnetic) case will be considered in subsequent work.

Operator for Electric Polarization. The electric polarization mode is determined by the solution of equation set (55). We assume that the nodal point P is at the boundary between four electrically dissimilar regions as shown in Figure 6. In this case, we assume that in each of the regions the electric field, E_y, can be locally approximated by a quadratic function $e_j(x,z)$, where the subscript denotes the jth prism ($j = 1$ to 4) adjacent to the point P. Each quadratic function, $e_j(x,z)$, can be expanded as a Taylor series in the vicinity of the point P, but in the jth region. For example, along either of the planes bounding region 1,

$$e_1(x,z) = e_1(0,0) + x\partial e_1/\partial x + z\partial e_1/\partial z + (x^2/2)\partial^2 e_1/\partial x^2 + (z^2/2)\partial^2 e_1/\partial z^2 \qquad (56)$$

with similar expressions for e_2, e_3 and e_4. Continuity of the tangential electric field requires that

$$e_1(0,0) \equiv e_2(0,0) \equiv e_3(0,0) \equiv e_4(0,0) \equiv e_P \quad , \qquad (57a)$$

along with the following conditions at each of the nodes shown in Figure 7:

$$e_1(0,-d_N) \equiv e_4(0,-d_N) \equiv e_N \quad , \qquad (57b)$$

$$e_1(-d_W,0) \equiv e_2(-d_W,0) \equiv e_W \quad , \qquad (57c)$$

$$e_2(0,d_S) \equiv e_3(0,d_S) \equiv e_S \quad , \qquad (57d)$$

$$e_3(d_E,0) \equiv e_4(d_E,0) \equiv e_E \quad . \qquad (57e)$$

Continuity of the tangential magnetic field across each interface implies, from (55b), that along the 1-2 interface

$$\partial e_1/\partial z = \partial e_2/\partial z \quad . \qquad (58a)$$

Along the 2-3 interface, (55c) implies

$$\partial e_2/\partial x = \partial e_3/\partial x \quad . \qquad (58b)$$

Along the 3-4 interface, (55b) implies

$$\partial e_3/\partial z = \partial e_4/\partial z \quad . \qquad (58c)$$

And finally, along the 4-1 interface, (55c) implies

$$\partial e_4/\partial x = \partial e_1/\partial x \quad . \qquad (58d)$$

Expressions for each e_j, written in the form (56), can be rearranged to determine the appropriate first partial derivatives which are needed for substitution into relations (58a) through (58d). These Taylor series approximations can be combined and rearranged by making use of the fact that in each region j the second derivatives of the electric field are related through the diffusion equation

$$\partial^2 e_j/\partial x^2 + \partial^2 e_j/\partial z^2 = i\omega\mu\sigma_j e_j \quad . \tag{59}$$

This leads to the following form for the electric polarization operator:

$$\begin{aligned} e_P &- (d_W + d_E)(e_N - e_P)/2d_N\beta_e - (d_W + d_E)(e_S - e_P)/2d_S\beta_e \\ &- (d_N + d_S)(e_W - e_P)/2d_W\beta_e - (d_N + d_S)(e_E - e_P)/2d_E\beta_e = 0 \quad , \end{aligned} \tag{60}$$

where β_e, the electric polarization induction parameter, is given by

$$\beta_e = i\omega\mu(\sigma_1 d_N d_W + \sigma_2 d_W d_S + \sigma_3 d_S d_E + \sigma_4 d_N d_E)/4 \quad . \tag{61}$$

Expression (60) is the finite difference operator we need for simulating the behavior of the electromagnetic fields at all nodal points interior to the boundaries of our modelling region, exclusive of the region of the source current itself.

Finite Difference Simulation of the Boundary Conditions, $z = \pm\infty$

It is straight-forward to replace the vertical derivatives in (46) or (48) with their appropriate finite forward or backward difference counterpart, such that they can be respectively written as

$$e_p - (1/\gamma_t)(e_s - e_p)/d_s = 0 \quad , \tag{62}$$

and

$$e_p + (1/\gamma_b)(e_p - e_n)/d_n = 0 \quad . \tag{63}$$

However, these expressions suffer some loss of accuracy because the forward and backward difference formulae are accurate to second degree only at the mid-point of the layer which is adjacent to the nodal point P (Forsythe and Wasow, 1960). We can compensate for curvature effects on the field quantities through taking into account second derivative terms as shown in the following section.

Top-most and Bottom-most Nodal Planes

We assume that $e_y(x,z)$ can be represented by a Taylor's series expression in the medium immediately adjacent to and below a representative node, P, at the top-most nodal plane $(z=z_t)$. The vertical derivative at $z=z_t$ can be expressed, to second degree accuracy, as

$$\partial E_y/\partial z\Big|_{z_t} \approx [(e_s-e_p)/d_s] - (d_s/2)\partial^2 e_y/\partial z^2 \quad . \qquad (64)$$

From the diffusion equation for E_y we have

$$\partial^2 e_y/\partial z^2 = i\omega\mu\sigma_t e_y - \partial^2 e_y/\partial x^2 \quad , \qquad (65)$$

which can be substituted into (64) to yield, in terms of finite difference forms,

$$(\partial E_y/\partial z)\Big|_{z_t} \approx [(e_s-e_p)/d_s] - (i\omega\mu\sigma_t d_s/2)e_p + (d_s/2)D_{xx}(e_y) \qquad (66)$$

where the operator,

$$\begin{aligned} D_{xx}(e_y) = {} & \{2/[d_E(d_W+d_E)]\}e_E - \{2/(d_E d_W)\}e_P \\ & +\{2/[d_W(d_W+d_E)]\}e_W \quad , \end{aligned} \qquad (67)$$

is the second finite difference simulation of $\partial^2 E_y/\partial x^2$ (Forsythe and Wasow, 1960). We now substitute (66) into (46) to obtain the following mixed boundary condition at $z=z_t$:

$$\gamma_t d_s e_p - [(e_s-e_p) - i\omega\mu\sigma_t d_s^2/2)e_p + (d_s^2/2)D_{xx}(e_y)] = 0 \quad . \qquad (68)$$

An analogous condition for the bottom-most nodal plane can be expressed as the following:

$$\gamma_b d_N e_p + [(e_p - e_N) + i\omega\mu\sigma_b d_N^2/2) e_p - (d_N^2/2) D_{xx}(e_y) = 0 \ . \qquad (69)$$

FINITE DIFFERENCE SIMULATION OF THE SOURCE FIELD WITHIN THE INTERIOR OF THE MESH

We assume for the purpose of this discussion that the source is a thin horizontal current sheet such that, as described above,

$$J_y = I_o \cos\theta_x \quad . \tag{70}$$

The geometry in Figure 8 represents a 5-point cell which contains the current sheet and whose center point, P, is immediately below the current sheet. We assume that for cells having dimensions small compared to the spatial wavelength of the source, λ_s, one can reasonably approximate Ampere's Circuital Law in integral form

$$\oint \underline{H} \cdot \underline{dl} = \iint J \cdot dA \quad , \tag{71}$$

with the expression

$$H_{x1}d_1 - H_{z2}d_2 - H_{x3}d_3 + H_{z4}d_4 = \int I_o \cos\theta_x d_x \quad , \tag{72}$$

where H_{x1}, for example with reference to Figure 8, represents the horizontal magnetic field component evaluated half-way along the line P-S and projected along the length of the contour element d_1. Furthermore, we assume that the length $d_1 = (d_W+d_E)/2$ and that the respective magnetic field components evaluated half-way along each nodal spacing can be reasonably approximated by finite difference expressions in the form of centered differences. In other words, we express the left hand side of

(72) as

$$\begin{aligned} & H_{x1}d_1 - H_{z2}d_2 - H_{x3}d_3 + H_{z4}d_4 = \\ & (1/i\omega\mu)(\partial E_y/\partial z)\Big|_S (d_W+d_E)/2 + (1/i\omega\mu)(\partial E_y/\partial x)\Big|_E (d_S+d_N)/2 \\ & -(1/i\omega\mu)(\partial E_y/\partial z)\Big|_N (d_W+d_E)/2 - (1/i\omega\mu)(\partial E_y/\partial x)\Big|_W (d_S+d_N)/2 \\ & = (1/i\omega\mu)[(d_W+d_E)/2][(e_s-e_p)/d_s] + (1/i\omega\mu)[(d_s+d_N)/2][e_E-e_p)/d_E] \\ & -(1/i\omega\mu)[(d_W+d_E)/2][(e_p-e_N)/d_N] - (1/i\omega\mu)[(d_s+d_N)/2][(e_p-e_W)/d_W] \ . \end{aligned} \tag{73}$$

The right hand side of expression (72) can be integrated analytically,

$$\iint J \cdot dA = I_o \int_{x_p-d_W/2}^{x_p+d_E/2} \cos[k(x-x_o)]dx \quad , \tag{74}$$

leading to

$$\iint J \cdot dA = (I_o/k)[\sin k(x_p-x_o+d_E/2) - \sin k(x_p-x_o-d_W/2)] \quad . \tag{75}$$

If k approaches 0, then the right hand side of (75) approaches $I_o(d_W+d_E)/2$, as one would expect.

Equating (73) to (75) provides the finite difference simulation of the source field condition at the nodal point P within the interior of the mesh.

RESULTS

Design Criteria for Mesh Spacing

The case when the source field itself has a finite dimension imposes additional considerations for the problem of designing adequate 2-D models. In general, the source field itself behaves according to the relation

$$H_x^o \propto \exp(-kz)[\cos(kx) + i\sin(kx)] \quad ,$$

where $k = 2\pi/\lambda_s$, x is the horizontal distance and z is the vertical distance. Hence the mesh spacing, Δs, must be sufficiently dense to allow quadratic forms employed by the numerical algorithm to adequately represent trigenometric functions in the horizontal direction and exponentially damped functions in the vertical dimension. This suggests that to account for the finite dimensions of the source field, $\Delta s \leq \lambda_s/12.5$, for well-designed models.

The induced field, of course, not only has a finite wave number equivalent to that of the source but may also be modulated by geometrical terms like

$$\exp(-d/\delta)$$

where d is a distance parameter and δ is the depth of penetration. In some cases, close to electrical discontinuities the induced field may behave more like $1/r$ or $1/r^2$. This often necessitates excessively close nodal spacing near electrical discontinuities.

For the case of uniform source fields incident on a 2-D earth, one often increases the nodal spacing to very large values as one approaches the edges of the model. Generally, this is inappropriate for finite source fields since, even as one approaches the edges of the model, it is required that $\Delta s \leq \lambda_s/12.5$.

Testing the Algorithm

This section describes several of many tests to which the computer code was subjected. Figure 9 shows the behavior of only the source field in the interior of a rectilinear modelling region. The conductivity of the earth was set equal to the value of free-space and the source field was assigned a spatial wavelength of 200 km. The model values are shown as solid points in the figure and the straight line indicates the corresponding theoretical results. Besides showing the good agreement between the model and the theoretical results, this figure also shows the rapidity with which source fields having wavelengths of 200 km or less are damped with distance below them - field amplitudes are reduced by an order of magnitude at a distance of only 70 km beneath the source.

The effects of attenuation due to induction in an earth having a finite resistivity are shown in Figure 10. Here the value of the electric field at a point within the earth is normalized by its amplitude at the surface of a homogeneous half-space having a resistivity of 1 ohm-m; the period of the source is 1 sec and its spatial wavelength is again 200 km. The values of these parameters are chosen so that electromagnetic induction effects clearly dominate the effects of the finite spatial wavelength (i.e. $|\omega\mu\sigma| >> k^2$). The solid points correspond to the model values and the straight line corresponds to the theoretical attenuation associated with a depth of penetration (δ) of 503 m.

Induction Near Lateral Heterogeneities

The simple model shown in Figure 11 was used to examine the typical range of influence associated with anomalous fields near the vicinity of a lateral discontinuity excited by a finite source field. The source has a wavelength of 500 km, a period of 1,684 sec and a current strength of 1 amp/m. The resistivity on either side of the vertical contact is 30 ohm-m and 15 ohm-m, respectively. Distances in Figure 11 are actually shown to scale relative to the source wavelength and the relevant skin depths in each medium.

Magnetic field values calculated for the model are shown as points in Figure 12; the open squares correspond to the values for H_x, the open circles correspond to the values for H_z. The solid lines correspond to the theoretical H_x and H_z fields for the equivalent source field above a homogeneous half-space having a resistivity of 30 ohm-m; the dashed lines correspond to the theoretical fields for a homogeneous half-space of 15 ohm-m.

It should be clear that at some distance to the left of the contact, the numerical results for both horizontal and vertical magnetic field values fall on the corresponding theoretical curve for a 30 ohm-m homogeneous half-space. Similarly, at some distance to the right of the contact, the numerical results correspond to the results for a homogeneous half-space of 15 ohm-m.

What is surprising is that the model makes the transition between these two asymptotic limits within a very small distance of the contact. To all practical purposes, the transition occurs with 20 km or so of the contact. This implies that the scale length of the perturbation due to the contact is much less than either the corresponding depth of penetration in the representative media, or of the spatial wavelength of the source field.

These results suggest that while fields may be perturbed in the close vicinity of lateral heterogeneities, at even modest offset distances from the contact the fields are more influenced by what is beneath the observer than by what is at some lateral distance away. This implies that in many cases, simple 1-D plane-layered models may be appropriately used in interpreting field data in a "piece-wise" sense, even when the total structure is more complicated laterally.

Magnetic Gradiometry Across Mega-Tectonic Features

The fact that the fields induced by finite sources tend to decouple fairly rapidly with distance to either side of a vertical discontinuity prompted us to consider the effects that this phenomenon has on magnetic gradiometric experiments. Schmucker (1970) and Kuckes (1973) have shown that one can determine an apparent conductivity (σ_a) for the earth through calculating the ratio of the horizontal gradient of the horizontal field ($\partial H_x/\partial x$) to the amplitude of the vertical field (H_z). The relevant expression when $\lambda_s >> \delta$, is

$$\sigma_a = (1/\omega\mu)\,|(\partial H_x/\partial x)/H_z|^2 \quad .$$

We have applied this relation to calculating the apparent resistivity ($\rho_a = 1/\sigma_a$) in the vicinity of a large scale discontinuity in the conductivity of the earth. Our model is simply a vertical discontinuity separating two quarter-spaces having resistivities of 30 ohm-m and 15 ohm-m respectively (Figure 13). A source field having a spatial wavelength of 20,000 km is located so that H_z is maximum over the contact and the gradient, $\partial H_x/\partial x$, is essentially linear. The period of the source is 10,800 sec (3 hr). After calculating the fields produced by such a model, two points were selected, point (1), in Figure 13, at -600 km, and point (2) at +400 km from the contact. A simple gradient, $\Delta H_x/10^6$m, was then calculated, providing an estimate for $\partial H_x/\partial x$. This <u>regional</u> gradient was then used to calculate <u>local</u> response functions by employing first the vertical field amplitude at point (1) and then the vertical field at point (2).

This allowed us to investigate the efficacy of employing local response functions in the vicinity of lateral discontinuities in the electrical conductivity.

The results of our simple calculations are shown in Table 1, where the true resistivity beneath each site is compared with the magnetotelluric apparent resistivity and with the magnetic gradiometric apparent resistivity. The close agreement between these values is encouraging in that, at least in some cases, regional gradients of the horizontal field (even where the sites span a major discontinuity) can be combined with local values of the vertical field, to yield estimates of electromagnetic response functions.

Comparison of Satellite and Ground-Based Magnetic Variations

We now consider the plane-earth equivalent of the situation illustrated in Figure 14. A satellite, at a nominal altitude of 400 km, passes above an ionospheric current system (at a height of 110 km), along a path which crosses a major geologic contact separating materials having a resistivity contrast of a factor of 2, not untypical of differences in gross continental lithologies. We represent the surface of the earth by an infinite horizontal plane and consider only two-dimensional heterogeneities. Although our numerical model can handle more complicated geologic structures, here we consider only the case of a vertical contact separating two quarter-spaces having resistivities of 30 ohm-m and 15 ohm-m, respectively.

Typical results from our model simulation for ionospheric currents flowing parallel to the geologic discontinuity are shown in Figure 15. Fields at the earth's surface are shown in Figure 15A, whereas fields at the satellite altitude are shown in Figure 15B. In both cases the results for a uniform source field are compared with those for a finite source field (λ_s = 20,000 km) at a period of 10,800 s (3 hr.).

At the earth's surface, there is little difference between the form of the H fields produced by the uniform and the finite source, respectively. The Z fields produced by either source are also quite similar in form. Clearly the behavior of the fields near the vertical discontinuity are dominated by local induction - in other words, the depth of penetration dominates the scaling relation.

The major difference between the results produced by either type of source is that the field amplitudes associated with the finite source field are slightly biased to lower values due to the geometrical spreading factor exp(-kz). For a source with $\lambda_s = 20,000$ km, at a height of 110 km, the field amplitudes at ground level will be reduced to 97% of their maximum values. This is approximately the magnitude of the offset indicated in Figure 15.

At satellite altitudes, the difference between the results for the uniform source field and those for the finite source field are more profound. The total horizontal field amplitude produced by the uniform source is approximately unity, suggesting that for remote sources in the magnetosphere the horizontal field is insensitive to the effects of lateral variations in the earth's conductivity.

On the other hand, the total horizontal field amplitude produced by the finite source field is reduced by more than an order of magnitude. This is due to the fact that the satellite is <u>above</u> the source and, while the H-field for the source itself is southward directed (-x) at satellite altitudes, the induced field is northward directed (+x). The two contributions therefore tend to cancel and the resultant H-field is quite small. At ground level the scale size of the anomalous H field is on the order of 300 km and appears to be controlled by induction effects, whereas at satellite altitudes the scale size is on the order of 1100 - 1200 km and appears to be dominated by the geometrical spreading factor exp(kz).

At satellite altitudes the vertical field produced by the uniform source field is quite small in amplitude and has a half-width of approximately 1000 km. At ground level the vertical field anomaly has a half-width of approximately 250 km and is approximately 5 times stronger in amplitude.

The finite source produces an anomalous vertical field at satellite altitudes which is of the same order of magnitude as that produced by the uniform source, the difference being an apparent skewing of the shape of the finite Z field due to the fact that the anomalous field locally associated with the vertical discontinuity is superimposed on a broad regional field which varies sinusoidally. This regional field is positive for $x < 0$ and negative for $x > 0$. The local anomalous field is negative, hence the sum appears to be skewed to the right (i.e. to $x > 0$) rather than having the symmetrical form of the perturbation associated with the uniform source.

ACKNOWLEDGMENTS

Preparation of this manuscript was supported by NASA Contract Number NAS5-26138 and NSF Contract Number EAR79-11283 to Brown University. Development of the theory and computer code was also supported by the above agencies in terms of its application to global satellite and ground-based magnetic observations. In addition, support was provided to Brown University by the U.S. Department of Energy Office of Basic Energy Sciences Contract Number DE-AC02-79ER10401, NSF Contract Number EAR80-18503, and Office of Naval Research Contract Number N00014-83-K-077 in terms of the application of these calculations to regional magnetic gradiometric interpretations.

REFERENCES

Coggon, J.H., Electromagnetic and electrical modeling by the finite element method, *Geophysics*, *36*, 132-155, 1971.

Forsythe, D.G. and W.R. Wasow, Finite-difference methods for partial differential equations: New York, John Wiley and Sons, 444 p., 1960.

Hermance, J.F., Model simulations of possible electromagnetic induction effects at MAGSAT altitudes, *Geophys. Res. Lett.*, *9*, 373-376, 1982.

Hermance, J.F., Electromagnetic induction by moving ionospheric current systems, *Geophys. J.*, *55*, 557-576, 1978.

Hermance, J.F., and W.R. Peltier, Magnetotelluric fields of a line current, *J. Geophys. Res.*, *75*, 3351-3356, 1970.

Hibbs, R.D., Jr. and F.W. Jones, Electromagnetic induction in the Earth by a non-Symmetric non-uniform source, *J. Geomag. Geoelectr.*, *25*, 75-86, 1973.

Hibbs, R.D., Jr. and F.W. Jones, Electromagnetic induction in the earth by an aperiodic non-uniform current source, *J. Geomag. Geoelec.*, *26*, 39-54, 1974.

Jones, F.W. and L.J. Pascoe, A general computer program to determine the perturbation of alternating electric currents in a two-dimensional model of a region of uniform conductivity with an embedded inhomogeneity, *Geophys. J.R. astr. Soc.*, *23*, 317-334, 1971.

Jones, F.W. and A.T. Price, The perturbations of alternating geomagnetic fields by conductivity anomalies, *Geophys. J.R. astr. Soc.*, *20*, 317-334, 1970.

Kuckes, A., Relations between electrical conductivity of a mantle and fluctuating magnetic fields, *Geophys. J.*, *32*, 119-131, 1973.

Madden, T.R. and C.M. Swift, Jr., Magnetotelluric studies of electrical conductivity structure of the crust and upper mantle, in *Geophys. Monograph 13*, *The Earth's Crust and Upper Mantle*, P.J. Hart, (ed.), 469-479, 1969.

Pascoe, L.J. and F.W. Jones, Boundary conditions and calculations of surface values for the general two-dimensional electromagnetic induction problem, Geophys. J.R. astr. Soc., 27, 179-193, 1972.

Peltier, W.R. and J.F. Hermance, Magnetotelluric fields of a gaussian electrojet, Can. J. Earth Sci., 8, 338-346, 1971.

Price,A.T., The theory of magnetotelluric methods when the source field is considered, J.Geophys.Res., 67, 1907-1918, 1962.

Price, A.T., Electromagnetic induction in a semi-infinite conductor with a plane boundary, Quart. J. Mech. Appl. Math., 3, 385-410, 1950.

Quon, C., K. Vozoff, M. Hoversten, H.F. Morrison, and K.-H. Lee, Localized source effects on magnetotelluric apparent resistivities, J. Geophys., 46, 291-299, 1979.

Schmucker, U., Anomalies of geomagnetic variations in the southwestern United States, Bull. Scripps Inst. Oceanography, 13, 165 pp., Univ. of California Press, Richmond, California, 1970.

Stoyer, C.H. and R.J. Greenfield, Numerical solutions of the response of a two-dimensional earth to an oscillating magnetic dipole, Geophysics, 41, 519-530, 1977.

Swift, C.M., Jr., Theoretical magnetotelluric and turam response from two-dimensional inhomogeneities, Geophys., 36, 38-52, 1971.

Wait, J.R., The fields of a line source of current over a stratified conductor, Appl. Sci. Res., Sec. B., 3, 279-292, 1953.

Ward, S.G., W.J. Peeples, and J. Ryu, Analysis of geoelectromagnetic data In, Methods of computational physics, B.A. Bolt, Ed., New York, Academic Press, p. 163-238, 1973.

Weaver, J.T. and D.J. Thomson, Induction in a non-uniform conducting half-space by an external line current, Geophys. J.R. astr. Soc. 28, 163-185, 1972.

Williamson, K., C. Hewlett and H.Y. Tammemagi, Computer modelling of electrical conductivity structures, Geophys. J.R. astr. Soc., 37, 533-536, 1974.

Wright, J.A., Anisotropic apparent resistivities arising from non-homogeneous two-dimensional structures, Can. J. Earth Sci., 7, 527-531, 1970.

TABLE 1. Comparison of Local Response Parameters Using Regional Horizontal Field Gradients

Source Field Wave-Length = 20,000 km
Period = 10,800 sec (3 hr)

	Resistivity, ohm-m		
	True	Magnetotelluric	Magnetic Gradiometric
Site 1	30	29	27
Site 2	15	15	16

FIGURE CAPTIONS

Figure 1. Geometry of the problem considered in this paper. An equivalent current source, $J_y(x)$ flows at some height parallel to the earth's surface and parallel to the axis of a 2-D inhomogeneity which has a characteristic scale dimension L.

Figure 2. One approach to the problem when typical wavelengths for the source field, λ_s, are much greater than the dimensions of the inhomogeneity L. Values for the source field and some average reflectance for the earth are assumed along the top plane of the modelling region.

Figure 3. A situation where only the source field is assumed to have appreciable magnitudes in some region of space (or the modelling region) and where all fields are assumed to tend to zero at the remote edges of the model. In general this requires that $\lambda_s << L$.

Figure 4. Details of the model considered in present paper. The finite source is located <u>within</u> the modelling region and characteristic impedance conditions for a finite source are imposed at the top-most and bottom-most edges. Earth structures, while having to be plane-layered, may be different at the left and right edges.

Figure 5. An equivalent current sheet source flowing parallel to the earth's surface.

Figure 6. The situation of four dissimilar materials abutting at a contact.

Figure 7. Convention for indicating nearest neighbor nodes surrounding the central node P (following Forsythe and Wasow; 1960). The various media surrounding the central node P are indicated by j = 1 to 4.

Figure 8. Geometry and conventions used to simulate a discontinuity in the horizontal sheet current density $J_y(x)$, flowing above, but adjacent to a nodal point P. The shaded region represents the amplitude of an infinitesimal thin sheet current J_y as a function of z. The dashed contour with arrows represents the line integral used to evaluate Ampere's Law.

Figure 9. Comparison of model results (solid points) and analytical results (solid line) for the source field alone.

Figure 10. Comparison of model results (solid points) and analytical results (solid line) when attenuation of the field due to electromagnetic induction dominates its behavior.

Figure 11. Model geometry used to illustrate the coupling of fields across a contact.

Figure 12. The behavior of model field values (see Figure 11) for H_x (squares) and H_z (circles) across a contact compared with analytical results for a homogeneous earth having a

resistivity of 30 ohm-m (solid line) and 15 ohm-m (dashed line).

Figure 13. A simulation of magnetic gradiometry across a vertical contact separating 30 ohm-m and 15 ohm-m materials. The source field has a spatial wavelength of 20,000 km and a period of 10,800 sec (3 hr). Results are summarized in Table 1.

Figure 14. Geometry representing a satellite orbiting at a height of 400 km, an ionospheric current source at a height of 110 km, and a vertical electrical contact separating gross earth lithologies having resistivities of 30 ohm-m and 15 ohm-m, respectively.

Figure 15. Comparison of simulated satellite and ground-based observations of magnetic variations. The H field is horizontal and directed toward increasing x; the Z field is vertical and directed downward. The signs in brackets are associated with the various branches of the curves used to denote the amplitude of the respective field amplitudes. Panel A: H and Z fields observed on the earth's surface; Panel B: H and Z fields observed at satellite altitudes (400 km). All field amplitudes represent the sum of the source <u>and</u> the induced field components.

TABLE 1. Comparison of Local Response Parameters Using Regional Horizontal Field Gradients

Source Field Wave-Length = 20,000 km
Period = 10,800 sec (3 hr)

	Resistivity, ohm-m		
	True	Magnetotelluric	Magnetic Gradiometric
Site 1	30	29	27
Site 2	15	15	16

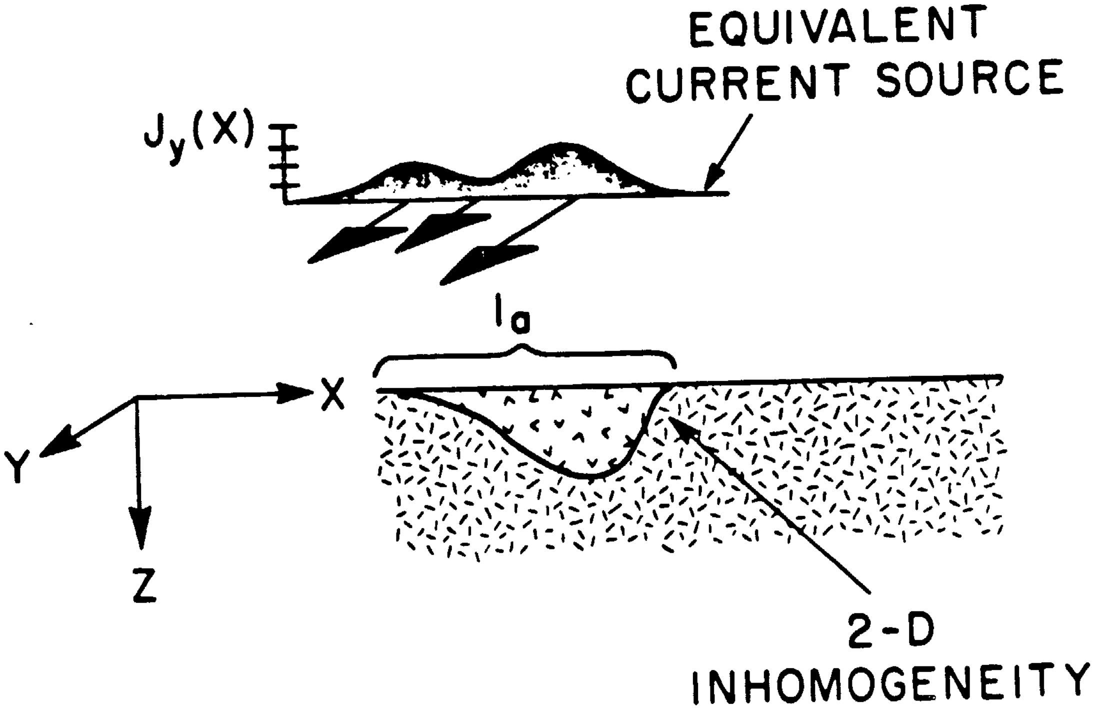

FIGURE 1.

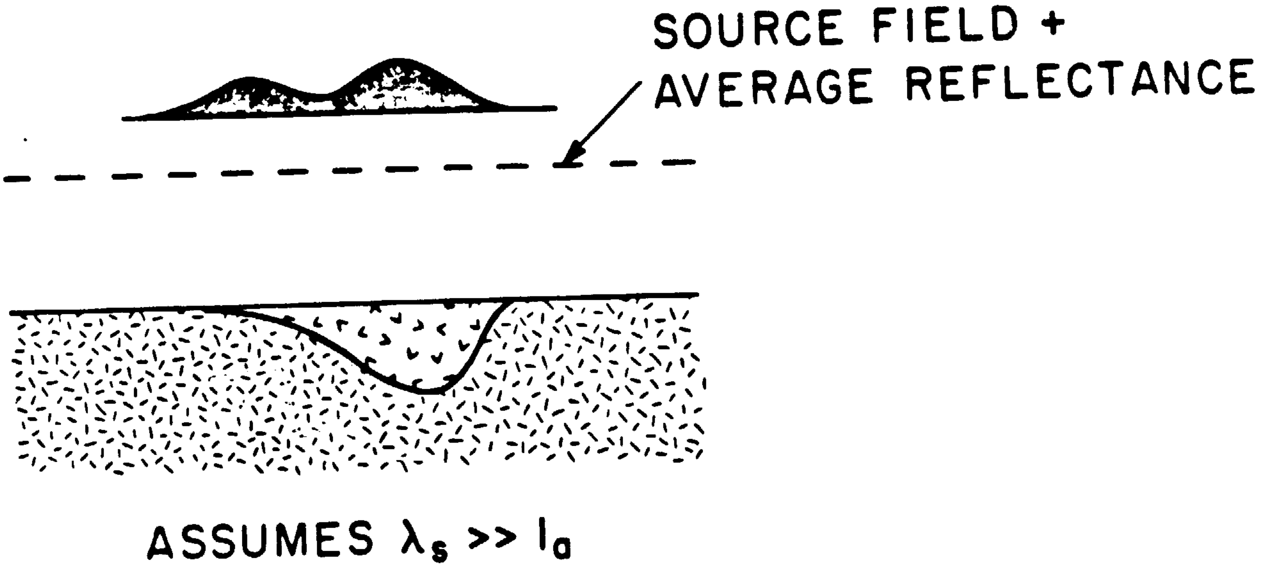

FIGURE 2.

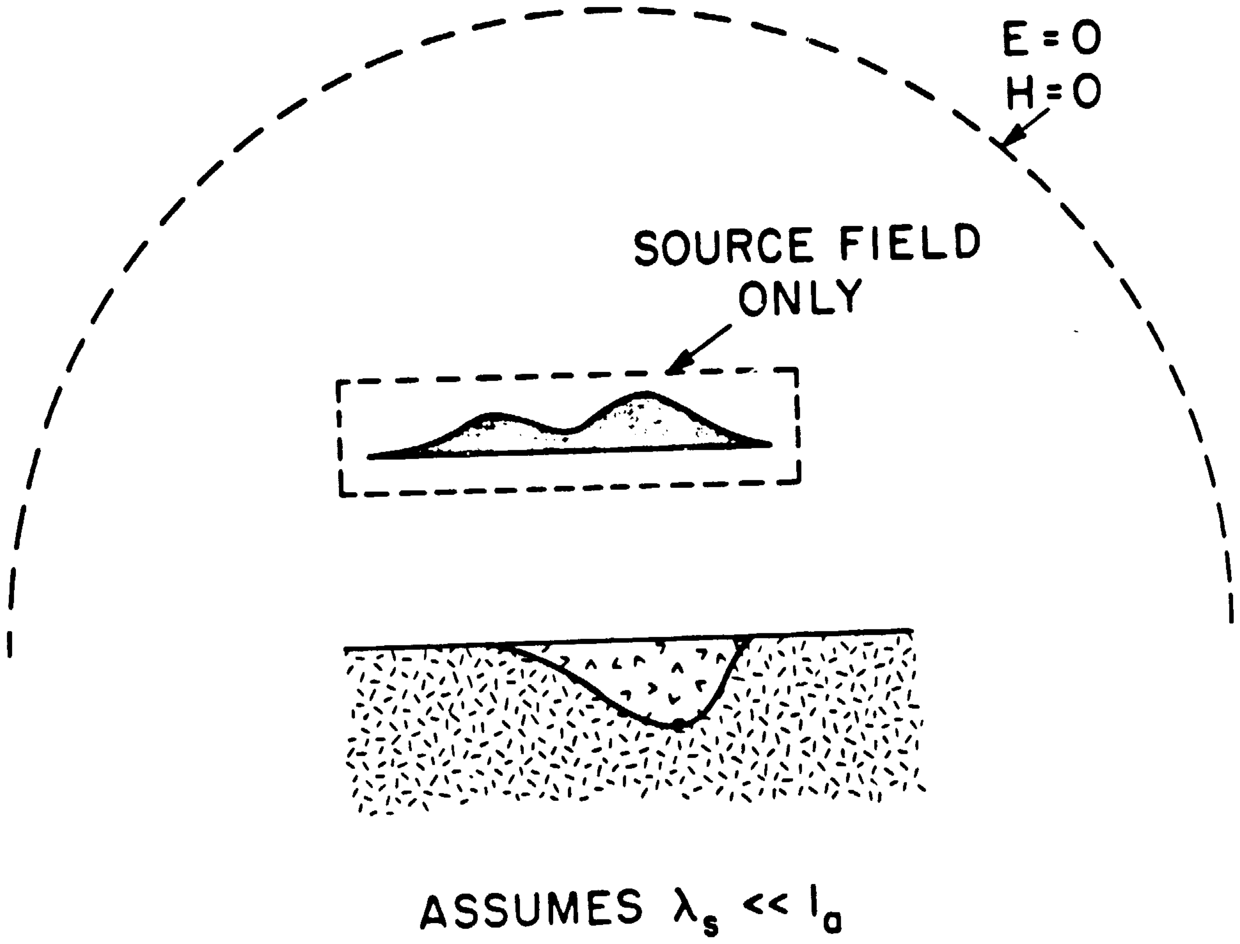

FIGURE 3.

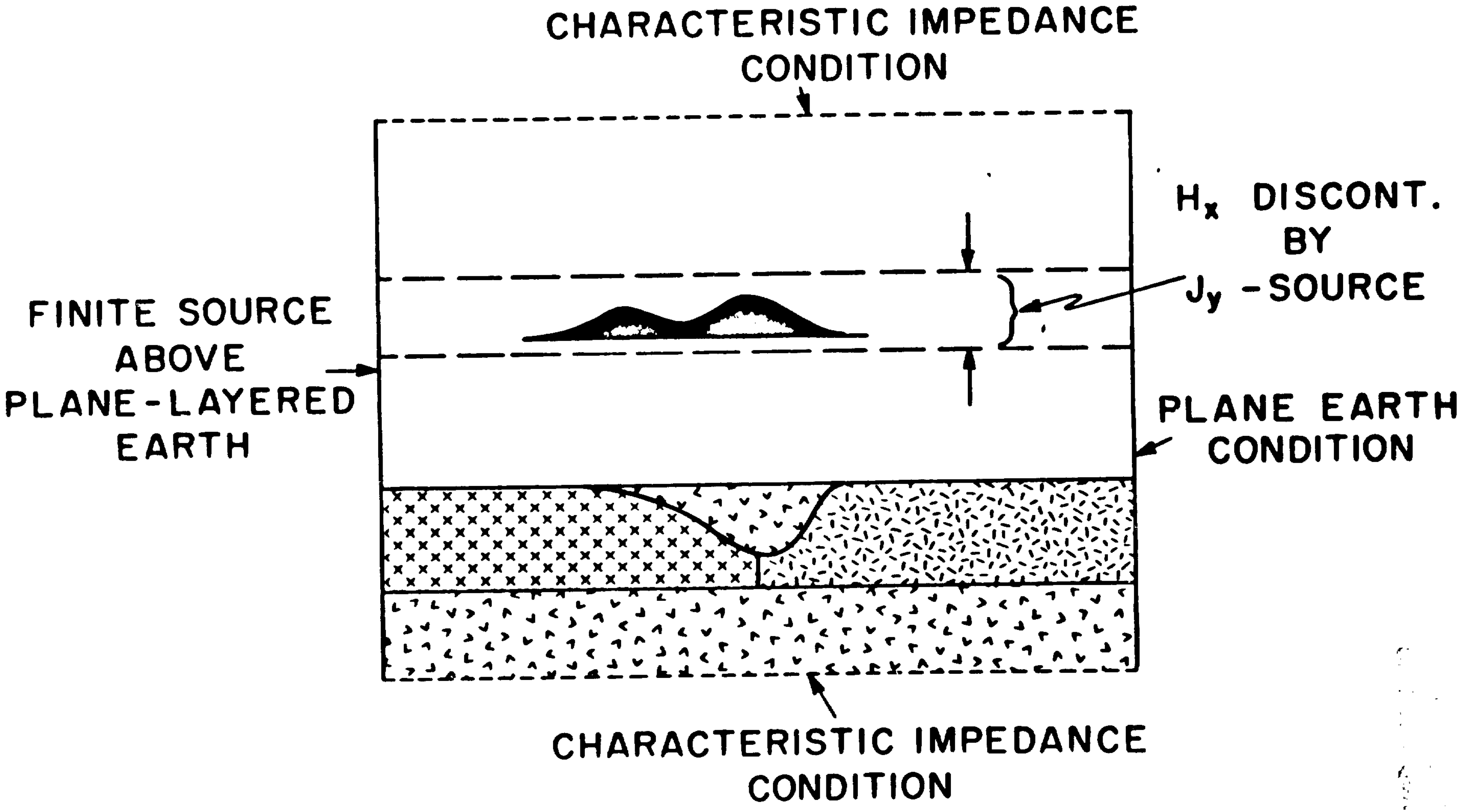
CHARACTERISTIC IMPEDANCE CONDITION
H_x DISCONT. BY J_y -SOURCE
FINITE SOURCE ABOVE PLANE-LAYERED EARTH
PLANE EARTH CONDITION
CHARACTERISTIC IMPEDANCE CONDITION

FIGURE 4.

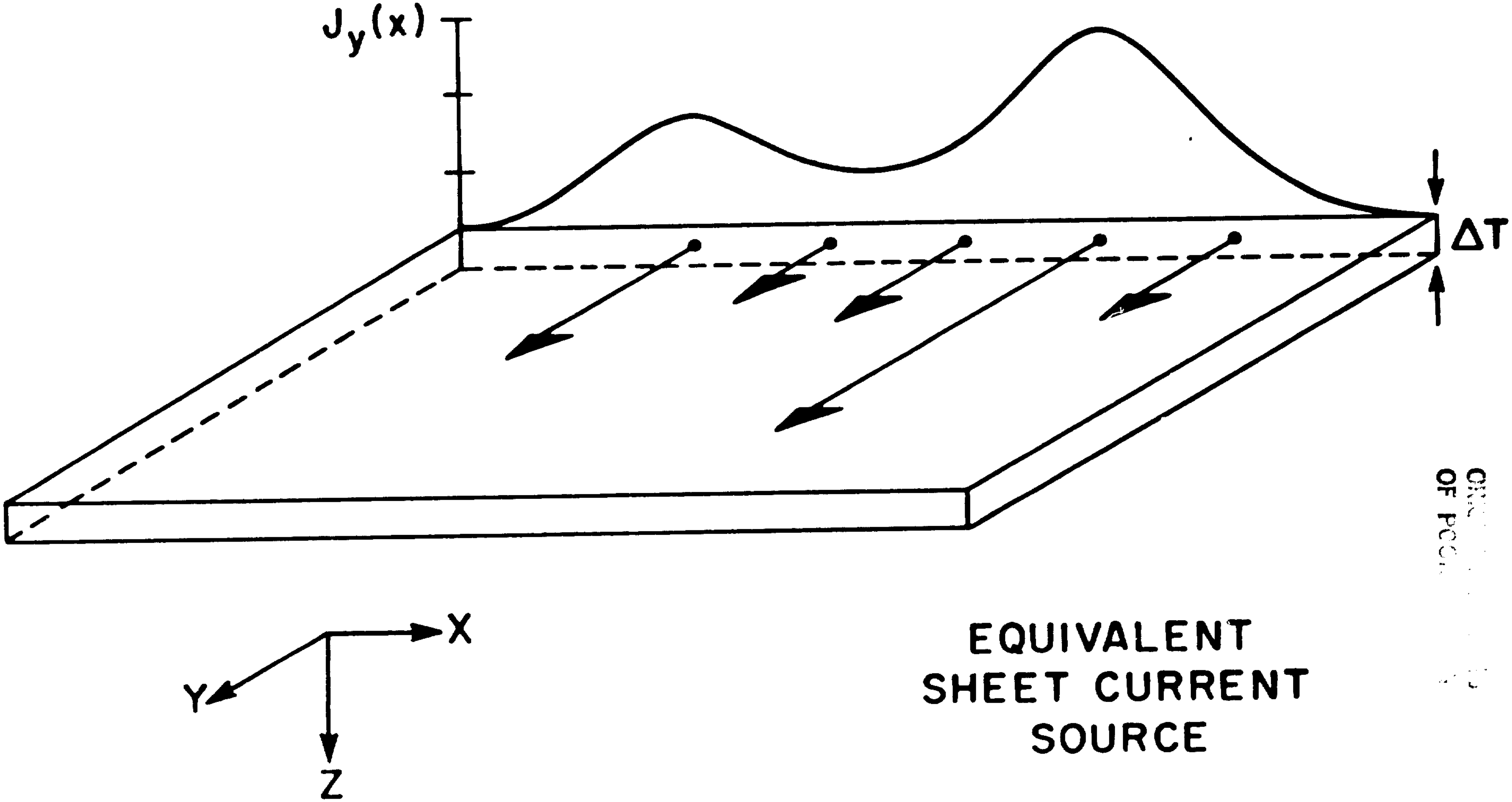

EQUIVALENT
SHEET CURRENT
SOURCE

FIGURE 5.

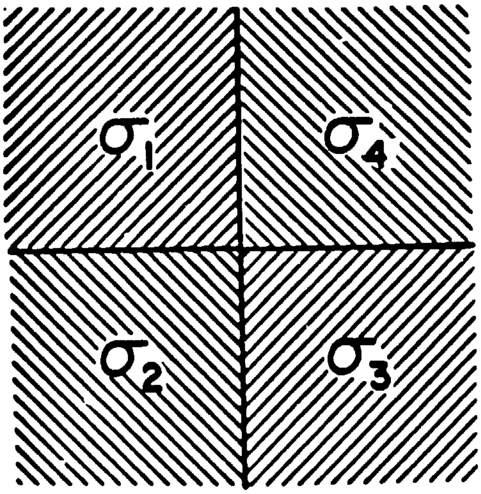

FIGURE 6.

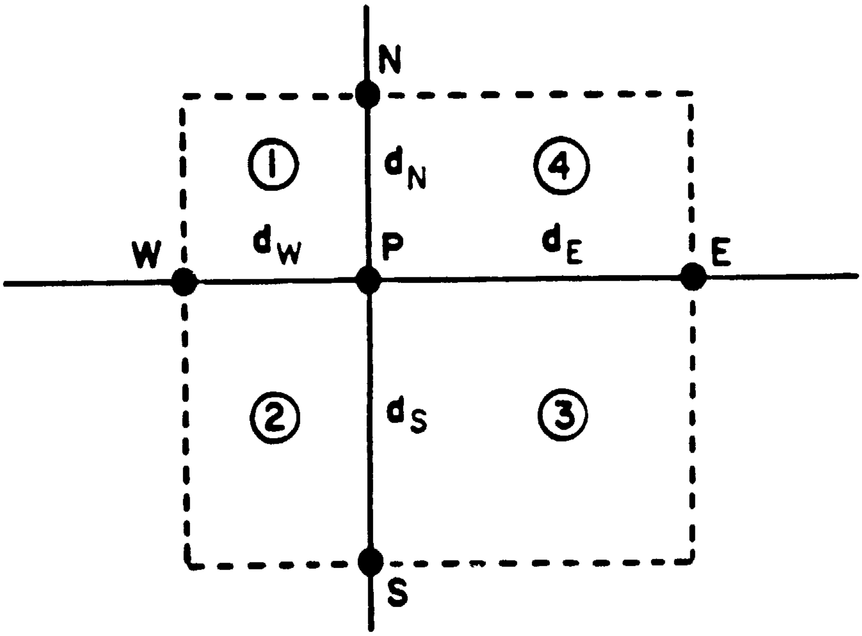

FIGURE 7.

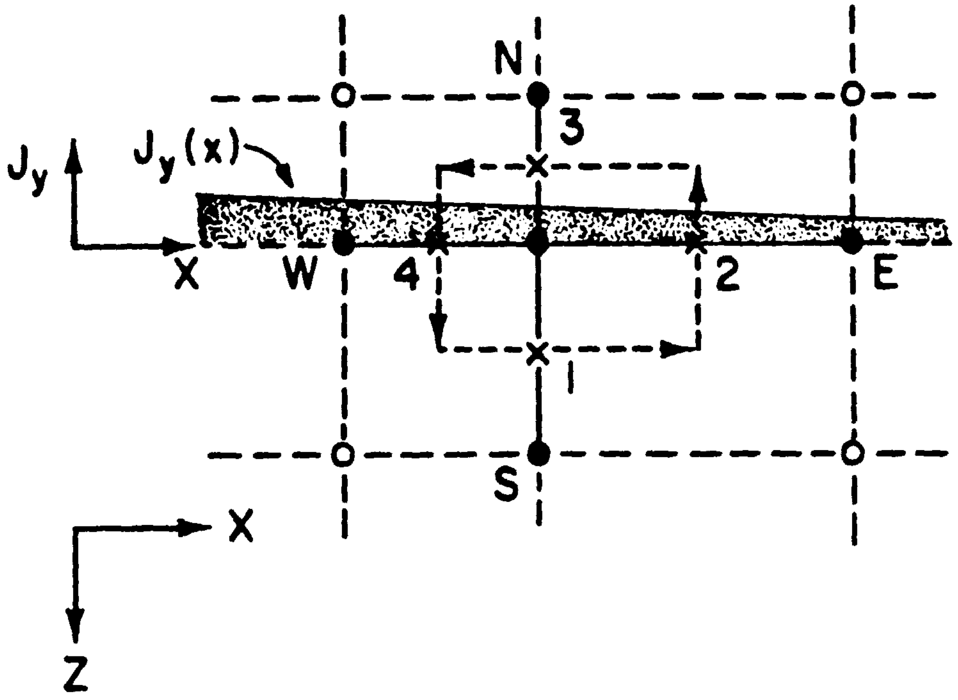

FIGURE 8.

ORIGINAL PAGE IS
OF POOR QUALITY

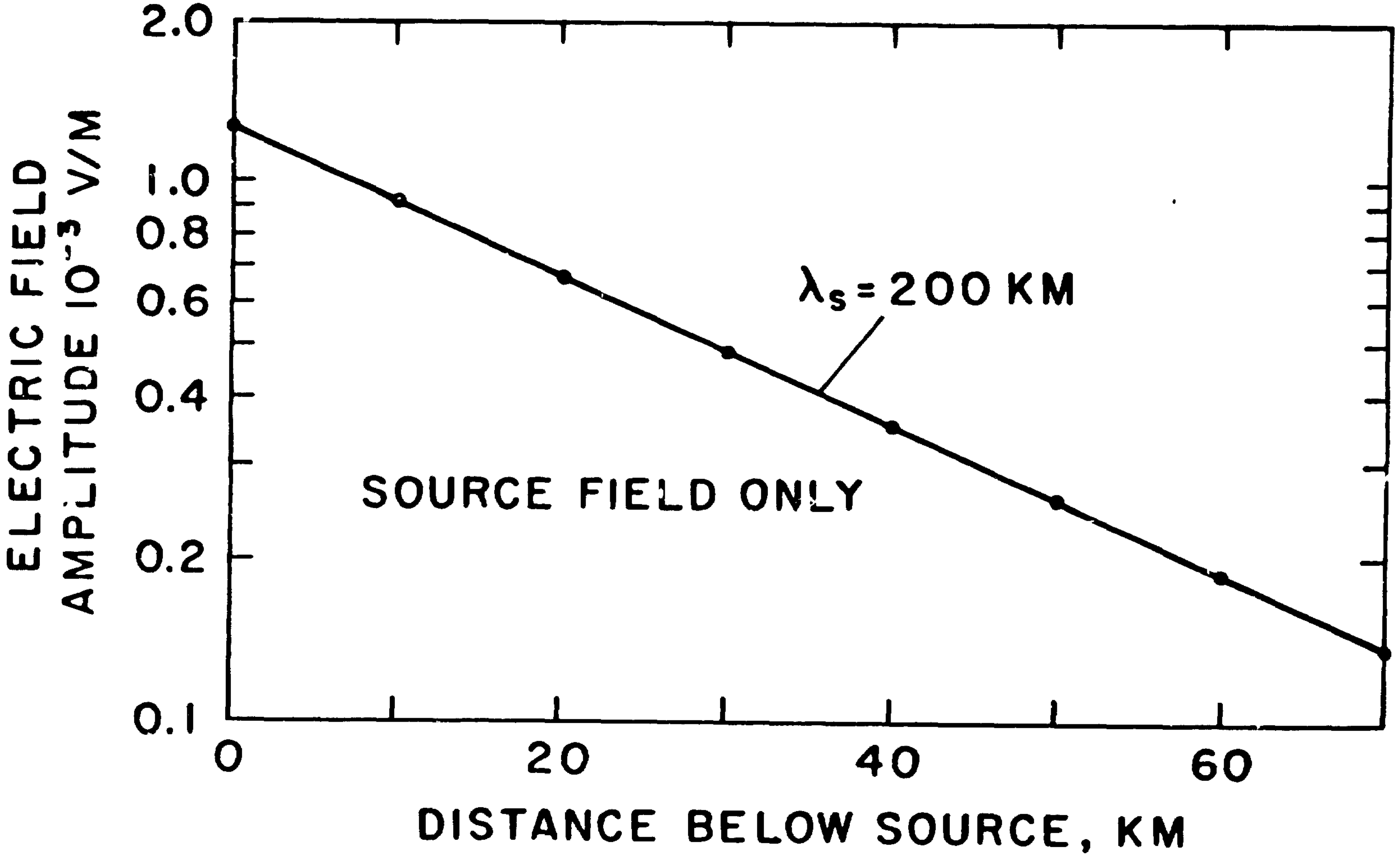

FIGURE 9.

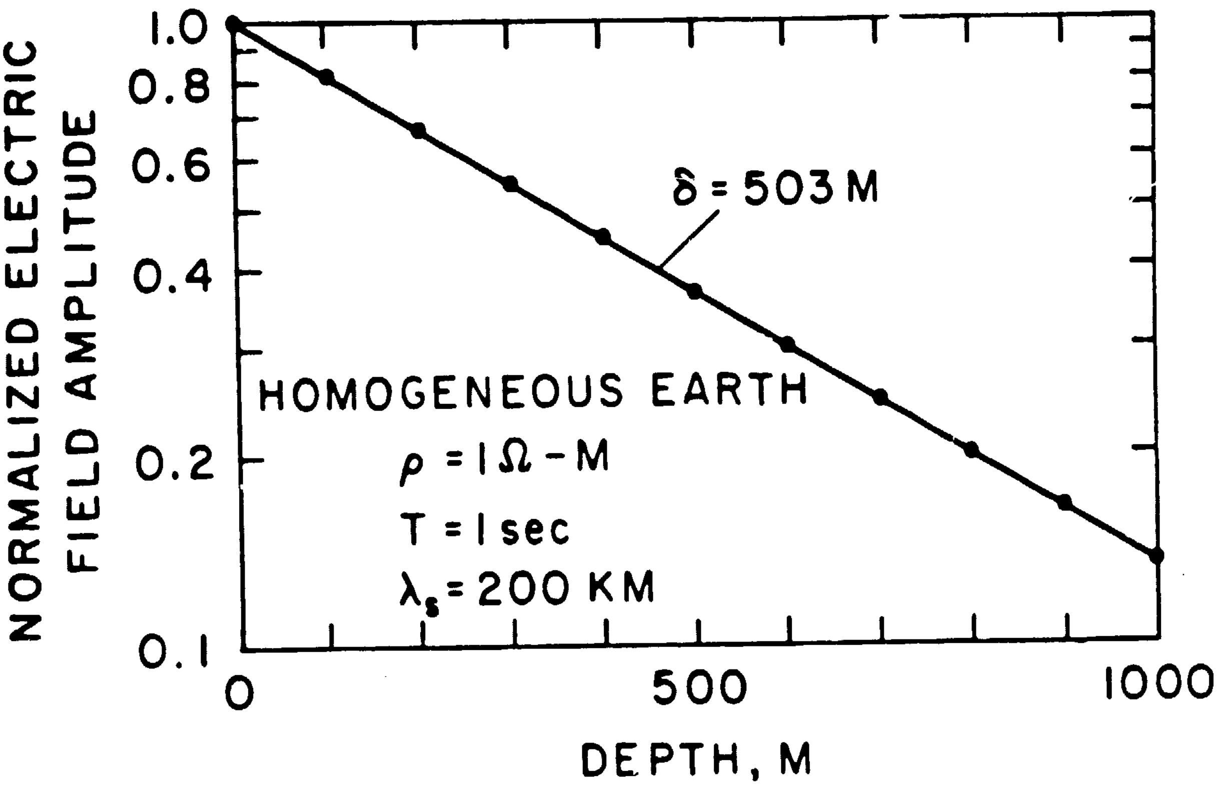
NORMALIZED ELECTRIC
FIELD AMPLITUDE
1.0
0.8
0.6
0.4
0.2
0.1
0
500
1000
DEPTH, M
δ = 503 M
HOMOGENEOUS EARTH
ρ = 1 Ω - M
T = 1 sec
λ_s = 200 KM

FIGURE 10.

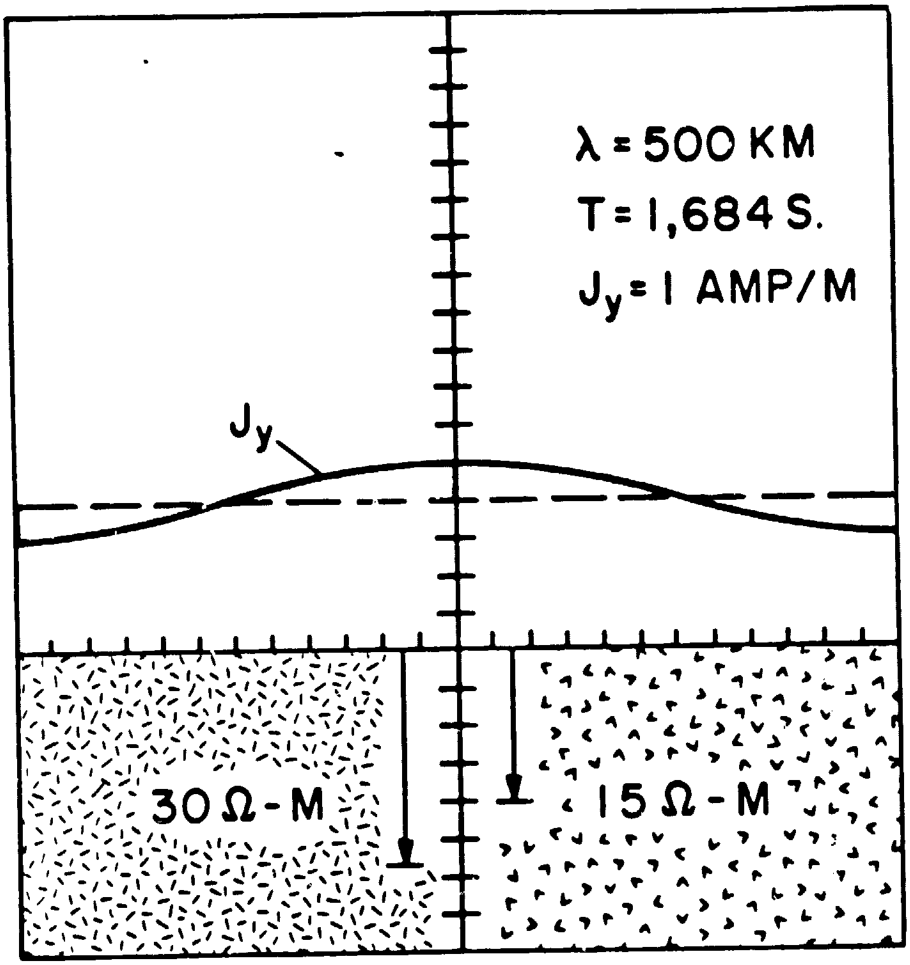

FIGURE 11.

ORIGINAL PAGE IS
OF POOR QUALITY

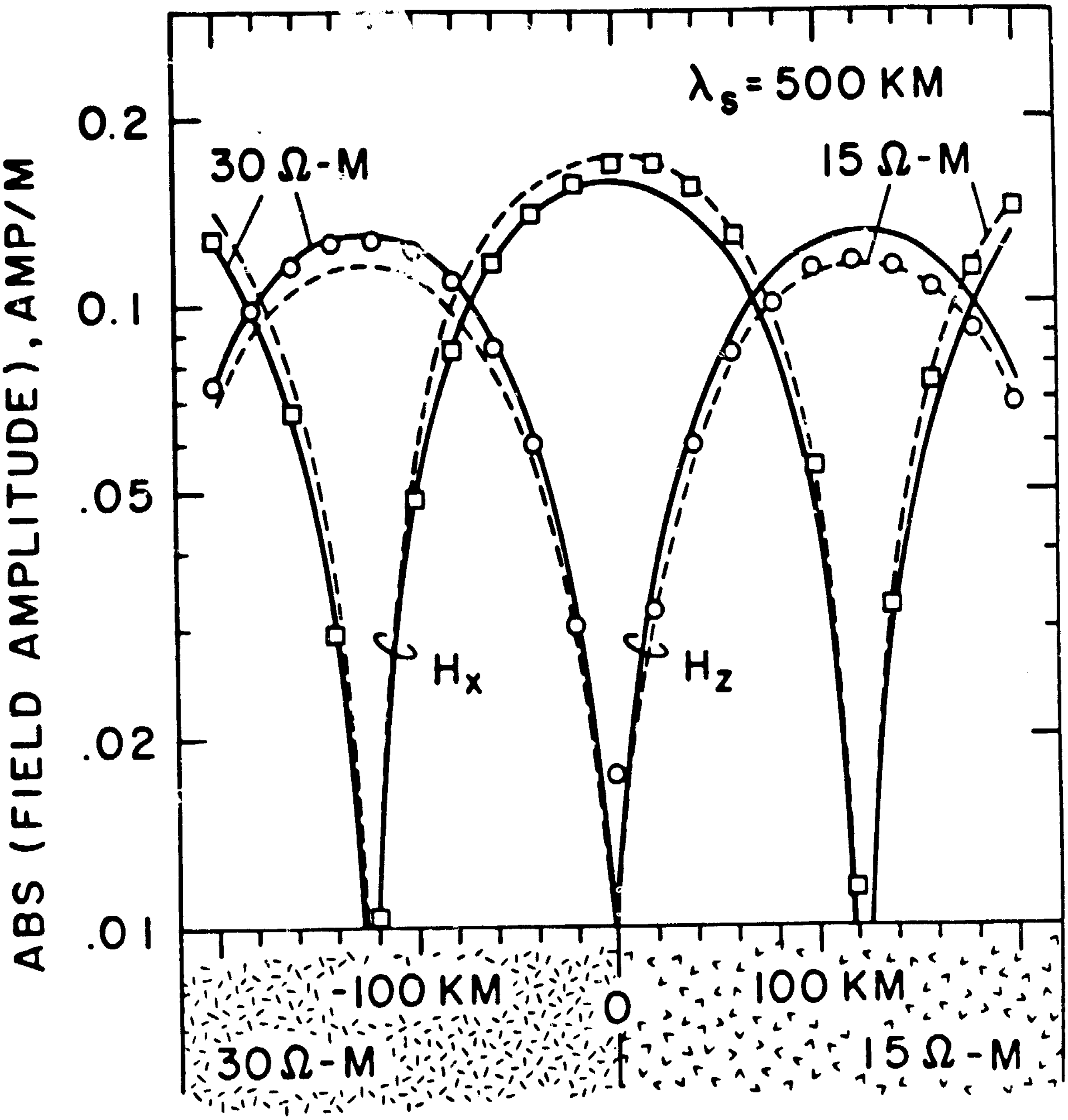

FIGURE 12.

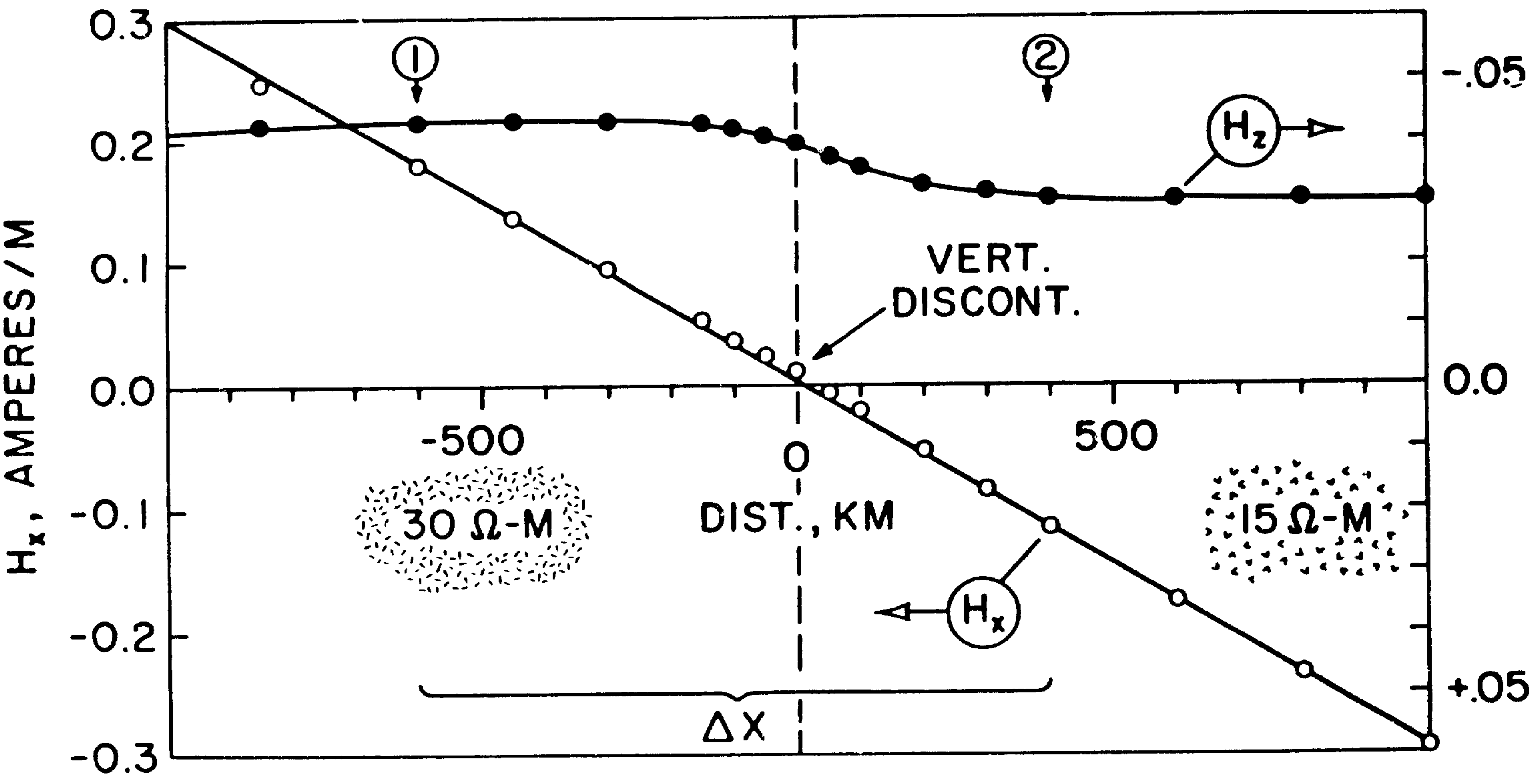
0.3
0.2
0.1
0.0
-0.1
-0.2
-0.3
H_x, AMPERES/M
-.05
0.0
+.05
H_z, AMPERES/M
-500
0
500
DIST., KM
①
②
H_z
H_x
VERT.
DISCONT.
30 Ω-M
15 Ω-M
ΔX

FIGURE 13.

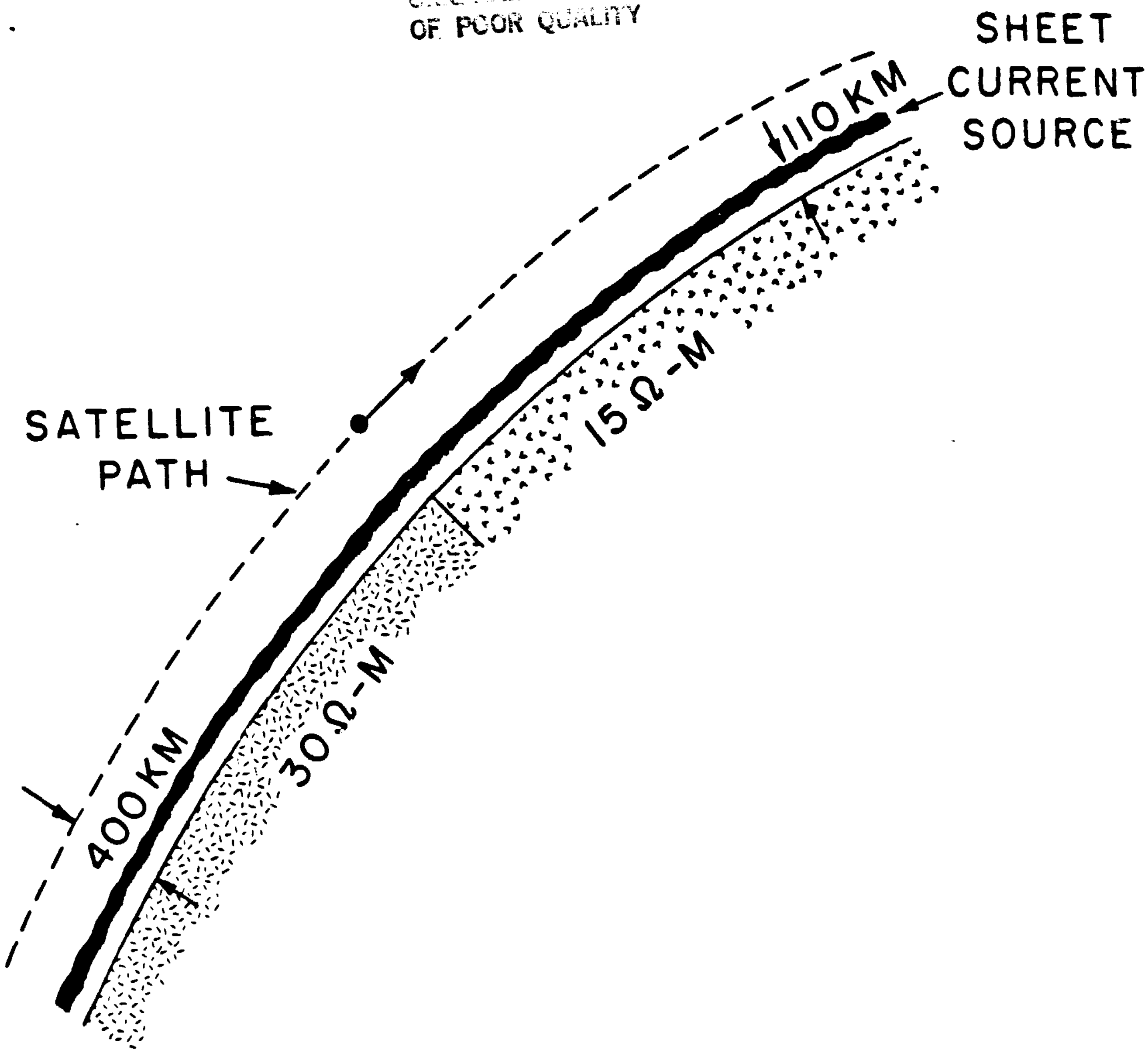

FIGURE 14.

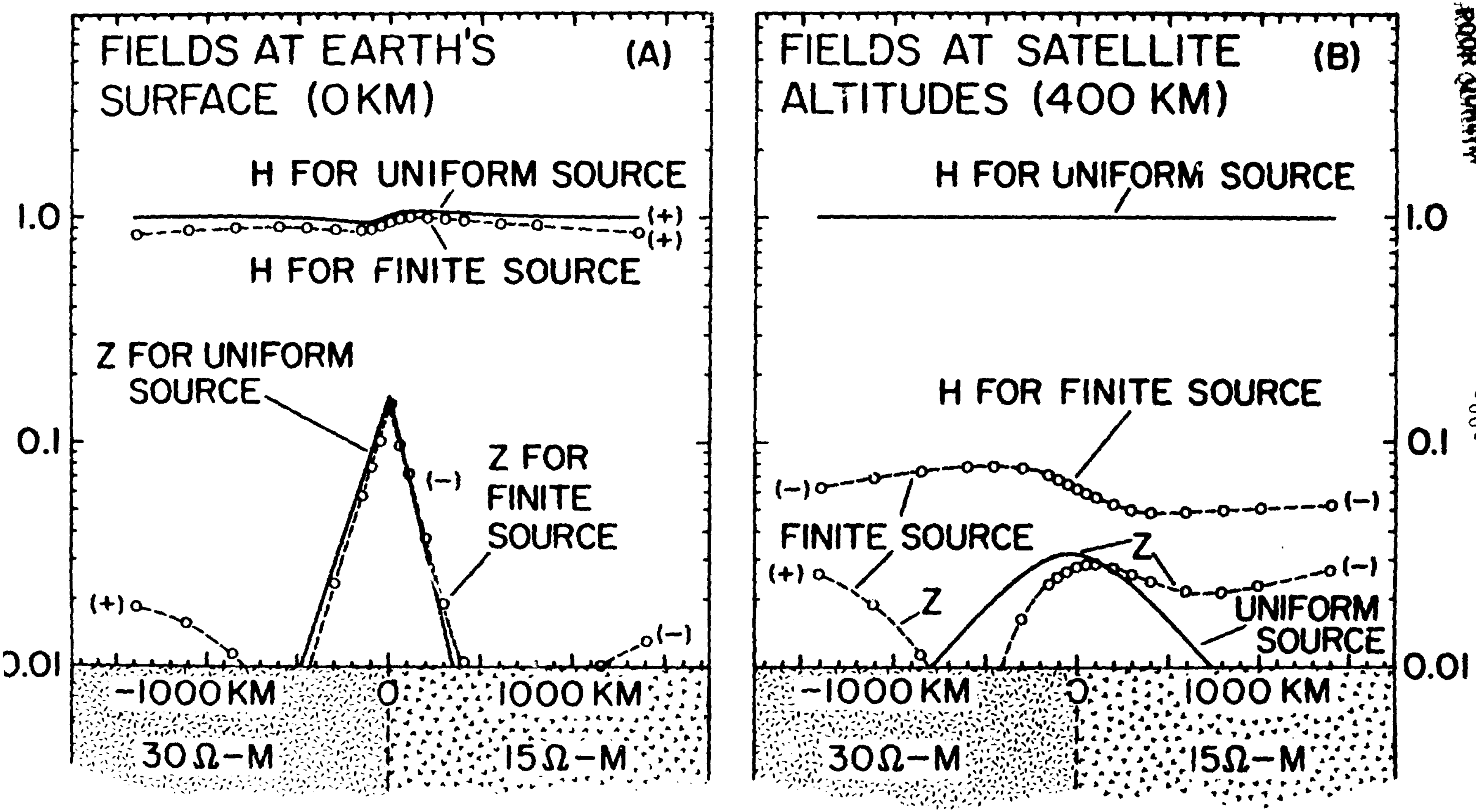
FIELDS AT EARTH'S SURFACE (0KM)
(A)
H FOR UNIFORM SOURCE
(+)
(+)
H FOR FINITE SOURCE
Z FOR UNIFORM SOURCE
Z FOR FINITE SOURCE
(−)
(+)
(−)
1.0
0.1
0.01
−1000 KM
0
1000 KM
30 Ω−M
15 Ω−M
FIELDS AT SATELLITE ALTITUDES (400 KM)
(B)
H FOR UNIFORM SOURCE
H FOR FINITE SOURCE
(−)
(−)
FINITE SOURCE
Z
Z
(+)
(−)
UNIFORM SOURCE
1.0
0.1
0.01
−1000 KM
0
1000 KM
30Ω−M
15Ω−M

FIGURE 15.